Geophysical Investigation of a Mineral Prospect on the Wortel Farm, Namaqua Belt, Northern Cape, South Africa

Minenhle Buthelezi

596280

A dissertation submitted to the Faculty of Science, University of the Witwatersrand, Johannesburg, in fulfilment of the requirements for the degree of Master of Science

October 2019

School of Geoscience, University of the Witwatersrand

Declaration

I declare that this dissertation is my own, unaided work. It is being submitted for the degree of Master of Science at the University of the Witwatersrand, Johannesburg. It has not been submitted before for any degree or examination at any other university.

Minenhle Carol Buthelezi

October 2019

Abstract

The Wortel Farm no. 42 is one of many areas in the Namaqua metamorphic terrain with mineral occurrences whose source, potential and extent have not been investigated. Mapped copper and tungsten mineral occurrences are identified on the farm, sitting on the Koeipoort granite of the Kheisian Period (~2.0 Ga); gneisses, schist, shale, amphibolite and quartzites of the Bushmanland Group and intruding dykes and sheets of the Gareskop Suite. The farm is located 20 km north of the well-known Aggeneys base metal sulphide deposits and 120 km north-east of the O'kiep copper district, all consisting similar lithologies with minor variations. This research was aimed at investigating (and delineating) the potential of the copper occurrence on the farm using multiple geophysical techniques. Gravity, aeromagnetic, DC resistivity and magnetotelluric methods were chosen to map the geology framework, both spatially and in depth, and induced polarization (IP) technique was used for the direct targeting of the mineralisation.

The Namaqua Sector of the Namaqua-Natal Mobile Belt, which is composed of low-to-high metamorphic grade rocks, experienced orogenic deformations that occurred between 2.0 – 0.95 Ga, resulting in strongly metamorphosed, overturned and deformed sequences, with a wide a range of mineral occurrences across the sector (only partially investigated).

Based on outcrop mapping and geophysical data interpretation, five previously unidentified faults at least 200 m long, and striking E-W, NW and NE, were identified in the various lithologies. Multiple folds were also mapped on surface through dip measurements and inferred from interpretations of the geophysical data and they ranged in strike length between centimetres and kilometres.

The geochemical analyses showed that the study area has elevated concentrations of Cr, Co, Cu, Fe, Li, Mg and Ni elements. Aeromagnetic data collected at 80 m flight height and 200 m line spacing were interpreted and modelled with the PyGMI software written in Python. The IP data were acquired over the high magnetic amplitude anomaly. A 2 km x 600 m zone of high magnetism (26380 nT or -265 nT with IGRF removed) is spatially coincident with parts of a 8 – 11 mV/V chargeability anomaly which is also correlated with the mapped Gareskop Suite dykes and Koeipoort granite. The high chargeabilities were interpreted as a possible source of the geochemical elements.

A resistivity anomaly (4 km x 500 m) coincides with most of the elevated chargeability anomaly, with a similar N-S strike and distribution. This is interpreted as an indicator that the possible mineral occurrence is structurally bound across granites, dykes and sand cover unlike the Aggeneys sulphide deposits that are strata-bound in the Gams Formation. Although Aggeneys and Wortel Farm are 20 km apart with minor differences in lithology their mineral occurences are different in nature: Aggeneys stratabound in Gams Formation and Wortel structurally bound.

The mapped geochemical anomalies and occurrences are hosted within the high chargeability zones. The structural confinement of these anomalous features indicate the source(s) of these mineral occurrences are of a pervasive nature as seen in the Springbok vicinity that the Namaqua region was subjected to mineralising fluids of post Namaqua age and yet unknown source. The porphyry system is inferred to be most probable mineralising system, occurring in and around the Gareskop Suite rocks.

Interpretation of magnetotelluric data revealed dome-like resistive crustal segments, shearing, folding, thrusting and faulting that may have been pathways for the mineralising hydrothermal fluids

and attributed to the final deposition and preservation of the mineralisation. Geology structures are well defined by the gravity data. From a palaeomagnetic study of the rocks surrounding the interpreted mineral occurrence both positive and negative inclination directions were obtained and discounting the effects of induced thermal remanence due to lightning strikes, is interpreted as that the rocks were magnetised at different times. As such a positive magnetic declination of the rocks indicates that the sampled rocks were magnetised when the magnetic north was to the east of the geographic north.

This research indicate that the Namaqua sulphide mineral deposits can occur in various forms even in areas with similar lithologies and close proximity, like the Wortel Farm and Aggeneys area. The nature of the Wortel Farm deposit resembles a magmatic segregation of disseminated sulphides while the Aggeneys deposit is of a SEDEX nature, based off the chargeability anomalies of similar amplitudes mapped as separate bodies coinciding with the amphibolite dykes. The geophysical methods chosen for the investigation successfully mapped the subsurface structure with great detail, and delineated the lateral extent of the possible mineralisation. The integration of different geophysical datasets proved crucial and a necessity and complemented other datasets (geology and geochemistry) to highlight various geological details that are required to delineate a base metal deposit in a complex metamorphic terrain.

Acknowledgements

I would like to extend my deepest gratitude to the following people, without whom this academic work would have not been complete:

- Prof. S. J. Webb for guidance during the course of the study and being available to brainstorm ideas that made the completion of this research possible.

- Dr M. Q. W. Jones for all the assistances with consolidating the initial ideas into a research topic and getting the research off the ground.

- Dr U. Weckmann and GFZ team for all the guidance and sharing their expertise on working with the magnetotelluric data.

- Dr D. T. Khoza, Dr E. Sakala and Mr E. Chirenje for technical advices and being available to assist at all times.

- Dr J. Cole for every extra hour spent reading every chapter, some that ended up on a cut, thank you for your grace and kindness!

- The Geophysics Unit who helped carry out all field work and shared their expertise in field surveys, you are champions!

- Friends and family for encouraging words, presence and giving of yourself, you have shown me grace and love. Thank you so much!

- The Council for Geoscience for sponsoring this research.

I am forever grateful!

Table of Contents

Table of Figures

List of Tables

List of Abbreviations and Nomenclature

AF	Alternating field
AMT	Audio-magnetotelluric
BosZ	Boven Rugzeer Shear Zone
CGS	Council for Geoscience
CSAMT	Controlled-source audiomagnetotellurics
DC	Direct current
DGPS	Differential global positioning system
EM	Electromagnetic
ERT	Electrical resistivity tomography
FFT	Fast Fourier transform
GPS	Global positioning system
GRS80	1980 geodetic reference system
IGRF	International geomagnetic reference field
IP	Induced polarisation
MT	Magnetotelluric
NNMB	Namaqua Natal Mobile Belt
NRM	Natural remanent magnetisation
RMS	Root measured square
SACS	South African Committee for Stratigraphy
SP	Self potential
TMI	Total magnetic intensity

Chapter 1: Introduction

The Namaqua-Natal Mobile Belt (NNMB) comprises low-to-high-grade metamorphic lithologies, complex geological structures, numerous deformation events and base metal deposits, especially, in the Namaqua Sector. In particular, Aggeneys and surrounding areas are known for hosting the lead-zinc-copper-silver deposits (Agenbacht and Oosterhuis, 2013; Bailie et al., 2007; Cornell et al., 2006). Mining in Aggeneys started in the late 1920s with the Black Mountain deposit, also known as Swartberg. More investigative studies of the neighbouring mineral prospects soon followed and continued over the years, resulting in the mining of the Broken Hill and Big Syncline deposits in the 1970s. In the 1990s, a shaft was sunk at the Deeps deposit following the success of diamond drilling that intercepted deeper high-grade mineralisation (Cornell et al., 2006; de Beer, 2015; Agenbacht, 2007). Recently, mining of the Gamsberg zinc deposit commenced. The other copper deposit in the sector is the Okiep copper district which is located 120 km southwest of Aggeneys. This copper district, which has been mined on and off over centuries dating back to the 1600s and studied extensively, is host to one of the largest copper deposit in the country (Barr and Reid, 1992; Cornell et al., 2006; Mobbs, 2004). Over the years, the Aggeneys mining town became one of the largest base metal producers in South Africa.

Various geoscientific studies have been conducted in the Namaqua Sector looking at structural settings, stratigraphy, chemical make-up of the rocks and carbon dating to determine rock ages; all done to investigate the formation of the Namaqua Sector (including the events responsible). Currently, more geoscientific studies are being conducted in the Namaqua Sector with authors reviewing and adding details to the existing data (Macey et al., 2017). A recent geophysical interpretation study of high-resolution data collected in Aggeneys and surrounding areas revealed magnetic anomalies that were previously not well mapped and defined due to regional mapping (Buthelezi, 2015). One of the interpreted magnetic anomalies shows similarities in intensity and magnetism to the Aggeneys deposits anomalies, especially the Broken Hill, Black Mountain and Big Syncline deposits. This observed anomaly coincides with mapped copper and tungsten mineral occurrences located on the Wortel Farm no. 42 – the study area for this project. The Wortel Farm study area (outlined in Figure 1.1) is 58 km north-east to the town of Pofadder and 20 km north of mining town of Aggeneys (Figure 1.1).

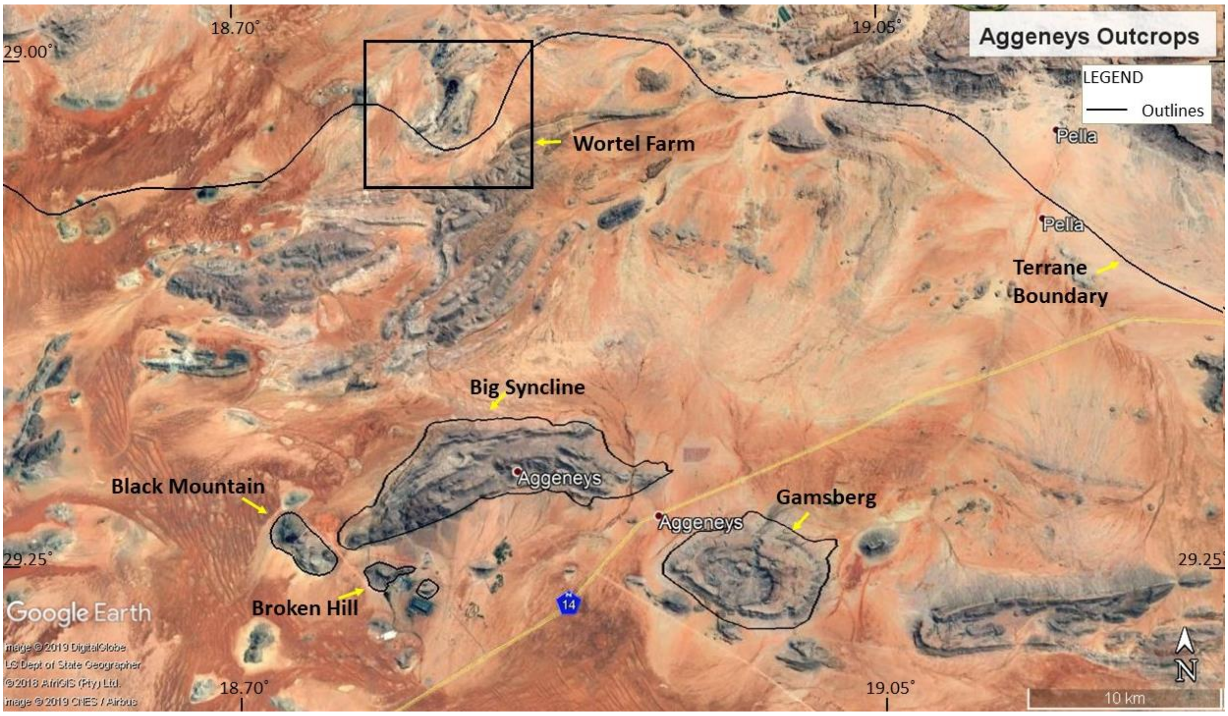

Figure 1.1. Google Earth terrain map of the Aggeneys area showing outcrops rocks with known deposits highlighted by irregular black boundaries and study area outlined by black rectangle. The Richtersveld Subprovince – Bushmanland Terrane boundary demarcated is geologically mapped on a 1:1 000 000 scale map (Google Earth, 2018).

The aim of this research is to map the mineral prospect on the Wortel Farm study area using geophysical techniques to determine the potential of the prospect. The hypothesis drawn from the magnetic data, lithologies present, mapped mineral occurrence and proximity to the Aggeneys deposit is: that the mapped mineral occurrences are part of a large mineral deposit occurring on the Wortel Farm and that the mineralisation is similar to that of the Aggeneys mineral deposits. The Wortel Farm deposits may have been separated from those at Aggeneys during the deformation events, ultimately ending up 20 km to the north. The objectives of this study are to 1) understand the geological framework of the farm and derive a comparison with the Aggeneys deposit geology through geophysical mapping, to 2) integrate all available geoscience datasets to determine a possible source and potential of the mineral occurrences, and to 3) determine the possible effect of the distance from the Aggeneys deposit and terrane boundary crossing the farm will have on the mineralisation and geology of the farm.

Geophysical studies encompass a number of methods that measure different physical properties of the rocks. The various datasets can be integrated to answer specific questions and derive a geological story of the subsurface. The geophysical methods have been successfully applied in various mapping, environmental, exploration and research studies and proven to be necessary tools. Below is a brief description of the geoscientific studies completed in the Aggeneys area largely focusing on the deposits, and the value added by geophysics.

Bailie et al. (2007); Colliston et al. (1989); Colliston and Schoch (2013, 2000); Foulkes (2014); Praekelt and Schoch (1997) are among a large group of scientist who have contributed to accumulating knowledge of the Namaqua-Natal Mobile Belt (NNMB), having studied the depositional age, metamorphism, effect of deformation, stratigraphy synthesis of some formations and groups, geochemical analysis to investigate the genesis and evolution of the mineralisation.

One of the geophysics contribution is reported by Colliston et al. (2014) where these authors studied the sixteen terranes of the NNMB, including the Aggeneys and Pofadder Terranes (here referred to as the Bushmanland Terrane and the Richtersveld Subprovince, respectively), to deduce the distribution of collisional terranes using regional geophysical data and selected detail profile studies. They compared the terrane boundary mapped from surface outcrop with the geophysical data. The results of their interpretation informed a revised extension to the mapped terrane boundaries especially in areas without outcrop i.e. under sand cover.

Walker and Terblanche (2010) calculated an electromagnetic model to characterise the Gamsberg deposit, a complexly folded synclinal major zinc deposit. The inverted model indicated that the depth of the conductor extended deeper than previously mapped. These results were refined and corroborated by the borehole data.

In his book, de Beer (2015) reports that, in the 1970s a drilled borehole on Black Mountain intersected economical mineralisation that was soon followed with geophysical and geological mapping. Since it was known that the ore in this area is directly associated with banded iron formations, a detailed ground magnetic survey was carried out. The survey revealed a number of high amplitude anomalies. What was also apparent from the data was the close relationship between the magnetite content and economic sulphide mineralisation. Subsequently the electromagnetic (EM) method, controlled-source audio-magnetotelluric in particular, detected a Black Mountain sulphide deposit at 400 m depth.

According to de Beer and Muller (2015), geophysics was amongst the most efficient tools used that contributed to determining the exploration potential of the Gamsberg zinc deposit. Geophysical surveys together with geochemistry and geological studies identified the Gamsberg as an exploration target. The stratigraphy of the deposit consists of barite, gossan and magnetite-quartzite rocks. The magnetic data showed an anomaly extending beyond the mapped outcropping gossan, indicating that the strike length extends at depth. These findings added to the assessment of the deposit. The magnetic survey was followed by extended induced polarization (IP) and EM geophysical surveys that detected the sulphide zone at 250 m depth. Targeted drilling followed and confirmed these findings. Consequently, high resolution aeromagnetic data acquired by mining companies locally were used as the basis for exploration drilling along synclinal structures described by high magnetic zones (de Beer and Muller, 2015). Geophysical data were, once more, instrumental in defining and elucidating of the Aggeneys complex base metal deposits (de Beer, 2015).

As part of his theses, Naicker (1993) compiled a database and map of acquired geophysical datasets in the area (Figure 1.2). The archived data includes: magnetic, electromagnetic (EM), induced polarization (IP), time domain EM and gravity datasets.

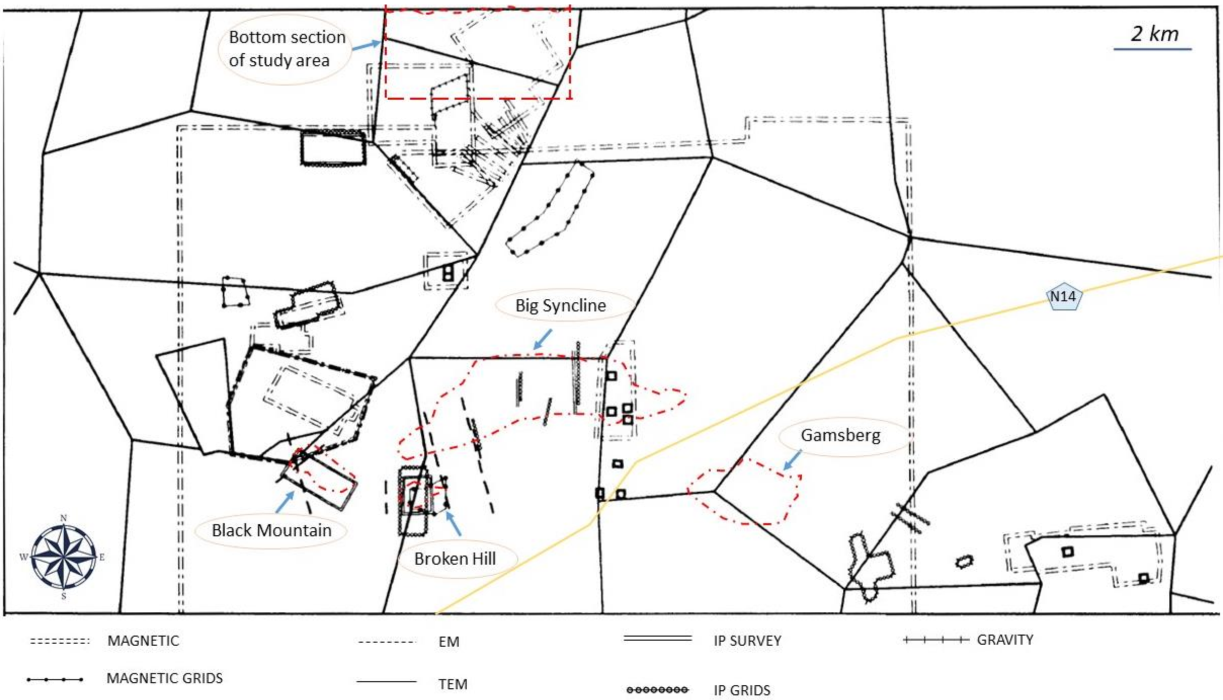

Figure 1.2. Test grids and survey lines map of the geophysical data acquired and available by 1993 (Naicker, 1993). The datasets include magnetic, gravity, EM, time domain EM and induced polarization. The outline of the Aggeneys deposits outcrop including parts of the Wortel Farm study area are overlain onto the map and indicated by the red dashed outlines. The bold black outlines are farm boundaries.

The case studies presented above show how instrumental geophysical data are to subsurface mapping especially when integrated with other geoscientific datasets. Geologically, the Namaqua Sector is enriched in base metal mineralisation however the area remains underexplored.

This dissertation is structured as follows: Chapter 2 is a discussion of the regional geological setting of the Namaqua Sector, Aggeneys region and the Wortel Farm, which includes the lithologies occurring in the area, structural and lithological deformations and mapped mineral occurrences. In addition, a brief discussion and comparison of the older low-resolution geophysical data and recently acquired high-resolution data is presented.

Chapter 3 consists of work completed during the course of this study: the methods chosen, survey design and data acquisition. The processing techniques employed for each dataset are also described here, including apparent features on the resulting maps. A brief description of palaeomagnetic rock sampling, analyses technique and resulting data is presented and compared with mapped magnetism in the area. Available geochemistry data of the farm is also presented and results summarised.

An interpretation of all the datasets is presented in Chapter 4. The geophysical datasets are compared and contrasted with the mapped geology to analyse and determine possible correlations with mapped geological structures and lithologies. Furthermore, a comparison of some datasets is presented in order to determine possible correlations – for example the IP and resistivity datasets.

An integration and discussion of all datasets with regard to geology and mineral potential in the area is presented in Chapter 5. Conclusions drawn from the results and a discussion, together with a comparison with the hypothesis are presented in Chapter 6. Recommendations are made.

Chapter 2: Geological and Geophysical Background

This chapter reviews the geological make-up of the Namaqua Sector, the Aggeneys region and the Wortel Farm study area. Geophysical datasets available in the area at the commencement of the project are presented and apparent features described briefly.

2.1 Geology

Rocks of the Namaqua Sector of NNMB (also known as the Namaqua-Natal Tectonic Province), cover large parts of the Northern Cape Province, South Africa. The Namaqua-Natal Tectonic Province extends from the south of Namibia through the Northern Cape, Western Cape, Eastern Cape and KwaZulu-Natal Provinces of South Africa. It is bounded in the north and east by the Rehoboth Province, Kheis Belt and Kaapvaal Craton (Cornell et al., 2006; Thomas et al., 1993; Webb, 2009) (Figure 2.1). The Cape Fold Belt and Gariep Belt borders the NNMB in the south and west, respectively. The Namaqua-Natal Tectonic Province consists of igneous and sedimentary rocks that have been metamorphosed during the Orange River Orogeny dated at 2 to 1.6 Ga and the Namaqua Orogeny that was active from 1.2 to 0.95 Ga (Cornell et al., 2006; de Villiers and Sohnge, 1959). Where these rocks outcrop in the KwaZulu-Natal and Northern Cape Provinces they are referred to as the Natal and Namaqua Sectors, respectively (Cornell et al., 2006).

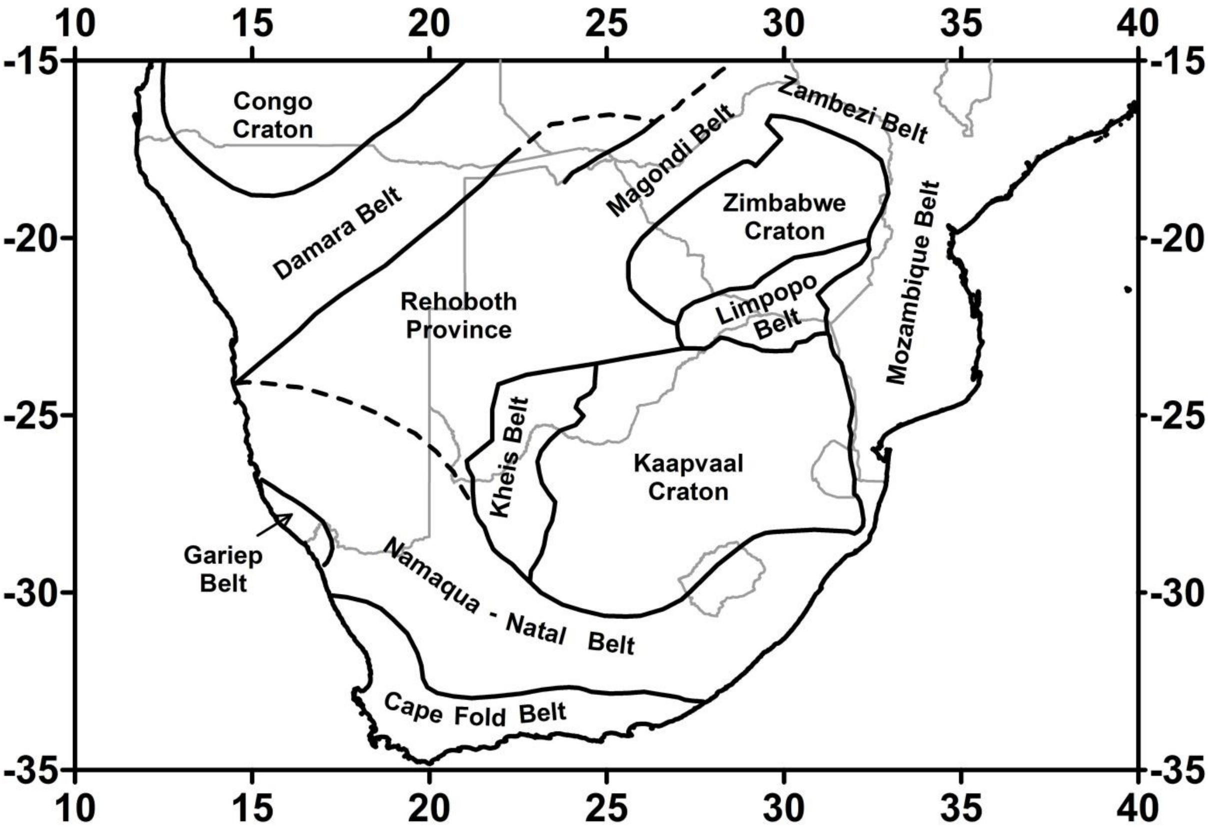

Figure 2.1. Tectonic map of Southern Africa, as illustrated by Thomas et al. (1993) and Webb (2009), outlining the extent of the Namaqua-Natal Belt and the adjoining Cape Fold and Gariep Belts, Congo Craton, Damara Belt, Rehoboth Province, Magondi and Kheis Belts, Kaapvaal Craton, Limpopo and Mozambique Belts, Zimbabwe Craton and the Zambezi Belt.

Various authors have divided the Namaqua Sector into numerous tectonostratigraphic subprovinces and terranes by (Cornell et al., 2006; Eglington, 2006; Evans et al., 2007). One of the regions, Richtersveld Subprovince, was upgraded to a province and the rest of the sector grouped as Namaqua Province (Van Der Merwe and Botha, 1989). Similarly, the Bushmanland Terrane is upgraded to the subprovince and combined with the Richtersveld Subprovince and then subdivided into at least six terranes by Colliston et al. (1989) (Agenbacht, 2007; Cornell et al., 2006) (Figure 2.2). Cornell et al. (2006) recognised five domains in the Namaqua Sector (from east to west): Kaaien Terrane, Koras Group, Areachap, Kakamas and Bushmanland Terranes and Richtersveld Subprovince (Figure 2.3). For this study we will be adhering to Cornell et al. (2006) subdivisions as approved by South African Committee for Stratigraphy (SACS). The stratigraphy details of the five domains are discussed below.

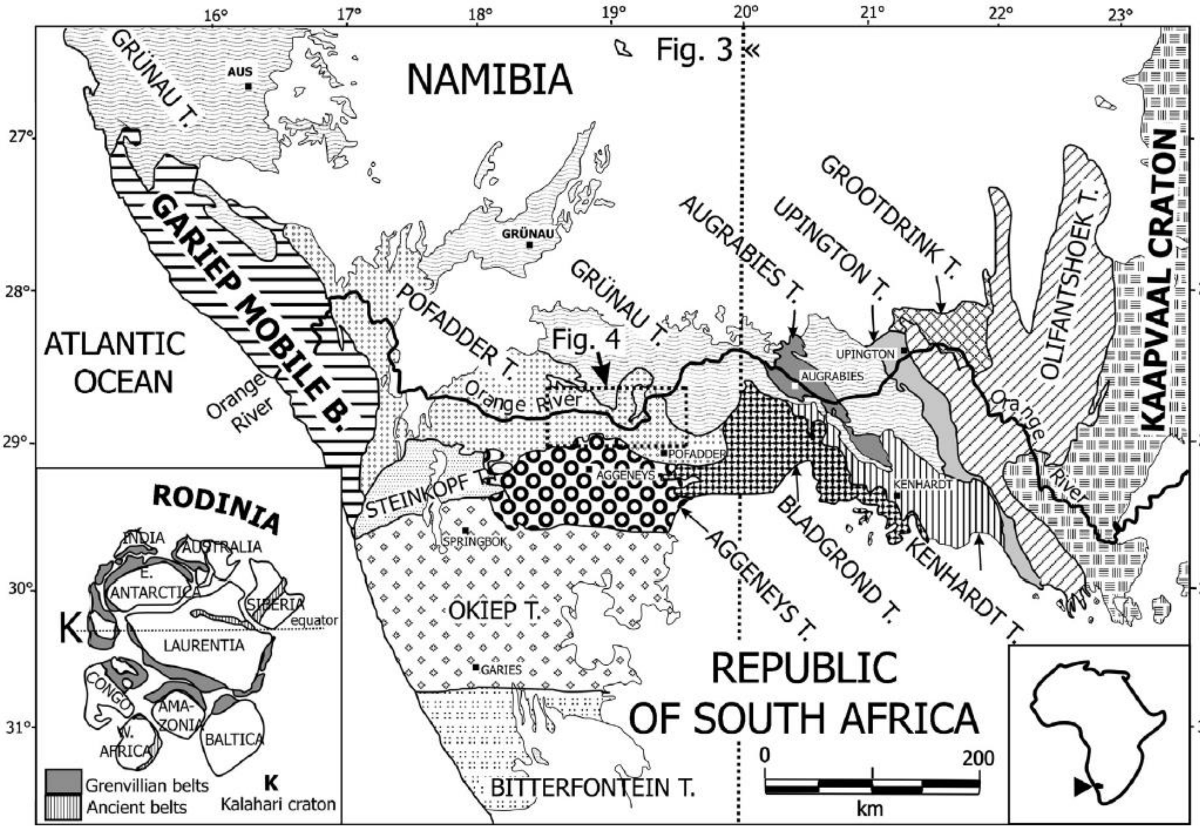

Figure 2.2. A simplified geology map of the Namaqua Sector with tectonostratigraphic subdivisions as described by Colliston and Schoch (2013).

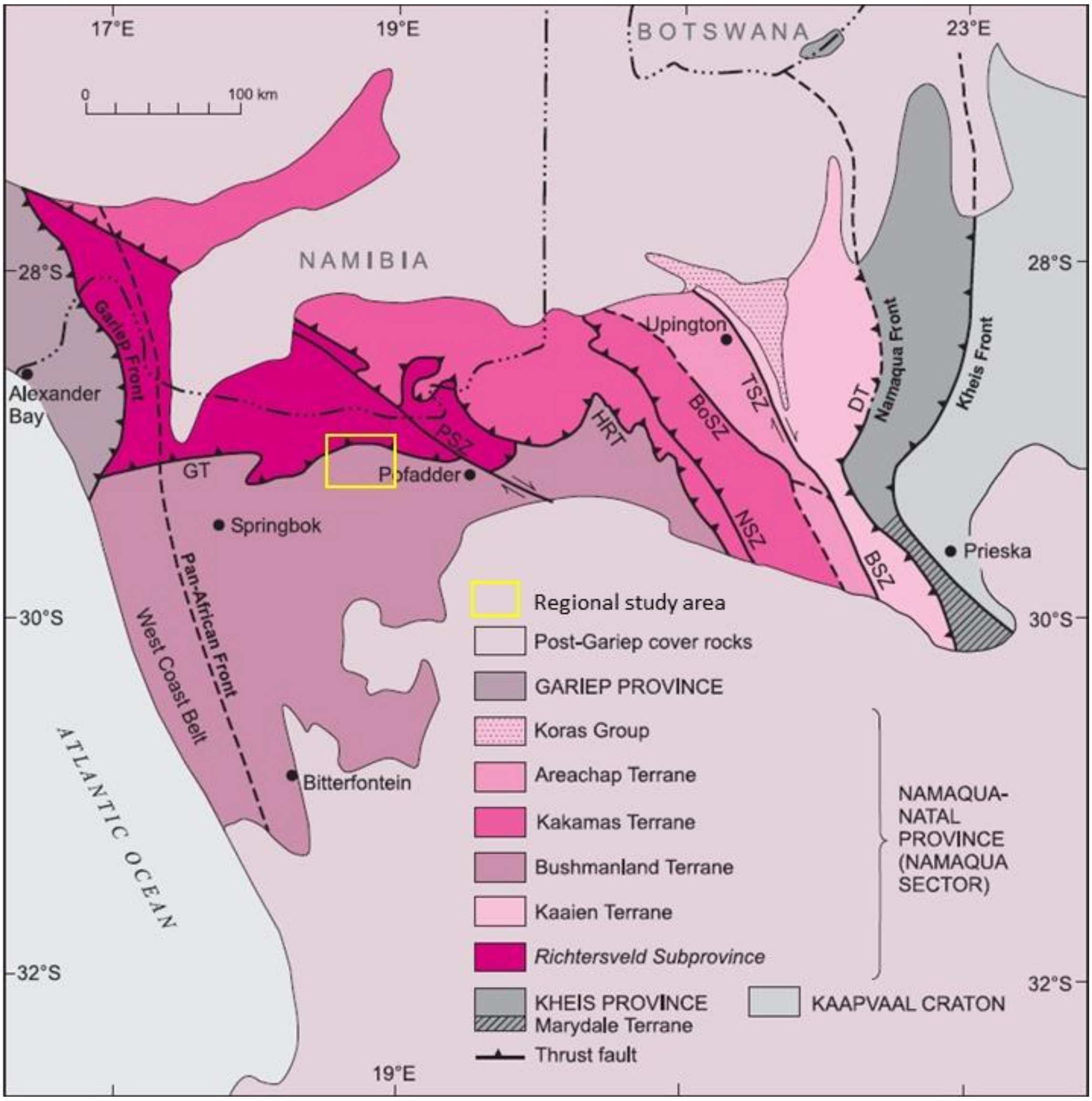

Figure 2.3. Tectonostratigraphic subdivision map of the Namaqua Sector of the Namaqua-Natal Belt according to Cornell et al. (2006) with the Aggeneys area outlined by a yellow rectangle.

The Kaaien Terrane forms the eastern foreland of the Namaqua Sector, bounded by the Dabeep Thrust (DT) to the east (Figure 2.3). The terrane is subdivided into three groups: the Brulpan, Vaalkoppies and Wilgenhousdrift Groups. The Brulpan Group consists of intrusions occurring as dykes and sheets and quartz-muscovite schist dated between 1930 Ma and 1300 Ma. The Vaalkoppies Group comprises quartzites and quartzite-schist rocks associated with Kheisian depositional age of 1750 to 1900 Ma. The Wilgenhoutsdrift Group consists of volcanogenic rocks dated around 1100 Ma (Cornell et al., 2006; Eglington, 2006). The terrane consists of low-grade metamorphosed rocks showing evidence of $D_1 - D_3$ (folding, shear movements, rejuvenation, fracturing) deformation. A mix of Kheisian (~2000 Ma) and Namaqua tectonic (1200 – 950 Ma) overprint is mapped in the terrane. The mineral occurrences in the terrane include copper stains mapped on fracture planes occurring in basalts of the Wilgenhoutsdrift Group; unexplored nickel deposit in the Vaalkoppies and Wilgenhoutsdrift Groups and asbestos in Kleinbegin (Cornell et al., 2006).

The Koras Group is sometimes described as the Kaaien Terrane subdivision although not all authors agree (Cornell et al., 2006). The Koras Group unconformably overlies the Kaaien Terrane to the north and east of Upington and comprises gneisses, granite and quartz-feldspar porphyry dykes dated at 1180 Ma. Deposition of parts of the group was controlled by continued fault movements, leading to the development of a talus fan and irregular distribution of lithostratigraphical units. Tilting and slumping are also mapped (Cornell et al., 2006).

The Areachap Terrane consists of a NNW-trending belt of amphibolite-grade metabasic and intermediate supracrustal gneisses of the Areachap Group rocks dated at 1300 Ma and granitoids of the Keimoes Suite dated at 1000 Ma. This terrane also comprises rocks associated with the Bushmanland and Kakamas Terranes. The Boven Rugzeer Shear Zone (BosZ) to the west and the Brakbosch-Trooilapspan Shear Zone to the east form the borders of the terrane (Figure 2.3). Some notable deformation events recorded on the terrane include rifting that led to the development of the ocean basin, the development of subduction zones and collision and overthrusting with the Kaapvaal Craton which lead to granitoid intrusions and M_1 metamorphism. Occurrence of $M_2 - M_4$ metamorphism were due to melting, uplift and cooling. Massive sulphides of pyrite and pyrrhotite with sphalerite and chalcopyrite were mined at Prieska Mines and Areachap (Cornell et al., 2006; Fransson, 2008).

The Kakamas Terrane is located west of the BosZ and is dated between 2000 and 1240 Ma depositional times (Figure 2.3). The terrane consists of supracrustal metapelite and Namaquan granitoids. This terrane has a NW-trending stratigraphy consisting of the Korannaland Group, Koelmanskop Metamorphic Suite and intrusions. The Korannaland Group is composed of high grade supracrustal rocks (arenite and calcarenite) and the suite comprises a supracrustal sequence of high-grade metapelite and biotite-garnet paragneisses. The age of these rocks is undetermined. Intrusions occurring on the terrane include the Keimoes Suite dated at 1200 to 1080 Ma and the Kenhardt pegmatite belt dated at 1000 to 945 Ma. Four major deformational events are identified on the terrane: $D_1 - D_3$ (various folding and thrusting) and major shearing associated with the BosZ, Cnydas and Pofadder shear zones. The only known mineralisation in the terrane is the lead deposit (silver, zinc, copper dated at 1200-1150 Ma) at Rozynenbosch, Kakamas town (Cornell et al., 2006; Fransson, 2008).

The Bushmanland Terrane is the largest crustal block of the sector located south of the Richtersveld Subprovince at the boundary defined by the Groothoek Thrust (Figure 2.3). The terrane consists of medium-to-high metamorphic grade rocks comprising granitic gneisses (basement complex) dated at 2000 Ma, amphibolite-grade supracrustal (sequence) rocks dated at 1600 to 1200 Ma and granitoids (intrusive) at 1200 to 1000 Ma. The base metal deposits in the terrane are hosted by supracrustal rocks. Two dominating tectonic episodes characterising the terrane are $D_2\ and\ D_3$ consisting of recumbent folds ranging between metre and kilometre scale. ENE-trending mapped mineral lineation are associated with S_2 foliation. A number of stratabound base metal deposits in the Bushmanland Terrane are hosted by supracrustal rocks including Aggeneys area major deposits of zinc, lead, copper and silver sulphides dated at 1350 – 1300 Ma. The Okiep Copper District consists of mafic intrusions most of which host copper sulphide mineralisation (Cornell et al., 2006; Bailie, Armstrong and Reid, 2007).

The Richtersveld Subprovince is bounded by the Bushmanland Terrane to the south and the Kakamas Terrane in the north (Figure 2.3). The subprovince is dated at 2000 Ma and consists of low-to-high grade metamorphic supracrustal rocks and intrusions (Cornell et al., 2006). The subprovince consists of the volcanosedimentary sequence of the Orange River Group and intrusions of the Vioosldrift Suite. The Orange River Group predominantly consists of subaerial volcanic rocks and reworked volcanoclastic sediments. The group is divided into the De Hoop and Haib Subgroups, both consisting of volcanic and volcanosedimentary rocks. The Orange River Orogeny deformation and metamorphism event greatly affected the Subprovince. Deformation event D_1 and folding structures $F_1 - F_3$ are evident in the rocks of the Subprovince. A number of plutons of the Vioolsdrift Suite show porphyry-type copper and molybdenum mineralisation in the Haib River and Lorelei areas in Namibia (Cornell et al., 2006; Miller, 2012). Barr and Reid (1992) reported that the Haib deposit is similar to the Okiep copper deposit. The study conducted on hydrothermally altered minerals showed that the alterations were associated with base metal mineralisation (Barr and Reid, 1992).

The area comprising the regional study area-Aggeneys area, outlined in Figure 2.3, is located in the northern parts of the Bushmanland Terrane and south of the Richtersveld Subprovince. The Aggeneys area is largely composed of gneisses and granites including the Aggeneys deposit, with most of the area covered by sand (Figure 2.4).

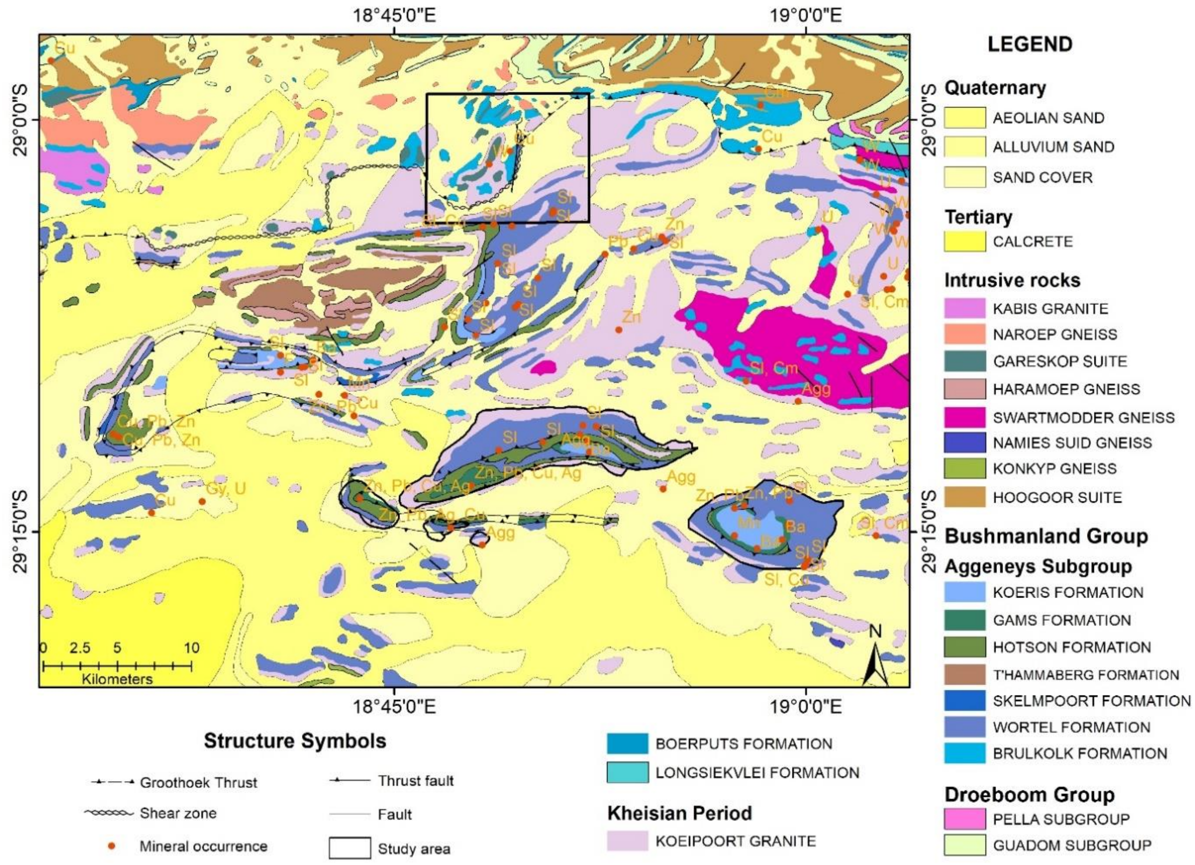

Figure 2.4. An excerpt from the 1:250 000 scale Pofadder and Onseepkans geology map of the Aggeneys area, as published by the Council for Geoscience (2007). The map shows lithological divisions, mapped structures including faults, folds, shear zones and mineral occurrences. The Aggeneys deposit outcrops are outlined by the irregular black boundaries and the Wortel Farm study area falls within the black rectangle.

The Bushmanland Group in the Aggeneys area consists of metavolcanic and metasedimentary rock units showing evidence of overturn and synformal infolds associated with granite gneisses. Sediments are present in the metaquartzite units of the group. The metasediments and metavolcanic rocks were intruded by granitic gneisses that obliterated the pre-existing basement (Bailie et al., 2007; Cornell et al., 2006; Foulkes, 2014).

The continental growth event dated at 1.21 – 0.95 Ga brought with magmatism, tectonism and metamorphism whose evidence is imprinted and observed in the rocks of Aggeneys. Other deformation events mapped across NNMB, classified and observed in the vicinity of Aggeneys are: D_2 defined by plunging folds, thrust and tectonic duplication; D_3 defined by ENE-trending asymmetric folds; D_4 defined by NNW- trending monoclonal folds and D_5 defined by NE-strike slip faults and shear zones (Bailie et al., 2007). The Bushmanland Group is dominated by ENE periclinal folds and E-W shear zones (Bailie et al., 2007; Cornell et al., 2006).

The mineralisation in the Aggeneys area is classified as a world-class economically significant source of lead and zinc in South Africa (Bailie et al., 2007). The Pb-Zn-Cu-Ag Aggeneys orebodies are stratabound in the Gams Formation (also known as the Aggeneys Formation) that consist of quartzite, shale, amphibolite associated with mineralisation and iron formation (Bailie et al., 2007; Cornell et al., 2006; Foulkes, 2014).

The Wortel Farm no. 42 study area, outlined in Figure 2.4 by a black rectangle, is largely covered by the rocks of Aggeneys Subgroup of the Bushmanland Group, Koeipoort Granite of Kheisian Period, intrusions and Quaternary sand. The Aggeneys Subgroup comprises supracrustal sequences dated at 1900 – 1200 Ma. The Wortel and Brulkolk Formations of the Aggeneys Subgroup outcrop on the farm. The Brulkolk Formation consists of medium-grained biotite-gneiss, conglomerate, amphibolite, limestone and muscovite schist. Shale, quartzite muscovite schist and white quartzites comprise the Wortel Formation. The Koeipoort Granite has been classified as a basal unit of the Aggeneys Subgroup and described as pink-weathering and medium-grained granite/gneiss with a NE-fabric (Agenbacht and Oosterhuis, 2013). Agenbacht (2007) describes the geology of the farm as the sheet of mafic rocks overlying the pegmatite-rich Koeipoort Granite/gneiss. The Gareskop Suite is composed of amphibolite dykes, metagabbro and ultramafic rocks and the Naroep Gneiss is described as medium-to-coarse grained leucocratic augen gneiss, both intruding the Koeipoort granite and Brulkolk Formation rocks (Cornell et al., 2006; Agenbacht and Oosterhuis, 2013; Bailie et al., 2007).

2.2 Geophysics

Airborne regional magnetic data of South Africa was acquired between the 1960s and 1990s by various contractors and published by the Council for Geoscience. Flight height ranged between 100 and 500 m, with most surveys maintaining 150 m altitude. Line spacing was on average 1 km apart with a few areas being flown at a significantly narrower or slightly wider line spacing: 250 m in Paalhuis and 1.6 km in Lichtenburg. The full survey specifications for each survey block can be found in the report by Ledwaba et al. (2009). The study area falls in the 22/75 Pofadder-Prieska survey block and the survey specifications are summarised in Table 2.1.

Table 2.1. Summary of survey specifications of the regional aeromagnetic data for the Pofadder – Prieska block.

Items	**Value**
Contractor	AOC Technical Services (Pty) Ltd
Survey date	June – September 1975
Aircraft	Decca Model 72 Doppler
Terrain clearance	~100 m
Line spacing	1 km
Tie line spacing	10 km
Line direction	E – W
Tie line direction	N – S
Aircraft speed	240 km/h
Equipment	Geometric G803 Proton magnetometer
Data recorded	Total Magnetic Field Intensity

The resulting data were gridded at 250 m cell size with an improved on minimum curvature algorithm (Briggs, 1974; Swain, 1976) which interpolates between data points to be gridded by calculating a continuous second horizontal derivative and minimal total squared curvature (Smith and Wessel, 1990) where after a constant mean value of 29578.9 nT was subtracted to highlight higher frequency local magnetic high and low. The resulting magnetic map of the Aggeneys area is presented in Figure 2.5.

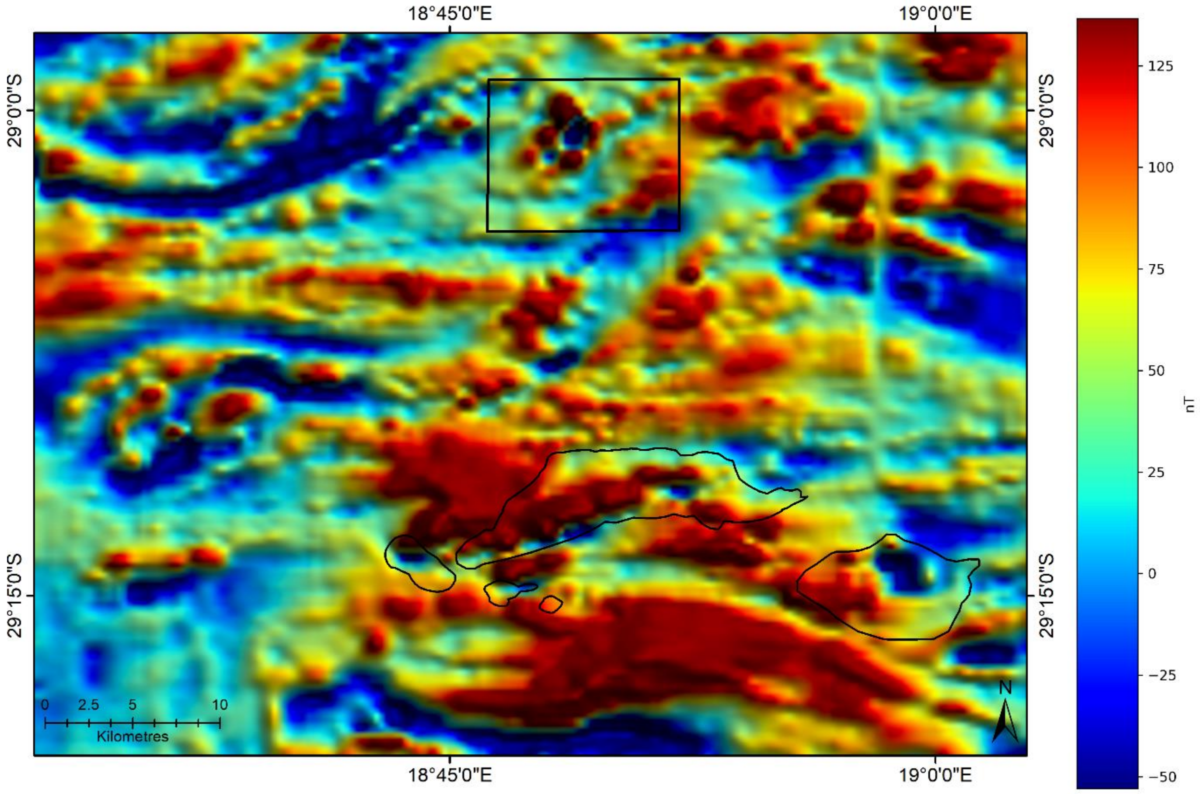

Figure 2.5. Regional magnetic map of the Aggeneys area overlain with the Aggeneys deposit outcrops outlined by the irregular boundary as well as the Wortel Farm study area by the rectangle. The map shows the residual total magnetic field with IGRF(2015) of 29578.9 nT removed, illustrating the magnetic fabric of the area.

The resulting map shows two distinct magnetic responses: magnetic highs or positives (red/magenta colour) and negative magnetic high (blue colour) with respect to the removed regional field. The southern part of the area is characterised by large amplitude positive magnetic signature with intensity of 125 nT, including the Aggeneys base metal deposits. These magnetic anomalies coincide with the magnetite quartzite, amphibolite and gossans of the Bushmanland Group which are possible sources of these anomalies. The northern section magnetic anomalies have shorter wavelengths and some have much lower magnetic intensity (50 nT) by comparison. Most of these short wavelength anomalies coincide with amphibolite and gneisses of the Brulkolk Formation, amphibolite dykes, granite intrusions and metamorphosed intrusions (gneisses). The sources of these anomalies could also due to buried sources. The resolution of this magnetic map is low, especially for the smaller magnetic bodies which obscure effective delineation, characterisation and detailed interpretation of the anomalies. Structures, lineaments and folding are observed to the east and west of the area including north-south and east-west striations correlating with tie line and flight line direction, respectively. The regional data show regional and larger magnetic structures very well.

The Wortel Farm study area, outlined in Figure 2.5 by rectangle, forms part of the high-amplitude short-wavelength anomalies. The intensity of this body reaches 125 nT with a -50 nT field strength signature associated with a remanently magnetized smaller body enclosed within. The amplitude of this body is larger than that of most of the surrounding anomalies, almost matching the intensity of the Aggeneys deposit anomalies. The anomalies on the farm coincides with amphibolite dykes of the Gareskop Suite and amphibolite and gneisses of the Brulkolk Formation. The low resolution of the data makes it difficult to draw conclusive interpretations.

The Council for Geoscience team acquired regional gravity data of South Africa between the 1950s and 2000s through three generations of geophysicists (Stettler and Kleywegt, 2010). The data were mainly acquired using La Coste-Romberg gravimeters and the elevation was measured using micro-barometers, spot heights, trigonometric beacons and global positioning system (GPS). The regional dataset constitutes approximately one gravity measurement per 12 km^2. The measurements were tied to the International Gravity Standardisation Net (IGSN) values and referred to the gravity formula based on the 1967 geodetic reference system. Latitude, Free-air and Bouguer slab corrections were applied to compute values with a mean crustal density of 2670 kg/m^3 using IGSN (1971) prepared by Morelli et al. (1974). The estimated accuracy of the regional data is 1.1 mGal (110 g.u.) and was further terrain corrected using the method as proposed by Kane (1962). The resulting Bouguer anomaly data were gridded at 1000 m cell size with a minimum curvature algorithm as given by Briggs (1974). The resulting Bouguer Anomaly (BA) gravity map of the Aggeneys area is presented in Figure 2.6. High gravity amplitudes bodies are indicated in red/magenta and low gravity amplitudes are depicted in blue.

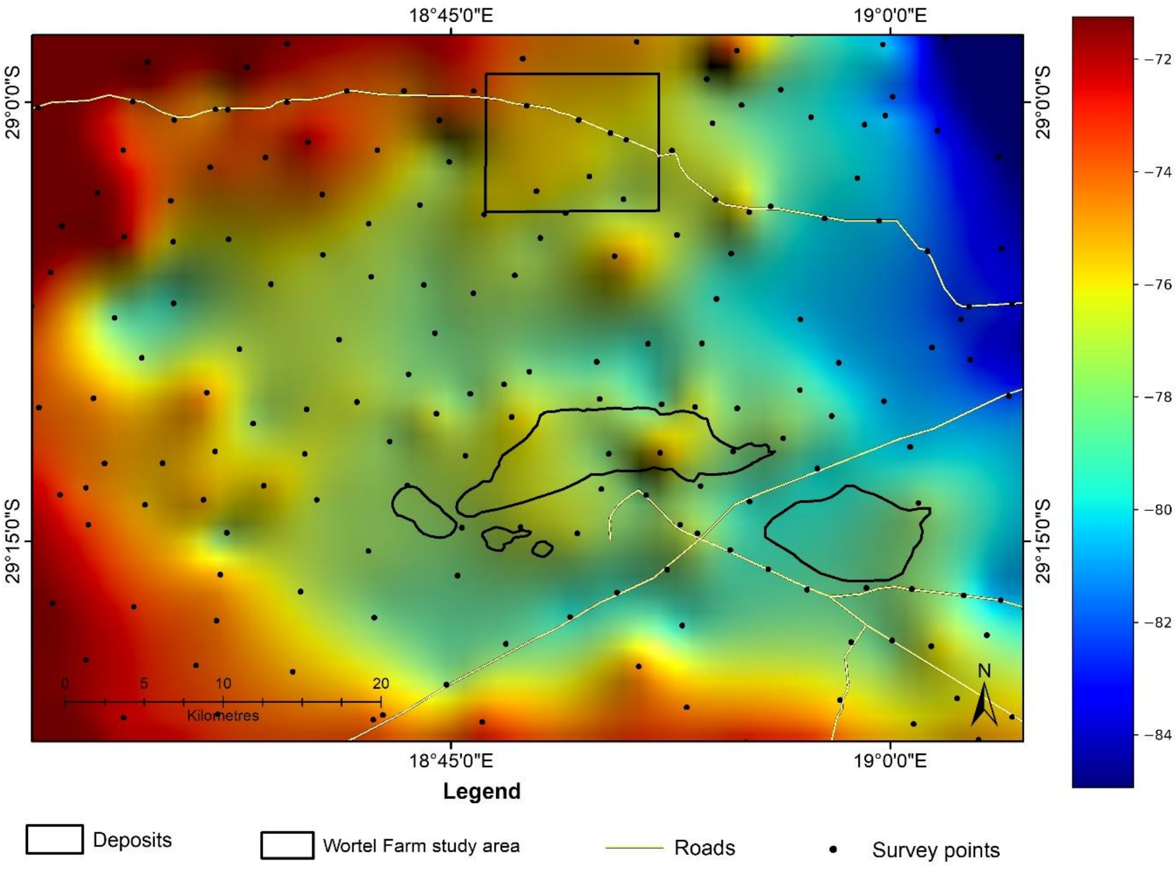

Figure 2.6. Regional Bouguer Anomaly gravity map of the Aggeneys area with inserted Aggeneys deposits outcrops outlined by irregular black boundaries and Wortel Farm study area by black rectangle. The gravity field map shows changes in structures based on gravity variations.

This BA gravity map due to the wide separation of measurement points does not show a lot of detail and most of the anomalies are due to regional features (Figure 2.6). High gravity amplitude bodies are observed in the north, west and south of the area and coinciding with mapped sand cover; shale, quartzite and schist of the Wortel Formation; amphibolite, gneiss and schist of the Brulkolk Formation and granites and gneisses. The central part of the area has lesser gravity intensity (-77 mGal) with few areas with anomalously high Bouguer Anomaly gravity values of -75 mGal BA. Some of the anomalies coincides with parts of the Aggeneys deposits. The rocks to the east of the area carry material with decreased gravity intensity, coinciding with abundant outcrops of the Koeipoort Granite, gneisses, granite intrusion and some sand cover. Since this gravity map attributes to regional gravity variations the high BA anomalies could be due to outcropping amphibolite and gneisses in the west and low BA anomalies in the east due to the dominant outcrops of the Koeipoort granite or undetermined buried sources. The gravity values on the farm gradually increase from the south-east toward north-west, the high BA gravity anomalies could be due to gneisses and amphibolite of the Brulkolk Formation. No further characterisation information can be drawn from this data, a high-resolution data are required.

High resolution airborne magnetic and radiometric data covering most parts of the Namaqua Sector were acquired by the Council for Geoscience (CGS) during year 2013 and 2014, at 200 m line spacing (five times the resolution of the regional data), ca 80 m flight clearance. These datasets were acquired as part of an initiative to conduct detailed mapping of South African geology. Detailed survey specifications are listed in Table 2.2.

Table 2.2. Summary of the survey specifications of the airborne data acquired over parts of the Namaqua Sector.

Items	**Value**
Contractor	CGG
Survey date	December 2013 – June 2014
Aircraft	Cessna C208B fixed wing
Terrain clearance	~80 m
Line spacing	200 m
Tie line spacing	2000 m
Line direction	90°
Tie line direction	0°
Aircraft speed	250 km/h
Equipment	Scintrex CS-3 caesium vapour Exploranium GR-820
Data recorded	Total magnetic field intensity Radiometric (Thorium, Potassium, Uranium and total count)

The airborne data are gridded at 50 m cell size with a minimum curvature algorithm. The resulting magnetic and radiometric maps are shown in Figure 2.7 and Figure 2.8, respectively.

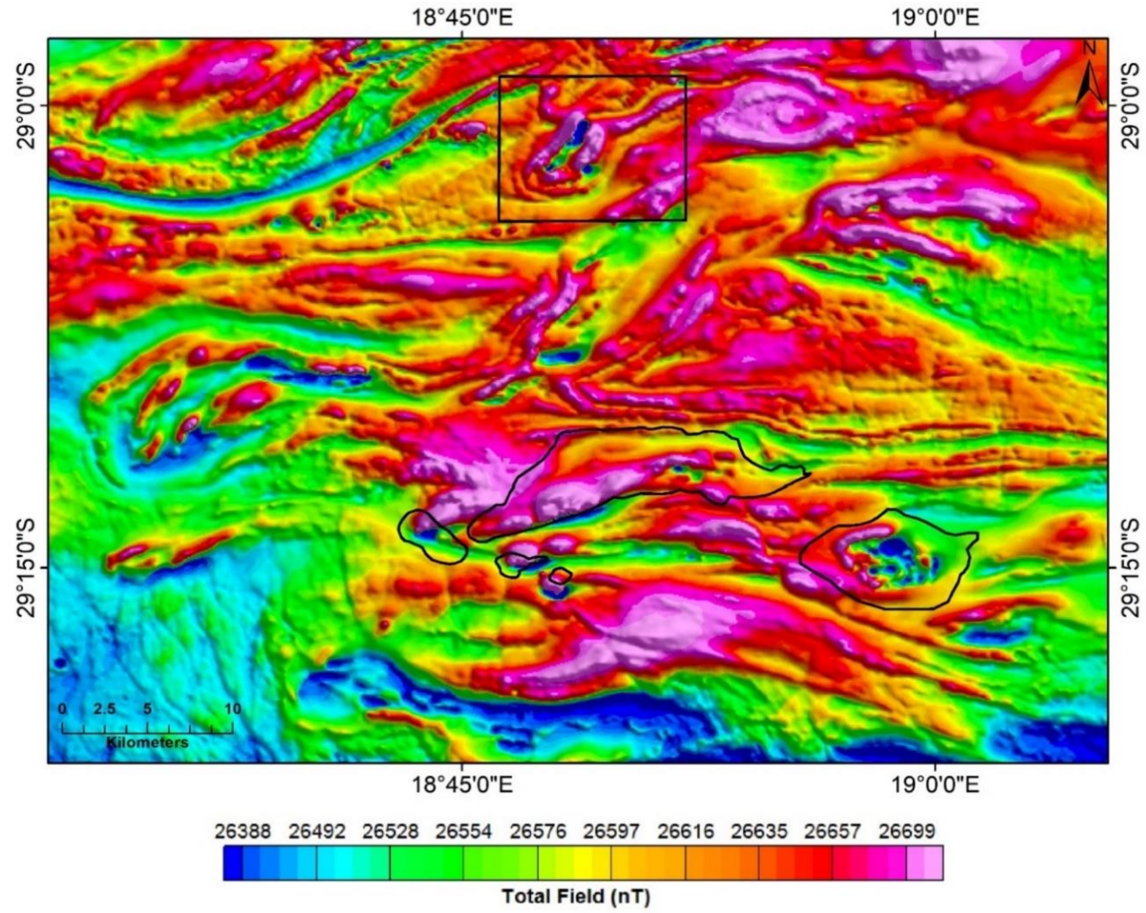

Figure 2.7. Airborne total field magnetic intensity (TMI) map of the Aggeneys area showing the magnetism of the area and much more concise definition of most of the anomalies. Aggeneys deposit outcrops and Wortel Farm study area are outlined by black boundaries.

Table 2.3 lists the international geomagnetic reference field (IGRF) data for the Aggeneys area calculated during the survey (National Oceanic and Atmospheric Administration, 2018).

Table 2.3. IGRF data of the terrane as calculated by the National Centre for Environmental Information.

Item	**Value**
Magnetic intensity	26 655 nT
Inclination	-66.19°
Declination	-19.82°
Latitude	-29.005° S
Longitude	18.812° E
Date	January 2014

The high resolution magnetic map replicates most of magnetic features which are visible on the regional map but much more well-defined than on the regional map (Figure 2.7). The Aggeneys deposits magnetic signature is well defined within its known geological boundaries. The following eye catching magnetic features are also correlated with the 1 km line spacing dataset: 1) high intensity (26700 nT), long wavelength (8 km across) anomalies mapped in the south remained high as seen on the regional magnetic map as well as Aggeneys deposits, 2) magnetised structural lineaments varying in strike length between few meters and kilometres are mapped largely from the centre down toward the south, 3) folded structures at the centre and western part of the area, ranging from few kilometres to 10 km in strike length are observed, 4) E-W and NE-striking bodies are identifiable matching the strike direction of the geologically mapped rocks, and 5) short wavelength smaller anomalies mapped on the regional data in the north section are well mapped and clearly defined on the high resolution data including the Wortel Farm anomalies. The farm anomaly indicated a highly magnetised rock type reaching a magnetic intensity of 26700 nT. This high amplitude anomalies at the centre of the farm encloses the low amplitude anomaly (peak low at 26300 nT).

The Aggeneys area shows much variation in magnetic field strength taken as indicating high concentrations of magnetic minerals that are distributed unevenly. The Aggeneys ore deposits are associated with high amplitude magnetism which is also seen in the Wortel Farm study area and much better defined on the high resolution magnetic data.

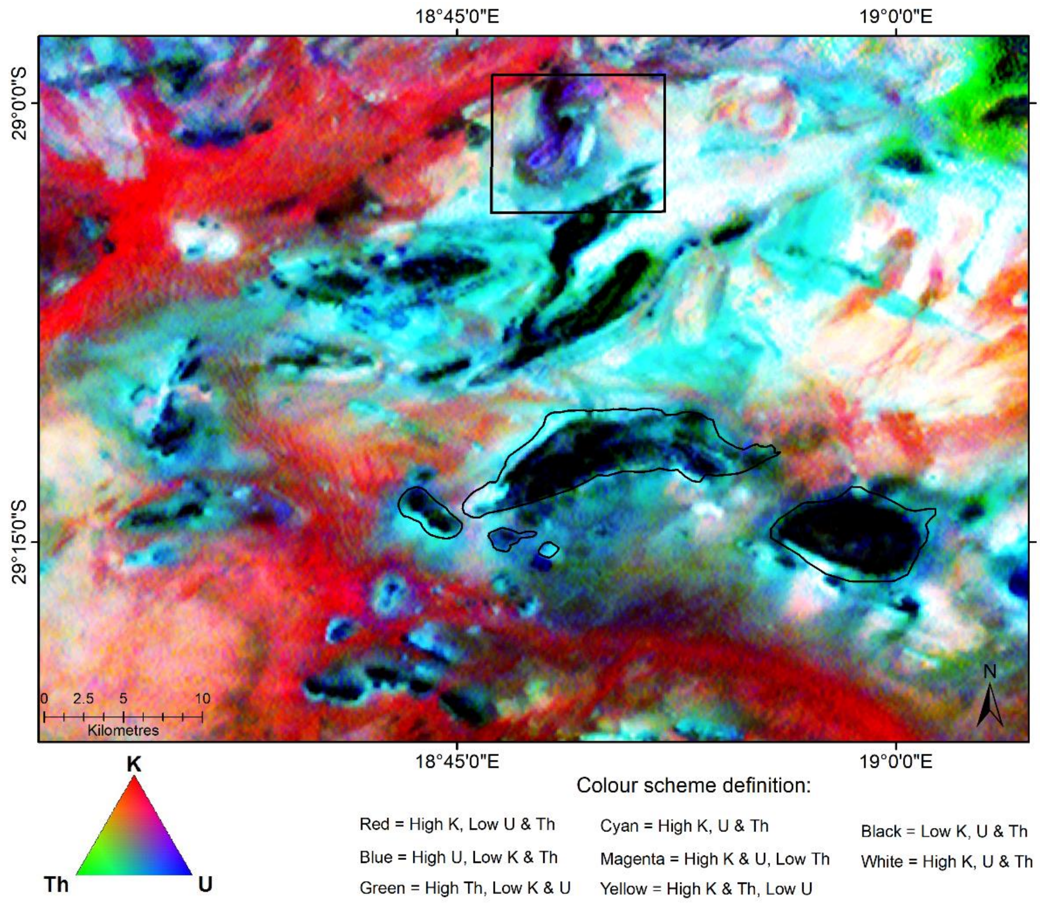

Figure 2.8. Airborne radiometric ternary (K, Th & U distribution) map of the Aggeneys area, showing the ratio distribution of the three elements on the surface. Aggeneys deposits outcrops are outlined by irregular black boundaries and the Wortel Farm study by the black rectangle.

The radiometrics ternary map show the ratio distribution of equivalent potassium (K), thorium (Th) and uranium (U) elements (Figure 2.8). The element concentration are called equivalent (i.e. eK, eU, eTh) because they have not been determined chemically in a laboratory. Few distinct colour schemes are observed on this map: red, cyan to white, green, blue to purple and black. High concentrations of eK (red colour) indicating rocks with a granitic or gneissic composition with abundant feldspar (Erdi-Krausz et al., 2003) are largely concentrated in the NW and southern parts of the area. Minor traces of eK are also mapped in the SE corner. The NE sections shows elevated concentrations of eTh and surrounding areas with little trace elements marked in black, are associated with rocks of mafic and ultra-mafic composition (Erdi-Krausz et al., 2003). The black anomalies are widely spread throughout the area. Elevated concentrations of eU and eTh, marked by cyan colour, are mapped in the west-central area and traces to the east. To the east and north east the eK concentrations increases mixing with the eTh and eU elements. The eastern part of the area shows a mixture of high eK elements surrounding an area with all three elements. Minor trace of eU are seen throughout the area. The northern part of the area has a slightly elevated concentration of eU including the study area. The Wortel Farm carries traces of all three elements. The south section has high concentrations of eU and eTh. Toward the north the eK element concentration increases. The central area is largely concentrated with eU with some sections having little trace elements.

The data presented here show that Namaqua Sector and the Aggeneys area, especially, are a geologically and structurally complex region hosting different types of mineralisation where the Aggeneys ore deposits are amongst the largest economical deposits. Similar lithologies as at Aggeneys, of the Bushmanland Group, were identified geologically on the Wortel Farm, showing only minor difference that is a missing Gams Formation, however with similar magnetic intensities.

The data presented further in this manuscript will provide a deeper understanding of the geological framework of the Wortel Farm (and some parts of the Aggeneys area). The airborne geophysical data that mapped the subsurface, its interpretation will be linked to the geologically mapped lithologies and various structures to determine correlations and possible physical properties sources. The airborne datasets together with the geological maps were integrated to aid the survey planning for the ground follow-up and to determine which geophysical methods should be chosen to most effectively address the objectives that area: better understanding of the local geology, determine the possible source of the minerals and their potential. The chosen methods, survey parameters, processing techniques and results are briefly discussed in Chapter 3.

Chapter 3: Geophysical and Geochemical Data

This chapter presents the geoscientific data acquired during the course of the study, briefly describing the theory of each method employed, survey parameters, processing schemes implemented and output maps. The geophysical methods employed are: induced polarization (IP), direct current (DC) resistivity, gravity, magnetotelluric (MT) and palaeomagnetic methods. All ground geophysical datasets were acquired by myself assisted by the CGS geophysics staff. The palaeomagnetic core samples were drilled in the field and analysed by the petrophysical laboratory personnel of the CGS. The geochemical data presented were acquired, analysed and gridded by the Geochemistry Department of the CGS.

At the commencement of the project, only airborne (regional and high resolution) magnetic (Figure 2.5 and Figure 2.7), regional gravity (Figure 2.6) and radiometric (Figure 2.8) datasets were available. Using the magnetic intensity map for the Wortel Farm study area as the reference and guide on the ground follow-up, a reconnaissance survey was in order. Despite the available data, the study area remained vast. A reconnaissance survey will assist in identifying focal areas for detailed ground follow-up. The mapped copper and tungsten mineral occurrences on the farm combined with verified base metal deposits of Aggeneys (Cornell et al., 2006; de Beer, 2015), the electrical methods were recommended and employed. The electrical geophysical methods are traditionally employed for base metal reconnaissance studies because of their ability to directly detect anomalous base metal targets, perceived low cost, speed and application success on base metal studies (Dentith and Mudge, 2014a). The IP (which maps chargeability of the ground) and DC resistivity (which maps resistivity/conductivity of the ground) electrical methods were employed here for reconnaissance following the basis that the sulphide minerals within a rock increases the electrode polarization thus making a rock very chargeable. Disseminated and massive sulphides produces a good induced polarization response as well as clay minerals. The resistivity method generally complement the IP method in mineral exploration surveys (Airo, 2015; Dentith and Mudge, 2014a) and provides structural set-up of-and-around chargeable materials.

The gravity method was selected because of its ability to map density variations due to lithology variations, structural features such as faults and folds and some deep geological structures which, in this project, could help elucidate the sources of the magnetic, chargeability and resistivity anomalies. The profiling resistivity method (electrical resistivity tomography (ERT)) is able to provide a detailed section map of resistivity variations at fairly limited depth from which geological structures can be inferred (including depth to bedrock). The MT method was chosen for its superior depth mapping ability of conductivity structures from which more geological structures can be inferred. A palaeomagnetic study was conducted to understand the source of the magnetism mapped on the farm. The data and its interpretation are then integrated to help understand the geological layout on the farm while possibly identifying areas of mineralisation.

Due to the complexity of the Namaqua region (Colliston and Schoch, 2013; Cornell et al., 2006) three MT datasets (two controlled source audio-MT (CSAMT) and one AMT) were acquired. The shallower CSAMT is to provide local geological structural details for the top few hundred of meter of the subsurface. The AMT data will provide regional structural set-up for few kilometres of depth. Acquired along the same traverse is a relatively deeper CSAMT data acquired to provide detail of the top 1 km of the subsurface for the AMT data. The combination of ERT (very shallow), CSAMT and AMT (regional and deeper) will provide a geological structural overview of the farm from smaller to a farm regional scale and relation to the mineralisation.

3.1. Electrical Methods: DC Resistivity and Induced Polarization Methods

The DC resistivity method uses an artificial current source that is introduced into the ground through points of electrodes inserted into the ground along a profile. The potential difference is measured between two other electrodes along the profile (Figure 3.1). The injected current (*I*) and resulting potential difference (ΔV) are recorded in order to determine the apparent resistivity (ρ_a) of the subsurface (Telford et al., 1990).

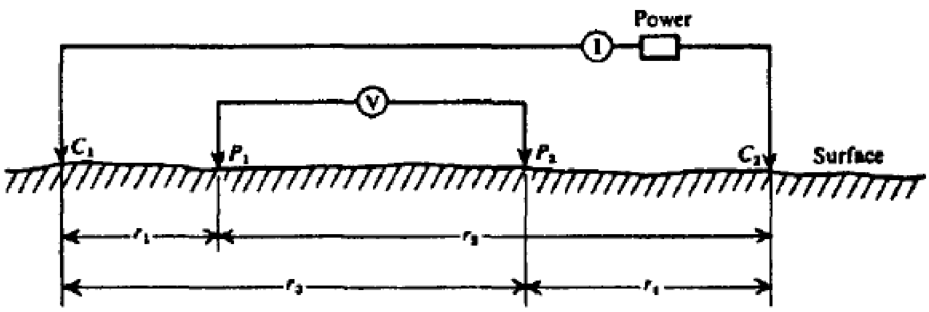

Figure 3.1. Ground DC resistivity setup of two current electrodes and two potential electrodes (Telford et al., 1990), where *C* are current inducing electrodes and *P* are potential difference electrodes.

The subsurface resistivity (*ρ)* of the setup shown in Figure 3.1 where there are four electrodes deployed at a certain distance (*r), is* given by equation 1 determined from Ohm's Law

$$\rho = \frac{2\pi \Delta V}{I} \left\{ \frac{1}{\left(\frac{1}{r_1} - \frac{1}{r_2}\right) - \left(\frac{1}{r_3} - \frac{1}{r_4}\right)} \right\} \qquad 1$$

Where the potential at P_1 due to C_1 is

$$V_1 = -A_1 / r_1 \text{ and } A_1 = -I\rho / 2\pi \qquad 2$$

Similarly for the potential at P_1 due to C_2 is

$$V_2 = -A_2 / r_2 \text{ and } A_2 = I\rho / 2\pi = -A_1 \qquad 3$$

Then adding $V_1 \, and \, V_2$ and introducing a second potential electrode, the resistivity between two current and potential electrodes is as illustrated in equation 1. In a homogeneous surface, if the current is kept constant, the ground resistivity will remain constant. The Earth's surface is inhomogeneous causing the values of resistivity to vary such that the resulting resistivity is an apparent resistivity ρ_a (Dentith and Mudge, 2014b; Telford et al., 1990).

The resistivity method is used to study horizontal and vertical discontinuities in the electrical properties of the ground. The resistivity of the rock is governed by porosity, weathering, metallic content of solid matrix, moisture content and mineral distribution in a rock. These effects can result in the resistivity of one rock type to vary greatly so that lithology cannot be determined readily just from the apparent resistivity values alone. Through the successful application of the resistivity method over the years electric properties of some rocks have been published (Figure 3.2) (Kearey and Brooks, 1991; Telford et al., 1976) and there is a considerable overlap between rock types.

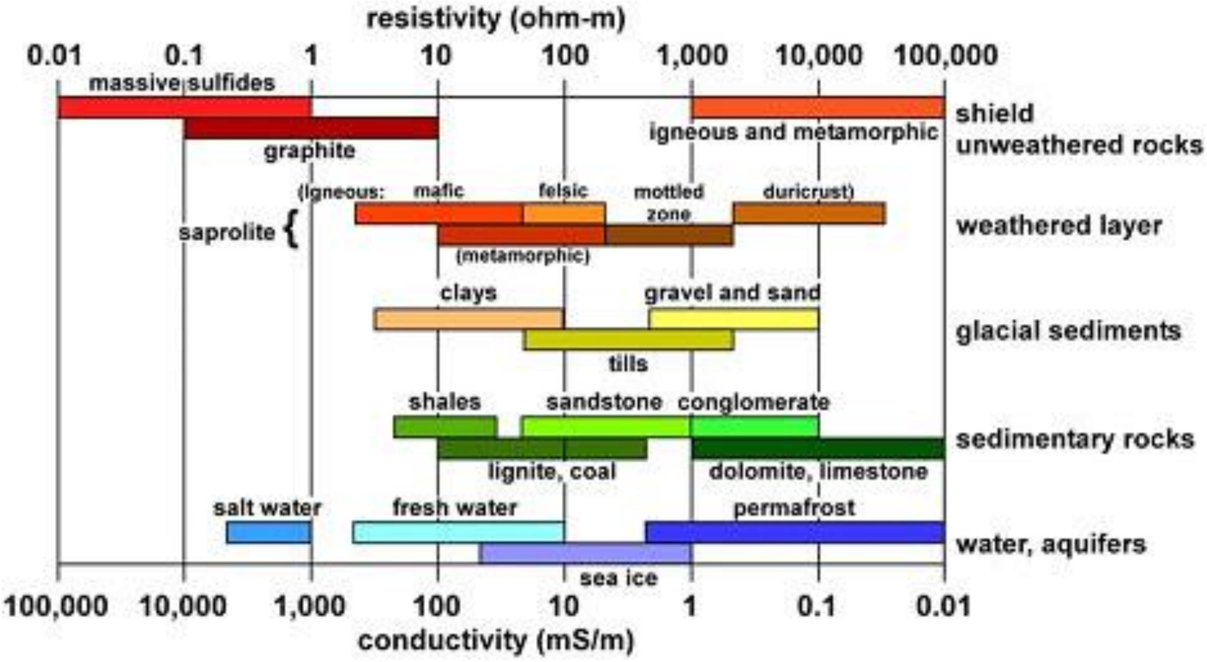

Figure 3.2. Electrical resistivity and conductivity values of some Earth material that have been recorded in literature over the years (Palacky, 1988).

The induced polarization (IP) method is very similar to the resistivity method, it uses an artificial current source as well to measure the chargeability of rocks. The ground setup is similar to that of the DC resistivity method. IP differs from the resistivity method in that it measures the response in voltage as a function of time after the current is switched on or off (Figure 3.3). The voltage decay can last from several seconds to minutes (Kearey et al., 2002).

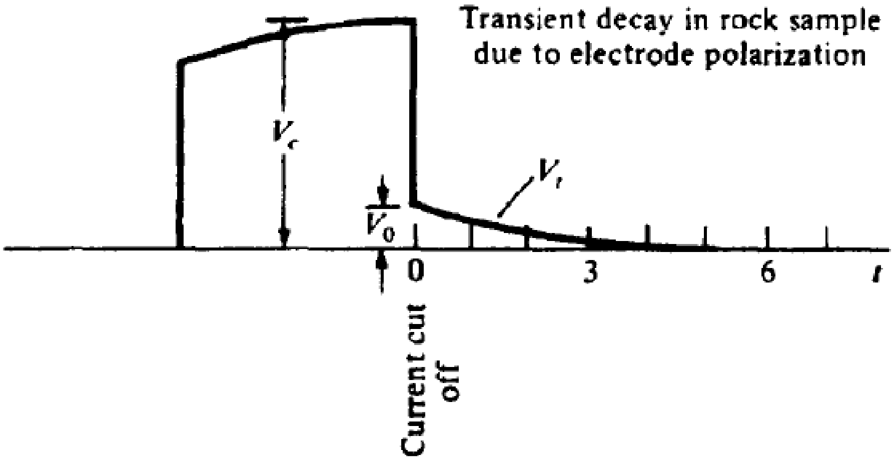

Figure 3.3. A graphical display of the potential behaviour when the current is switched on and then off over time (Telford et al., 1990).

With reference to Figure 3.3, chargeability is defined as:

$$M = \frac{1}{V_c}\int_{t_1}^{t_2} V(t)dt \qquad 4$$

Where *V(t)* is the time dependent voltage and V_c is the peak voltage. Chargeability has units of millivolt per volt (mV/V). This parameter depends on the electrical properties of rocks and experimental set up (Telford et al., 1990). Similarly to the electrical resistivity method, IP readings are also affected by porosity, weathering, moisture content, metallic content of solid matrix and texture of the rock (Figure 3.2). The IP method has been found valuable for detection of disseminated sulphides (Airo, 2015).

The IP and DC resistivity datasets were collected using the IRIS Elrec 6 receiver and IRIS VIP4000 transmitter. The receiver is a 6-channel unit (in-taking 7 electrodes including the ground) that measures chargeability and resistivity datasets concurrently. The receiver automatically synchronises with the transmitter signal ensuring high measurement repeatability. The receiver has been integrated with power line rejection and self-potential drift correction as well as quality control. It has an impedance of 100 MΩ and 1 µV accuracy. The transmitter is designed to continuously inject constant DC current onto the ground and can be set for both frequency and time domain surveys, outputting up to 4 kW of power with accuracy of 1 mA. The pulse duration ranges between 500 m.sec – 8 sec.(IRIS Instruments, 2003a, 2003b).

The survey lines position, orientation and length were chosen according to the high amplitude magnetic anomaly on the farm and mapped geology (Figure 3.4). The stainless steel electrodes and copper wires were used for both transmitter and receiver. The transmitter was set to output 1.5 – 2 A current over a 6 km long cable (Figure 3.4). The chargeability and resistivity were measured with the gradient array. The gradient array maps near surface changes in resistivity while keeping the current constant (Telford et al., 1990). The electrodes were 50 m apart, survey lines were ±2 km long, approximately 400 m apart and orientated in the NW-SE direction (Figure 3.4). An overlap of 50 m was implemented for each roll-along. The survey parameters are summarised in Table 3.1.

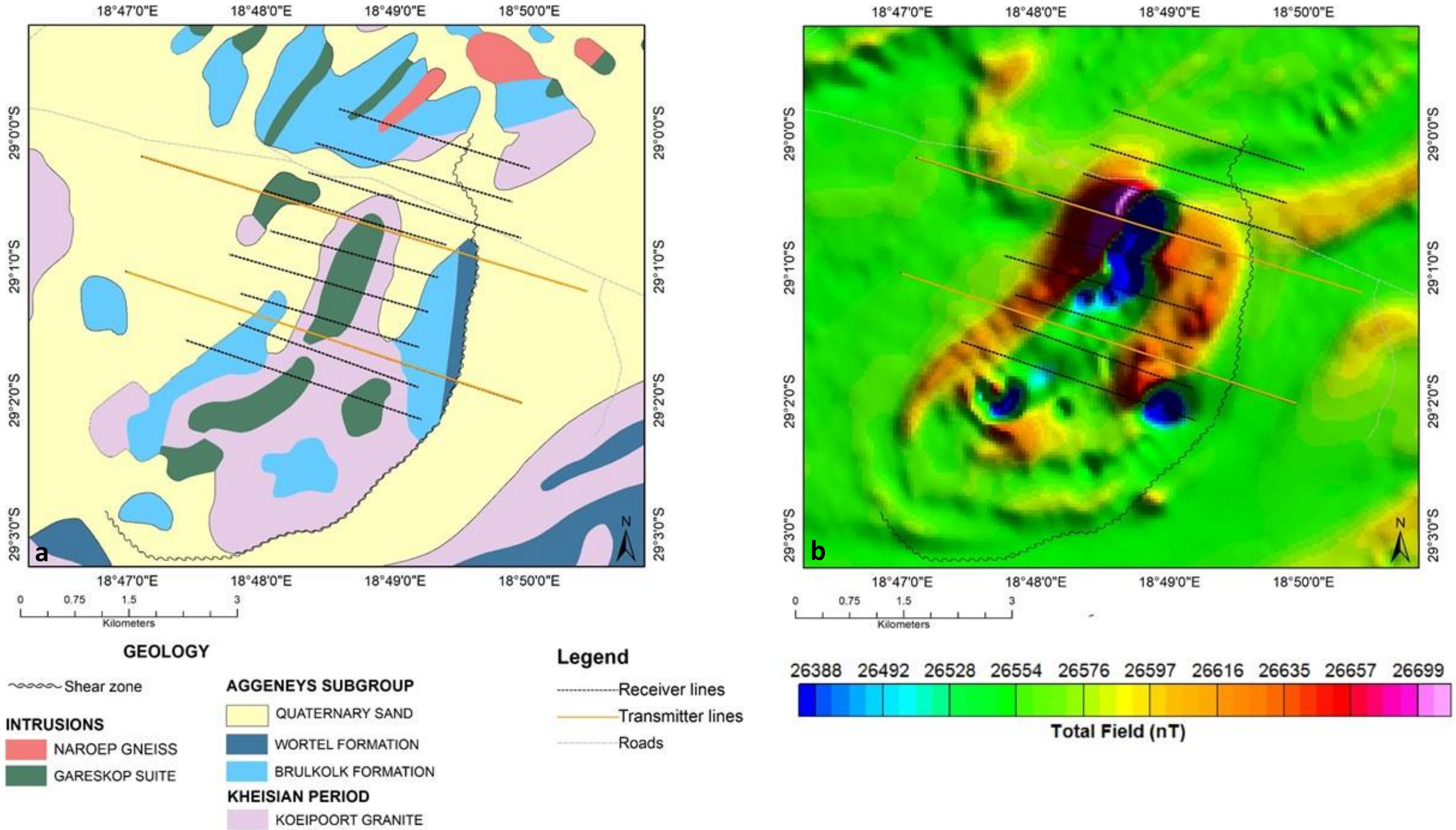

Figure 3.4. a) An excerpt from the 1:250 000 scale Pofadder geology map of the Wortel Farm study area, as published by Council for Geoscience (2007) and b) a total magnetic field map of the study area, both overlaid with the IP and DC resistivity survey grid.

Table 3.1. Summary of survey specifications for the DC resistivity and IP surveys.

Induced Polarization & DC Resistivity Methods	
Item	**Value**
Instrumentation	IRIS Elrec 6 receiver VIP4000 transmitter
Receiver electrode spacing	50 m
Spread overlap	50 m
Line spacing	400 m
Transmitted current	1.5 – 2 A
Array	Gradient

The reconnaissance raw data was pre-processed manually to remove outliers and obvious bad points. The resulting datasets are gridded at 100 m cell size with minimum curvature algorithm which interpolates data to be gridded by calculating continuous second derivatives and minimal total squared curvature along surface to produce an optimally smooth surface (Smith and Wessel, 1990). The algorithm was ran on the Oasis Montaj Geosoft software as well as editing of the data was also done in Geosoft. The resulting IP (Figure 3.5) and resistivity (Figure 3.6) maps are presented below.

The IP map shows lateral chargeability distributions on the farm (Figure 3.5) with the longer wavelength anomaly spatially constrained to the centre of the area and striking N-S. Within the anomaly are two areas with higher chargeability intensity (11 mV/V), one to the south and the other to the north with dimensions that are at least 500 m x 250 m. The concentration of chargeable material decreases considerable to the east, west and south-west. Further analyses, correlation and interpretation are presented in Chapter 4.

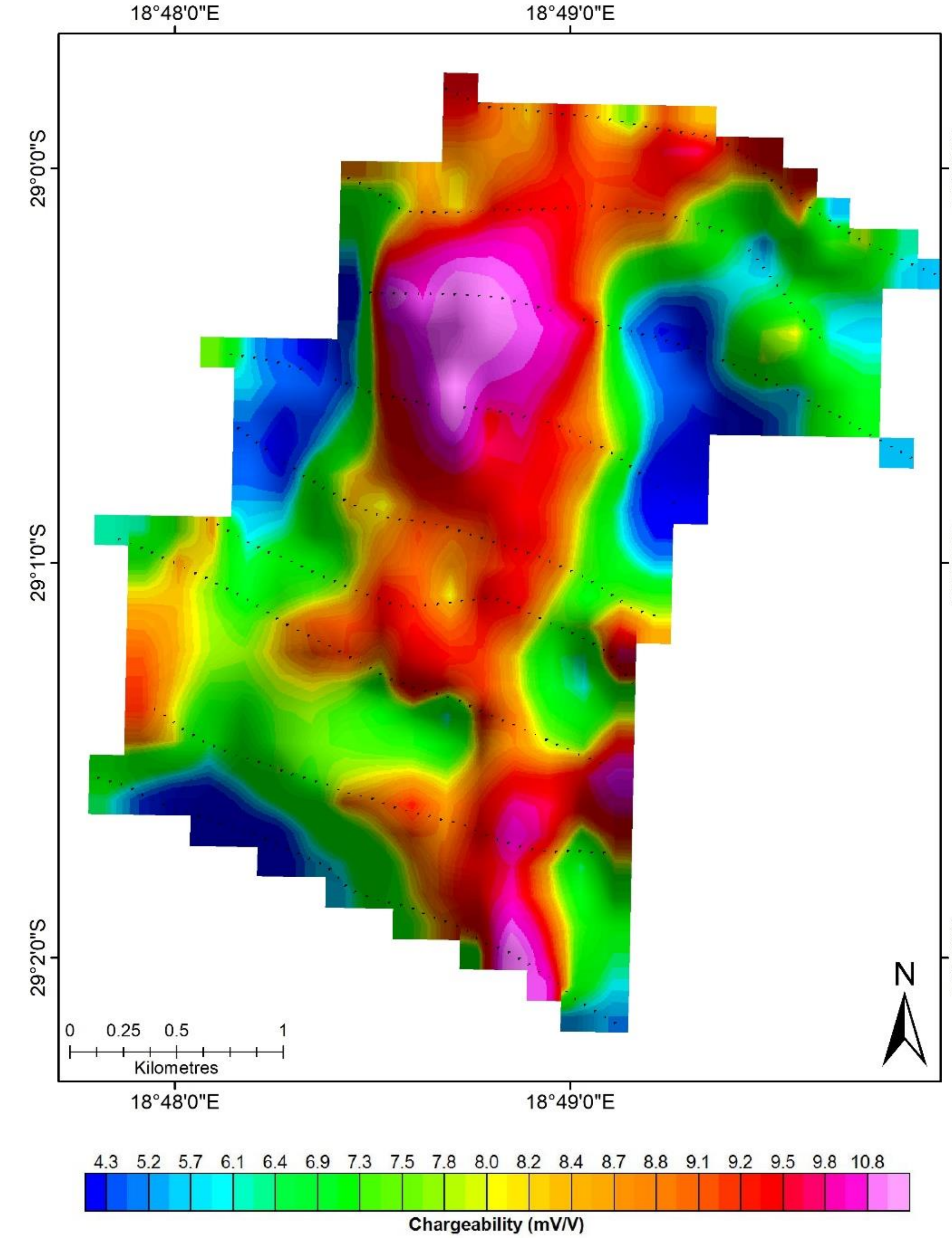

Figure 3.5. Chargeability map derived from the IP data, showing the distribution of the chargeable material on the farm. The dotted lines represents electrode location during acquisition.

The DC resistivity map shows that the rocks resistivities ranges from at least 2 kOhm.m to 15 kOhm.m (Figure 3.6). The high amplitude resistivities are spatially confined to the centre of the area striking in the N-S direction, similar to the chargeability anomalies, over a 4 km length and width of few meters to over 1 km. Areas with higher resistivity intensities are mapped in the south, lower west and toward north with 14 kOhm.m resistivities. These anomalies are elongated to forming a lineament. The lower resistivities are mainly confined to the east, west and south-western boundaries of the area.

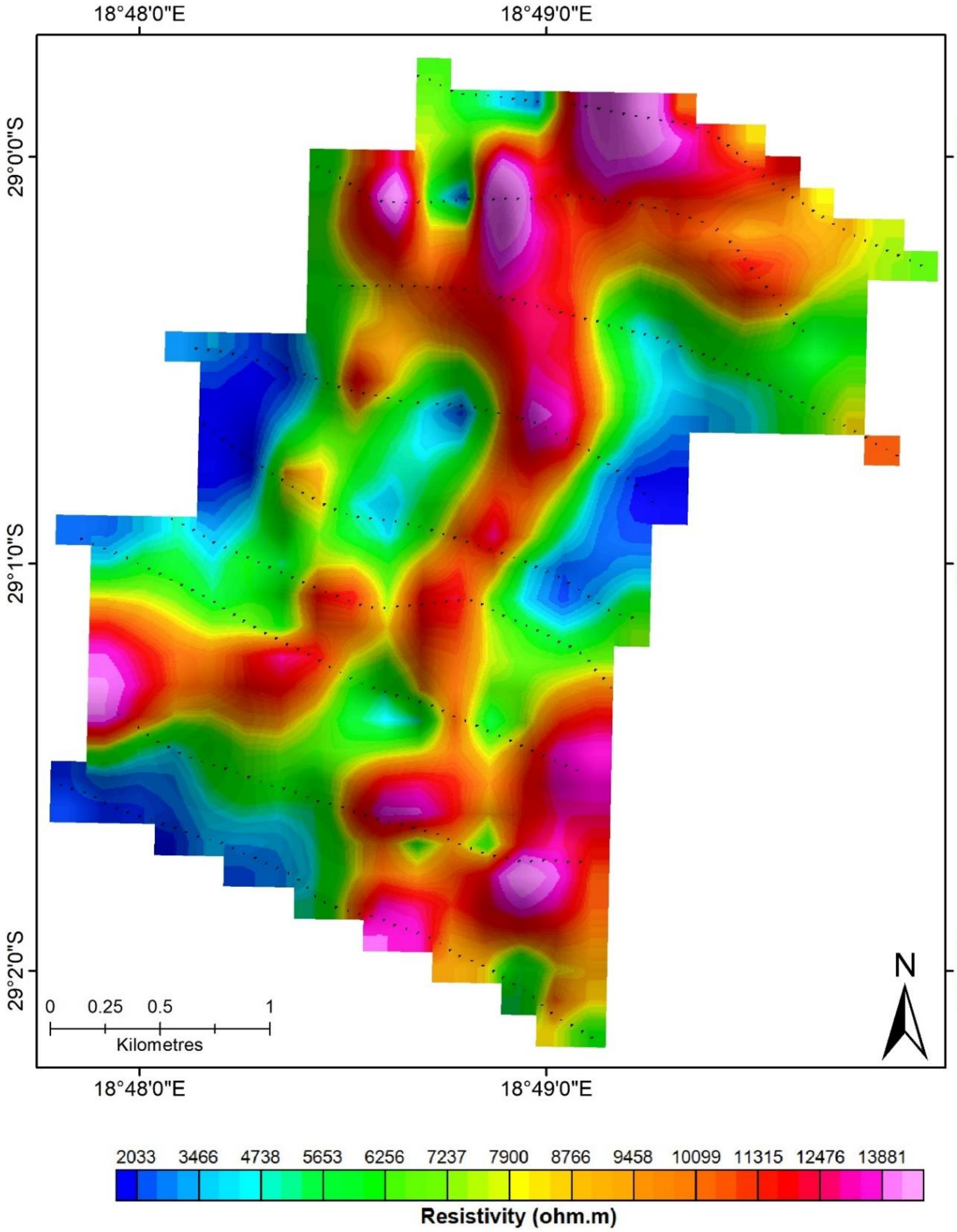

Figure 3.6. DC resistivity map of parts of the study area acquired along the same lines of the IP data. The dotted lines represents electrodes location during acquisition.

The resulting IP and resistivity data together with terrain data and access were used to further guide the ground follow-up surveys (Figure 3.7).

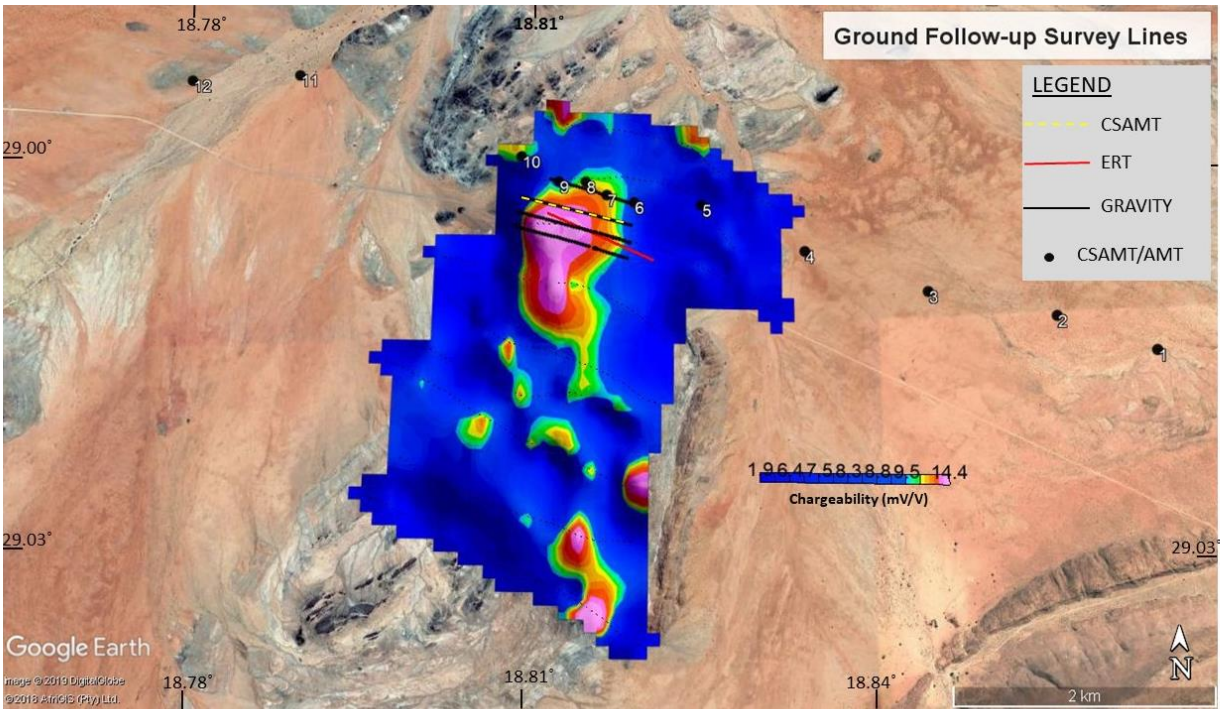

Figure 3.7. Google Earth terrain map of the study area overlaid with chargeability (IP) shaded map and survey lines for gravity (black), ERT (red) and MT lines (dashed yellow and labelled stations) as guided by the chargeability, resistivity, topography and access datasets (Google Earth, 2018a).

The ERT DC data were acquired with the IRIS Syscal Pro 10-channel receiver that can take up to 72 electrodes. This instrumentation is an all-in-one multimode resistivity meter with an inbuilt 250 W internal transmitter. The receiver can measures self-potential (SP) and resistivity soundings, profiling 2D and 3D data. For this survey the receiver was used to acquire profiling data. A power line rejection and SP linear drift correction are integrated in the instrument. The receiver has a pulse duration of 250 msec – 8 sec. The transmitter can inject current between 0 - 2500 mA. This instrumentation has an input impedance of 100 MΩ and accuracy of 1 µV. The instrumentation supports various survey arrays (IRIS Instruments, 2003c).

The ERT profile covers part of the IP anomaly (Figure 3.7) and coincides with mapped sand cover on the geology map (Figure 3.8). The electrodes were 10 m apart covering 360 m distance per spread. A 90 m roll-along was implemented to achieve a good overlap and repeatability. A total of 1.1 km profile was mapped. The data were acquired using the Schlumberger array which fixes the potential electrodes while moving the current electrodes further apart, allowing deeper penetration. This array allows for efficient acquisition, improved spatial resolution and greater depth sensitivity (Parasnis, 1979; Telford et al., 1990). Stainless steel electrodes were used. Survey parameters are summarised in Table 3.2.

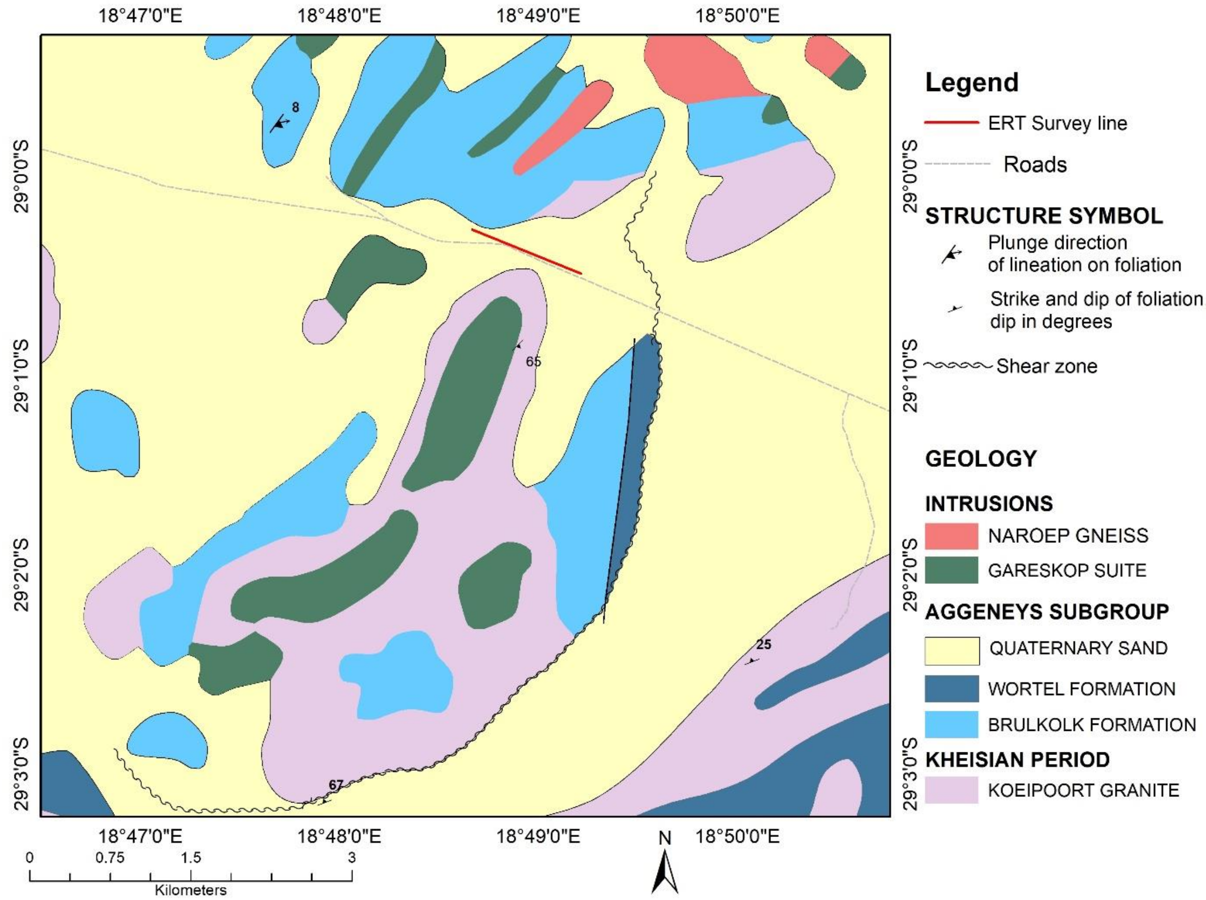

Figure 3.8. An excerpt from the 1:250 000 scale Pofadder geology map of the Wortel Farm study area, as published by Council for Geoscience (2007), overlain with the ERT survey line.

Table 3.2. Summary of the survey specifications for the ERT survey.

Electrical Resistivity Tomography Method	
Item	**Value**
Instrumentation	IRIS Syscal Pro
Electrode spacing	10 m
Roll along	90 m
Array	Schlumberger

The ERT data were pre-processed to remove outliers and obvious bad points. The resulting data are inverted using a smoothness-constrained least-square inversion technique which determines the best fit to the data by minimizing the difference between measured and calculated data (Loke et al., 2003; Sasaki, 1992). The algorithm is based off the equation:

$$(J^T J + \mu F)d = J^T g \qquad 5$$

where *F* is the sum of horizontal and vertical flatness filters, *J* is the matrix of partial derivatives, μ *is* the damping factor*, d* is the model perturbation vector and *g* the discrepancy vector. To achieve the minimal difference measured in root mean square (RMS) the inversion is reiterated. For this study the inversion was initially set at 10 iterations and converged at 10% RMS error in 4 iterations. The RMS (minimal difference) is calculated with equation:

$$RMS = \sqrt{\frac{1}{n}\sum_{i=1}^{n}(\rho_c - \rho_m)^2} \quad 6$$

where ρ_c is the calculated apparent resistivity, ρ_m is the measured apparent resistivity and *n* the number of data points. The data are inverted with IRIS inversion software RES2DINV and resulting depth section is presented in Figure 3.9**.**

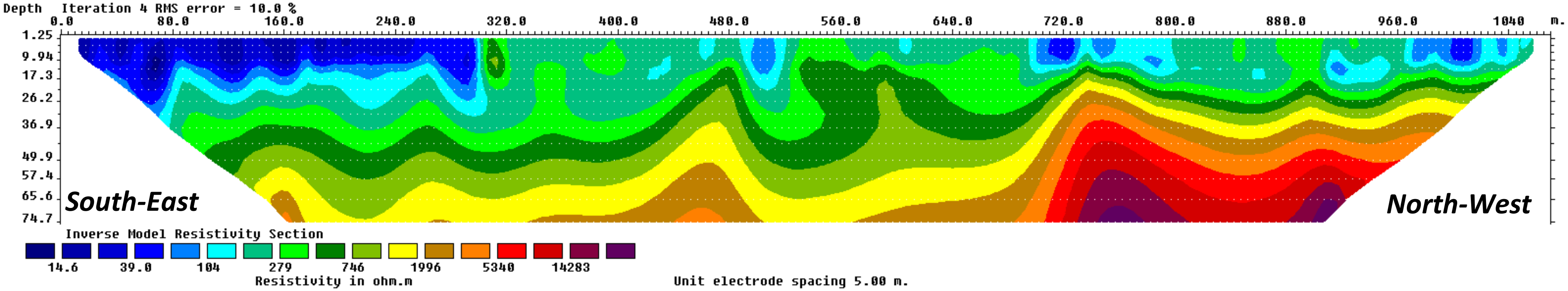

Figure 3.9. 2D ERT inversion cross section map measured near the gravity survey line and over the northern part of the chargeability anomaly.

The ERT inversion map showed resistivity features up to a 75 m depth, a general increase from less resistive (more conductive) material at surface and increasing in resistivity with depth, and revealing structural variation laterally and with depth (Figure 3.9). The top layer is conductive showing low resistivity values (14 ohm.m) to the south-east and increasing resistivity to the north-west (10-300 ohm.m). This conductive layer is approximately 10 – 30 m thick. Below this is a slightly more resistive layers that show undulation. At distance 720 - 1040 m along the traverse the highly resistive structure is interpreted to be uplifted while at 0 - 720 m distance the same or similar structure is mapped deeper, extending from 35 m to 75 m depth.

3.2. Potential Fields: Gravity Method

Gravity method is a natural source technique that measures small variations in the Earth's gravitational field. This method measures gravity field due to the rocks from surface downwards using a highly sensitive instrumentation. The measured gravity field is interpreted as due to density variations associated with lithology and geological structures. The principle of this method is based on Newton's law for gravitational theory, given by

$$F = -G\frac{m_1 m_2}{r^2}\hat{r} \qquad 7$$

where *F* is the gravitational force between two masses m_1 and m_2 separated by distance *r* and *G* is the gravitational constant (6.670 x10^{-11} $m^3/kg.s^2$). Then acceleration of m_2 due to m_1 is

$$g = \frac{F}{m_2} = -G\frac{m_1}{r^2}\hat{r} \qquad 8$$

where g is the acceleration of gravity and m_1 is the mass of the Earth. The gravitational field is measured in gravity work and has units of acceleration ($cm.s^{-2} = gal$). The gal is too large a unit in exploration so milligal (mgal) or gravity units (gu) are commonly used, where 1 mgal = 10 gu (Telford et al., 1990). The Earth's surface gravity mean value is approximately 9.8 m/s^2. The variations in the gravity caused by density variation, shape of the source and depth to source in the subsurface are of the order of 0.01 mGal (Kearey et al., 2002; Telford et al., 1990).

The gravity data was acquired using the Geometrix Scintrex CG-5 automated gravity meter that senses the position of the test mass by a capacitive displacement transducer. The feedback circuit applies DC voltage to the capacitor plates producing an electrostatic force due to the mass. The relative value of gravity at a reading site is measured by the feedback voltage which is then converted into a relative gravitational attraction at that point. The gravimeter readings has a resolution of 0.001 mGal, 0.005 mGal standard deviation and 0.02 mGal/day drift and equipped with an inbuilt radio frequency remote that helps maintain instrument stability after levelling (Scintrex Limited, 2012). A GPS accompanied the gravimeter and measured position and elevation at the same gravity survey point to attain an accurate elevation data for the free-air and Bouguer gravity corrections. A Trimble differential GPS (DGPS) was used in this survey. The DGPS consist of two components: the rover R10 and base R8. These unit connects with each other via Bluetooth and radio frequencies while also connected to multiple satellite to increase the measurements precision. The Trimble DGPS has less than 1 mm precision in a 1 Hz bandwidth, spatially measuring accurately to the nearest centimetre (Trimble Geospatial, 2018; Trimble Navigation Limited, 2008). The measured gravity stations were tied into the National Gravity Base Station Network of the Council for Geoscience, namely the Pofadder (POFA) and CGS (SIL1) gravity bases, located in Pofadder town CGS headquater – Pretoria, respectively (CGS, 2019a).

The station spacing was 25 m apart for both gravity and DGPS and approximately at a 100 m line spacing interval (Figure 3.10). The two instruments (gravimeter and DGPS) acquired data following each other to assure the measurements are taken at the same point. Survey specifications are summarised in Table 3.3.

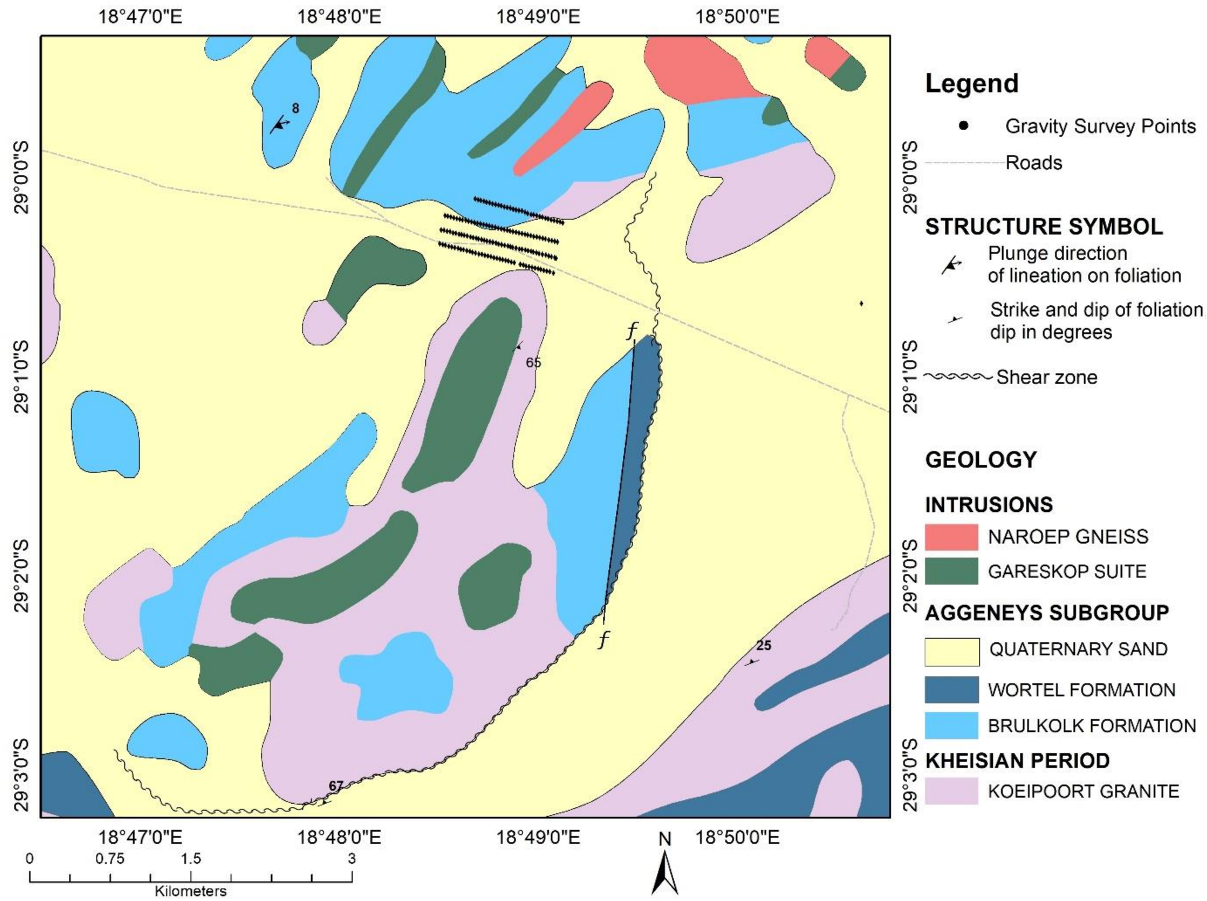

Figure 3.10. An excerpt from the 1:250 000 scale Pofadder geology map of the Wortel Farm study area, as published by Council for Geoscience (2007), overlaid with the gravity and DGPS survey grid. The gravity survey grid follows the northern parts of the IP anomaly.

Table 3.3. Summary of survey specifications for the gravity survey.

Gravity Method	
Item	**Value**
Instrumentation	Geomatrix Scintrex CG-5 Trimble DGPS R10 & R8
Station spacing	25 m
Line spacing	100 m

The measured gravity value at the point is influenced by other attractions that as a result processing schemes were developed to reduce the effect of these attraction on a surveyed station. The following reductions were applied to the gravitational measured data: drift, latitude, atmosphere, free-air and Bouguer corrections. The temperature and/or pressure changes experienced during the survey or over time tend to cause instrument drift that may affect the mechanics of the instruments (Dentith and Mudge, 2014a; Kearey et al., 2002). The drift is corrected by repeating readings at the base station and other noted points at recorded times throughout the day. 5% of survey points were repeated each day, including the base station. The repeated readings were plotted against time and the difference between the base values and repeated point is subtracted from the observed value.

The latitude correction removes the effect of an elliptic Earth that causes the gravity to decrease from the poles to equator including a mass and rotation effect (Hinze et al., 2005; Parasnis, 1979). The 1980 Geodetic Reference System (GRS80) (Vajda and Panisova, 2005) is the latest ellipsoid recommended by the International Union of Geodesy and Geophysics, and the theoretical gravity g_T-value on this ellipsoid at latitude φ is

$$g_T = \frac{g_e(1+ksin^2\varphi)}{\sqrt{(1-e^2sin^2\varphi)}} \qquad 9$$

where the g_e is the gravity value at the equator ($g_e = 978032.67715$ mGal), *e* is eccentricity (e^2 = 0.0066943800299) and *k* = 0.001931851353. The resulting g_T is subtracted from the drift corrected gravitational data (Hinze et al., 2005; Moritz, 1980).

The atmosphere correction removes the effect of the mass above a station with the equation

$$\delta_{g_{atm}} = 0.874 - 9.9x10^{-5}h + 3.356x10^{-9}h \qquad 10$$

where the atmospheric effect is in mGal, *h* is the height of the station relative to the GRS80 in meters and the correction is subtracted from the absolute g_T value (Hinze et al., 2005; Tenzer et al., 2010).

The free-air corrections removes the effect of atmosphere based on the elevation above geoid. The second-order approximation formula is used to improve the accuracy of the height correction, the effect is

$$\delta_{g_h} = -(0.3087691 - 0.0004398sin^2\varphi)h + 7.2125x10^{-8}h^2 \qquad 11$$

where *h* is the height above the ellipsoid and the effect of gravity is in mGals (Hinze et al., 2005; Parasnis, 1979).

Bouguer correction accounts for the gravitational attraction of the rock present between datum and observation point. The correction removes the effect by approximating the rock layer beneath the observation point to an infinite horizontal slab with a thickness equal to the elevation of the observation above datum. The Bouguer correction is given by

$$\delta_{g_{BC}} = 2\pi G\sigma h = 4.193x10^{-5}\sigma h \qquad 12$$

where *G* is the gravitational constant, σ the density of the slab and *h* is the height of the station in meter relative to the ellipsoid (Hinze et al., 2005; Kearey et al., 2002). The resulting gravity data are Bouguer anomaly (BA) data. The density of the slab used for this surveys reduction was 2.67 g/cm^3.

The above mentioned reduction equations were coded into a microsoft excel based software called *GravTool* processing software developed by Council for Geoscience (Dingoko et al., 2010) which has since been added on the open source PyGMI software (Cole, 2012).

The resulting Bouguer Anomaly (BA) data are gridded at 50 m cell size with minimum curvature algorithm on Oasis Montaj Geosoft software (Figure 3.11). The BA data was further processed with upward continuation algorithm which calculates the potential field at specified height from the plane on which the gravity is measured (Yossi, 2015). The gravity data was upward continued to 200 m calculating the regional effect (Figure 3.12) which is later subtracted from the BA dataset resulting in a residual gravity map (Figure 3.13).

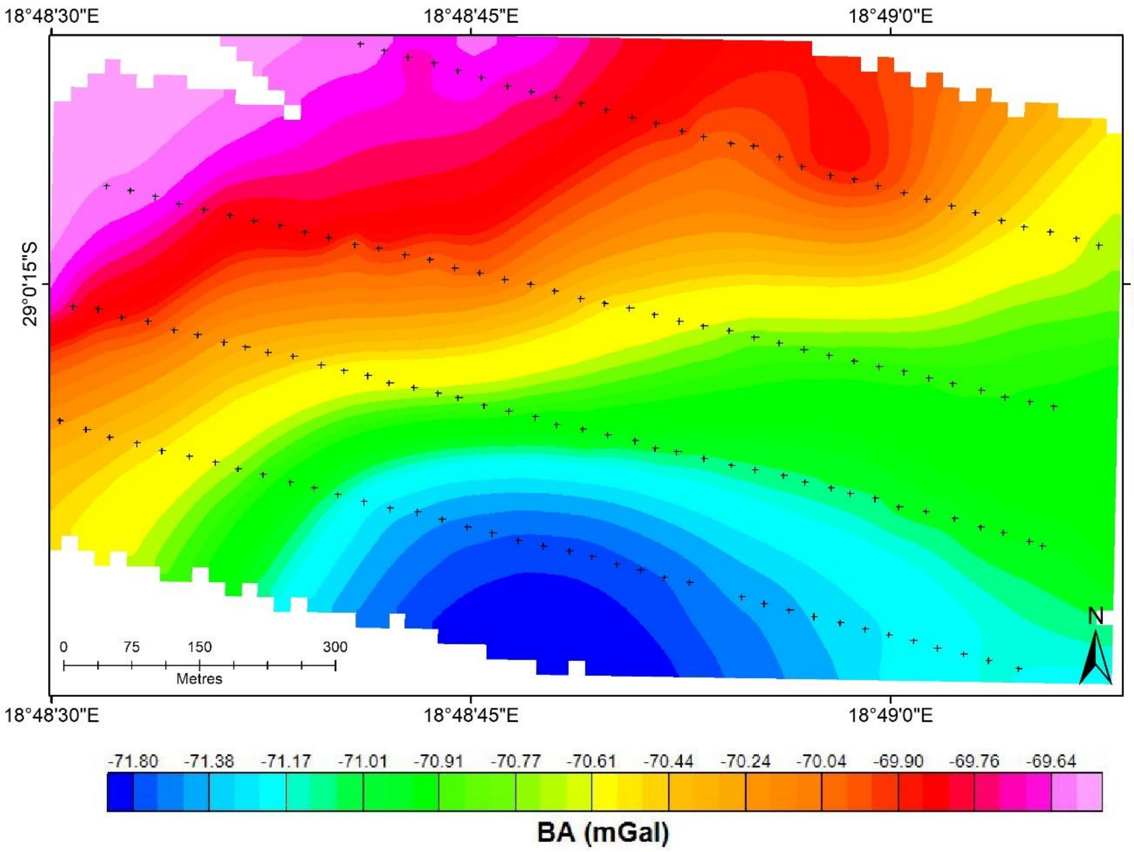

Figure 3.11. Bouguer Anomaly gravity map resulting from gravity reductions applied to the measured gravity data. The data shows that the relative gravity gradually decreases from NW to SE.

The Bouguer Anomaly map shows gravity features distribution in the area (Figure 3.11). The BA gravity amplitudes are generally higher in the NW and gradually decrease toward the S-SE. The high gravity feature (-70.6 – (-69.6) mGal) are NE-trending and low gravity feature (-71.8 – (-71.1) mGal) are confined to the south of the area.

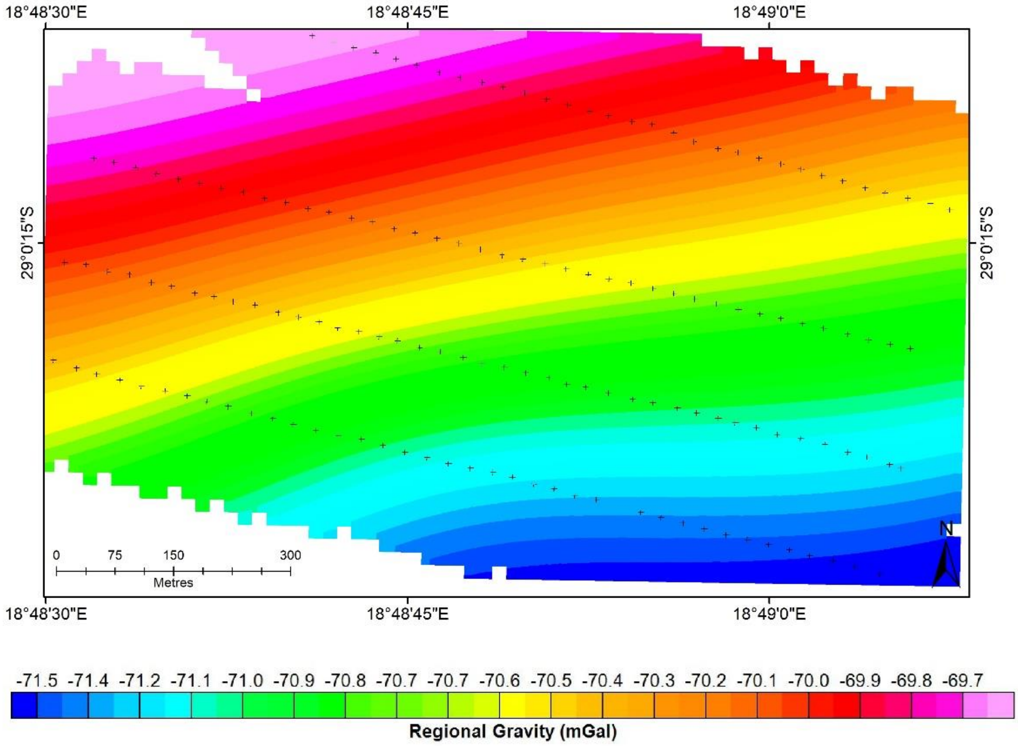

Figure 3.12. Regional gravity map calculated at 200 m height from the measured BA gravity data presented in Figure 3.11. This map shows a gradual decrease in gravity values from the northwest toward the southeast.

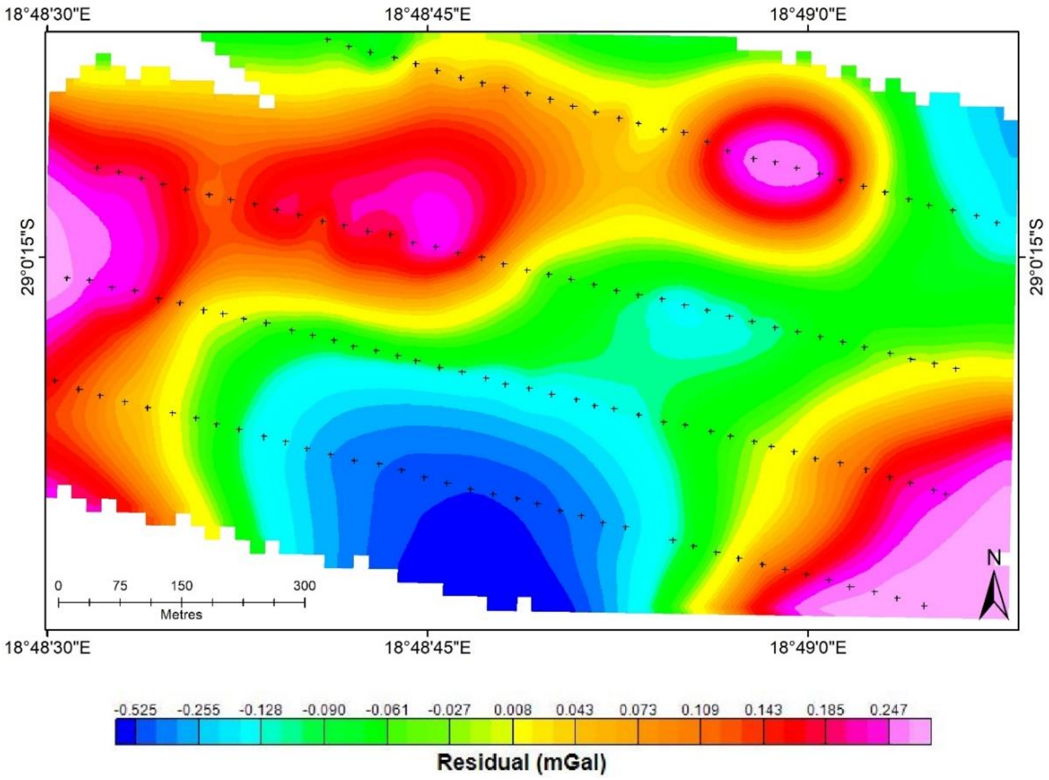

Figure 3.13. Residual gravity map that resulted from a 200m upward continued regional data removed from the BA data. This data reveal the outlines and general strike direction for the local rocks. The black ticks are survey points.

The residual gravity data revealed high and low gravity features in the area (Figure 3.13). Most of this section is dominated by high gravity features that are E-W-trending. These bodies dimension are at least 300 x 300 m. The residual gravity amplitudes of the high gravity amplitude bodies forms pockets of discontinuous material. The low gravity feature (-0.52 – (-0.130) mGal) is spatially confined to the south and NE. The low gravity amplitude body's decrease toward its centre.

3.3. Electromagnetic Method: Magnetotelluric Method

The electromagnetic (EM) method measures a combination of electric and magnetic fields, from which the bulk conductivity of the subsurface is derived. The magnetotelluric (MT) method is a frequency domain electromagnetic (FDEM) method that measures a combination of electric and magnetic fields. This method can use either naturally induced currents into the Earth by solar wind or artificial current sources when it is termed as controlled source audio-frequency magnetotelluric (CSAMT). With ordinary FDEM induced secondary EM fields may be screened off by superficial layers of high conductivity e.g. graphite sheets, clay, etc, that make the detection of deeper conductors much more difficult (Kearey et al., 2002; Parasnis, 1979; Telford et al., 1990). For this survey the magnetotelluric (MT) was chosen given its superior depth of penetration and generally high lateral resolution, for this study the MT method to provide local and regional structural detail of the farm.

The magnetotelluric (MT) geophysical method is a passive exploration electromagnetic method that uses a broad spectrum of naturally occurring current variations as a power source i.e. lightning, thunderstorms and solar plasma emissions. It measures fluctuations in the natural magnetic and electrical fields in perpendicular directions at the surface of the Earth to determine subsurface conductivity structure. The propagation of electromagnetic waves through a homogenous medium is given by

$$y = \sqrt{\omega\mu(i\sigma - \omega\varepsilon)} \qquad 13$$

where y is a complex propagation constant, ε is electric permittivity, σ is electric conductivity, μ is magnetic permeability and ω is angular frequency. The magnetic permeability may be taken as the free-space value μ_0 in nearly all Earth material. The angular frequency and electric permittivity are negligible at the frequencies used by MT, resulting in electromagnetic fields to be not governed by the wave equation but the diffusion equation embedded in the Maxwell equations. An approximation of the depth of penetration of electromagnetic inductions also known as skin depth, is given by

$$p(T) = (T/\pi\mu\sigma)^{1/2} \qquad 14$$

where *p(T)* is electromagnetic skin depth in metres and *T* is period in seconds. The skin depth theory describes exponential decay of electromagnetic fields as they diffuse into a medium. The depth of investigation ranges from a few metres to hundreds of kilometres (Chave, A. D., Jones, 2012; Simpson and Bahr, 2005; Weckmann et al., 2005).

The controlled-source audio-magnetotelluric (CSAMT) is an electromagnetic sounding technique used to map the apparent resistivity of the Earth's crust up to 3 km with good resolution. The 2D and 3D models generated from CSAMT data can exhibit the structures, lithology, mineralisation, electrochemical alteration, ground water changes and permeability (Zonge and Hughes, 1988). The method has been successfully applied in mineral exploration (de Beer, 2015; Simpson and Bahr, 2005).

Simpson and Bahr (2005) compiled a resistivity table of common rocks and Earth material from data obtained from laboratory studies as well as MT surveys (Figure 3.14).

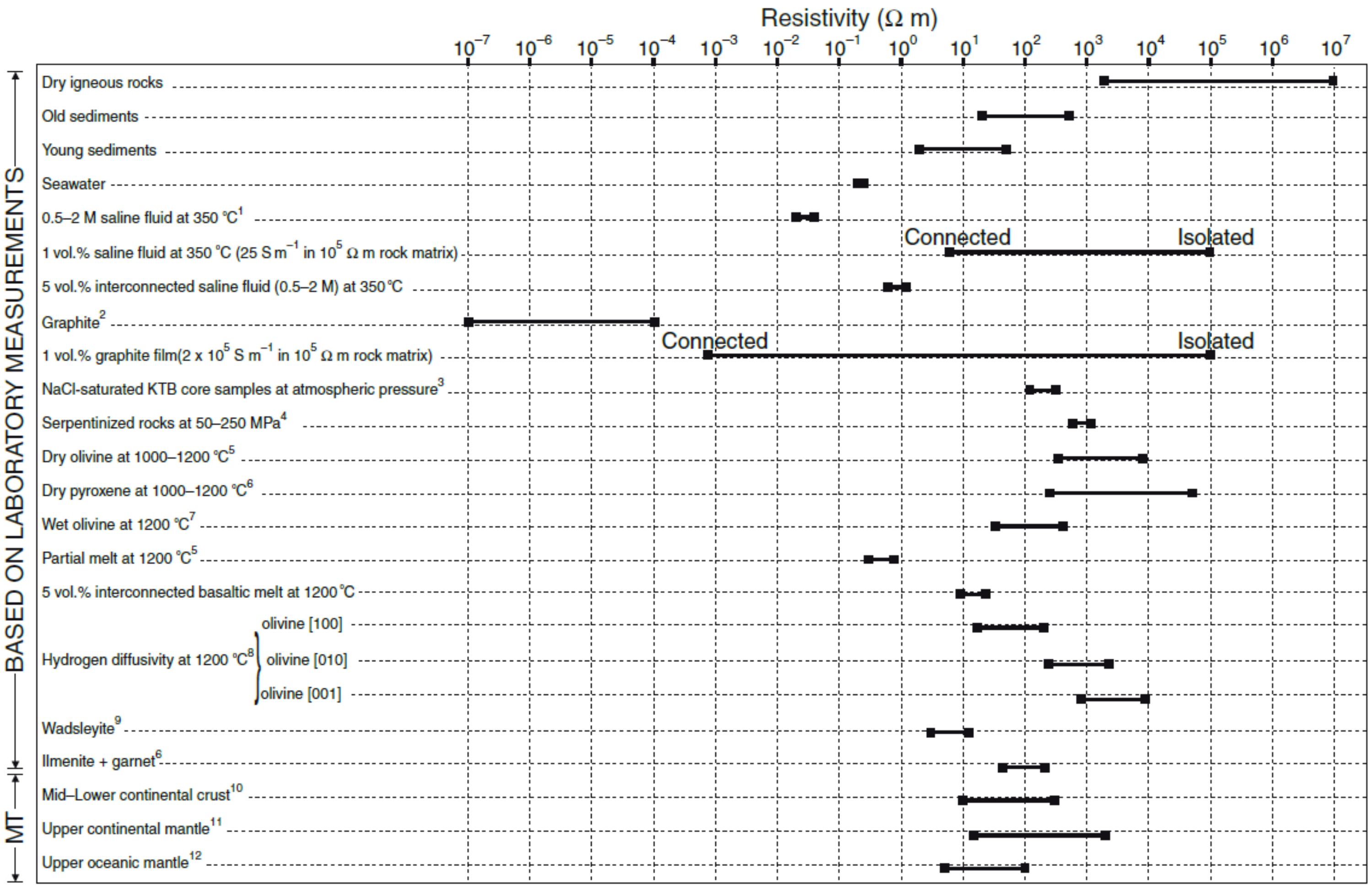

Figure 3.14. Electrical resistivities of common rocks and Earth materials measured in a laboratory as well as derived from MT datasets (Simpson and Bahr, 2005).

The magnetotelllurics (MT) data were acquired using two instrumentations: Stratagem and Phoenix. The Stratagem EH4 instrument which acquires both natural and controlled source-AMT data is a 4-channel system manufactured by Geometrics. The Stratagem is a high resolution electromagnetics conductivity imaging instrument that can map up to 500 m depth with good resolution. It measures electric and magnetic fields magnitudes and present the data as time-series. The measured data include: time series, cross-power spectra, spectral amplitude, scalar resistivity, tensor resistivity, phase and coherency datasets. The measured data can be presented as 1D and 2D resistivity plots. Stratagem can measure frequencies from 10 Hz – 92 kHz. The accompanying transmitter generate frequencies from 1 kHz up to 70 kHz and 400 $Amp - m^2$ (Geometrics Inc., 2011).

The CSAMT survey station spacing varied between 50 m over the chargeability anomaly and 1 km on the AMT stations. Some stations were recorded using the transmitter and others using natural source (Figure 3.7 and Figure 3.15). Survey specifications are summarised in Table 3.4.

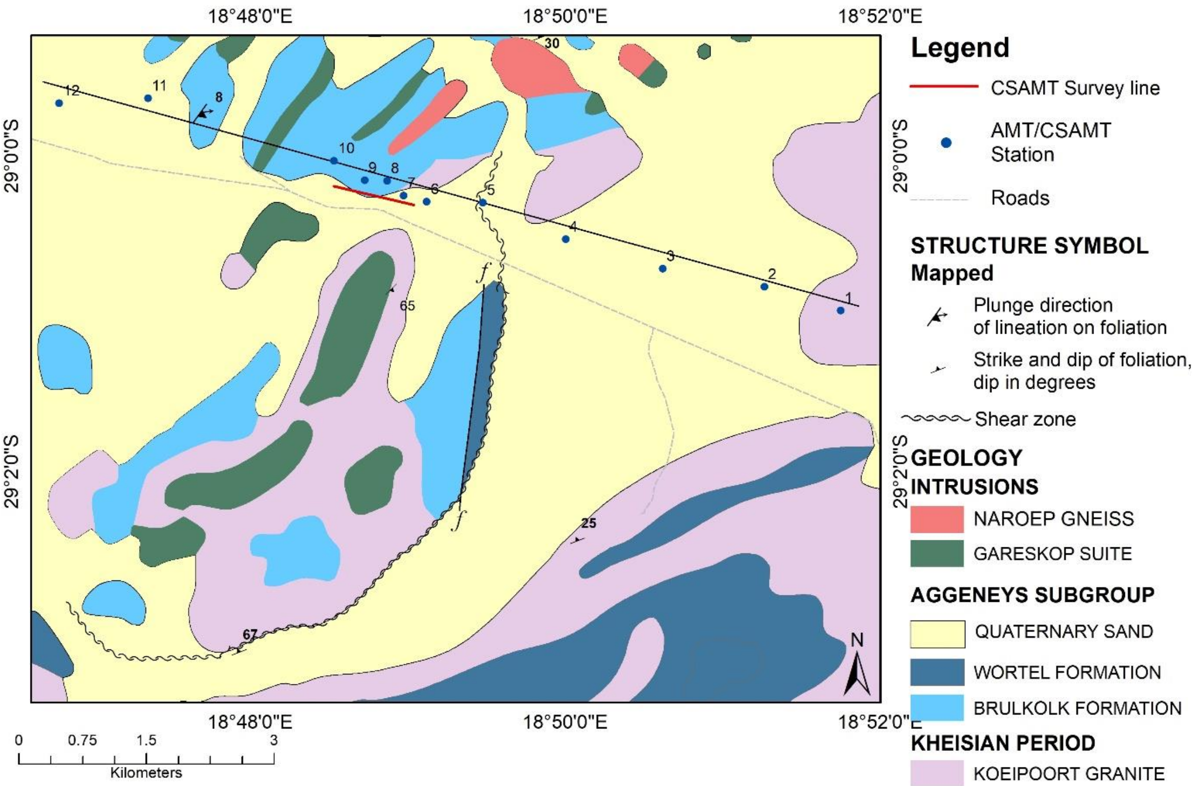

Figure 3.15. An excerpt from the 1:250 000 scale Pofadder geology map of the Wortel Farm study area, as published by the Council for Geoscience (2007), overlaid with CSAMT and AMT survey lines and stations.

The Phoenix MTU-5A is a natural source MT and Audio-MT (AMT) unit that can acquire up to 5-channels of data (three magnetic coils and two electric dipoles). The magnetic coils can measure 10 kHz – 1 Hz frequencies for AMT and 400 Hz – 50 ksec for MT. Similar to the Stratagem system, the measured electric and magnetic field data are presented as time-series. The electrodes used for the dipole measurements were the non-polarized PE4 (Rogers, 2015).

The AMT was acquired at 250 m station distance over the IP anomaly (stations 6 – 10) and 1 km elsewhere and coinciding with the Koeipoort granites; gneiss, amphibolite and schist of the Brulkolk

Formation and sand cover on the geology map (Figure 3.15). The survey specification for CSAMT and AMT are summarised in Table 3.4 below.

Table 3.4. Summary of the survey specifications for the CSAMT and AMT survey.

Magnetotelluric method - CSAMT	
Item	**Value**
Instrumentation	Geometrics Stratagem (EH4)
Surveyed frequencies	92 kHz – 10 Hz
Station spacing	50 m – 1 km

Magnetotelluric method - AMT	
Item	**Value**
Instrumentation	Phoenix MTU-5A
Surveyed frequencies	10 kHz – 1 Hz
Station spacing	250 m – 1 km

The CSAMT apparent resistivity data are calculated by the least-square regression analysis of the measured electric and magnetic fields data from spectra data converted from time-series datasets (Simpson and Bahr, 2005). The time series are converted to spectra data by calculating the fast Fourier transform (FFTs) of the measured 4-channels which is then converted to time series with the sampling rate. The least-square regression method minimizes the sum of squared residual by determining the optimal value for each survey point, where the regression model data is subtracted from the measured data and the resulting data is residual, is given by:

$$S = \sum_{i=1}^{n} {r_i}^2 \quad 15$$

where *S* is the sum of squared residual, *r* the residual of measured and calculated value and *n* the number of data points (Simpson and Bahr, 2005). The sum of squared residual (S) is calculated for each measured electric and magnetic field (*E & H*) at a point and direction (*x & y*). The resulting *S* for electric (E_x & E_y) and magnetic (H_x & H_y) field is then used to calculate impendences with the following equations:

$$\rho_x = (0.2/freq) * {E_x}^2/{H_y}^2 \quad 16$$

$$\rho_y = (0.2/freq) * {E_y}^2/{H_x}^2 \quad 17$$

The resulting apparent resistivities are gridded with 25 m cell size for 50 m station spacing and 500 m cell size for 250 m – 1 km station spacing profiles with minimum curvature algorithm on Oasis Montaj Geosoft software.

The Phoenix AMT time-series data were processed with the following steps to calculate impedances: transformation of the selected time window into frequency domain using Fourier Transform, cleaning the data of electromagnetic noise by coherency and rho variance and impedance computation with least-square regression analysis. The resulting impedances were processed further in preparation for inversion: calculation of regional geological strike of all sites and frequencies using the Bahr (1988) tensor decomposition scheme, rotation of the data to the N35˚E calculated geological strike (Figure 3.16), data correction for static shift caused by galvanic effect due to the electric dipole on the surface by using DC vertical soundings data, and removal of bad data and outliers. The data was then inverted using nonlinear conjugate gradients to determine regularized solutions to a 2D inverse problem (Geosystem SRL, 2011). This inversion routine was developed by Randy Mackie and applied with the WinGLink software. The starting model was set at 100 ohm.m half space and the inversion converged at RMS 5.46 in 30 iterations.

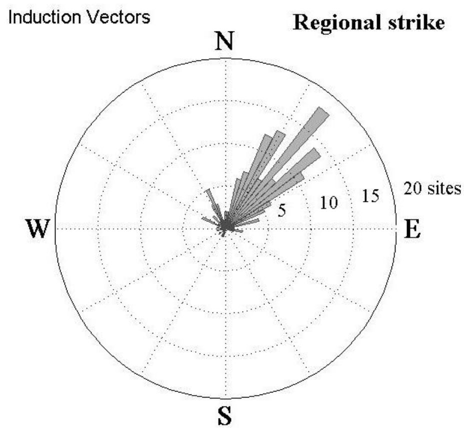

Figure 3.16. Rose diagram indicating strike direction at 10 000 – 1 Hz calculated from induction vectors data, calculated using the Bahr (1988) tensor decomposition scheme. The regional strike ranges between 15°-60°, 35° is the major axis used to rotate the inverted data.

Figure 3.17 is a contrast display of AMT data before (a) and after processing (b), data presented are apparent resistivity, phases and induction arrows (Hz) plotted against frequency (period in seconds) before rotation, static shift correction and removal of outliers and after.

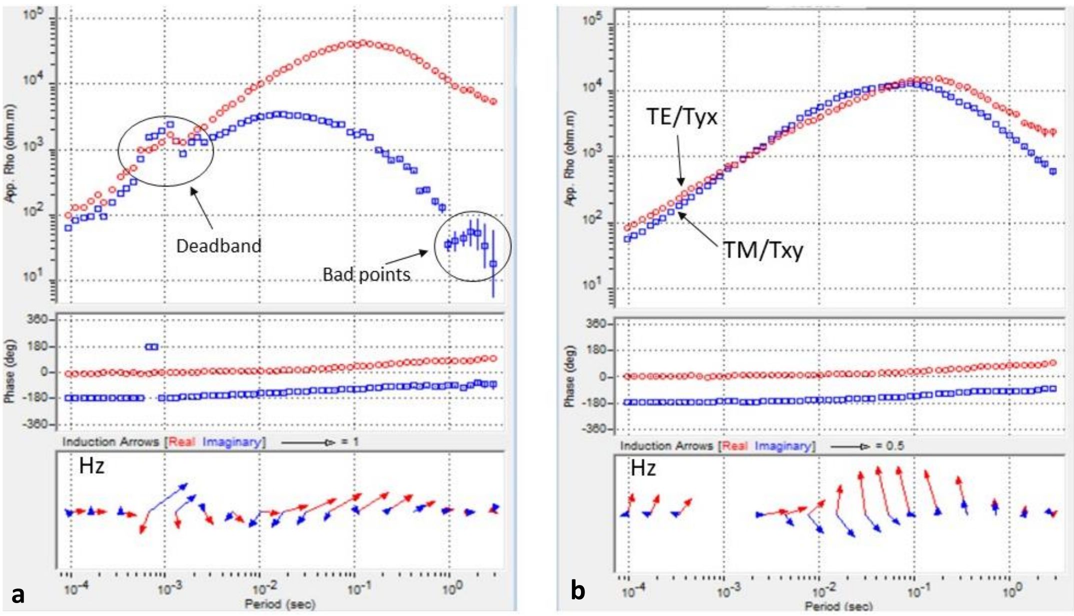

Figure 3.17. Comparison figure of a) the raw apparent resistivity sounding, phases and vertical transfer functions (Hz) before rotation, static shift correction and removal of bad points, with b) the resulting processed AMT sounding curve used for modelling and inversion. This is station 5 dataset.

The CSAMT resistivity 2D cross section show the changes of resistivity both laterally and with depth (Figure 3.18). The top layer consist of material with lower resistivities (very conductive) except between 600 and 700 m horizontal distance. This layer reaches a depth of 80 m to the southeast and up to 100 m in the northwest. At 600 and 750 m distance is an outcropping high resistivity amplitude feature. With depth this feature become wider and more resistive, laterally reaching 250 m distance to the east and appear continuous toward the west, beyond the mapped section, and reaching 200 m depth. Below the resistive layer to the west, at 200 m depth, is another conductive layer that extends to 400 m depth. The thickness of this layer varies between 50 and 100 m. Below the conductive layer, at 750 m horizontal distance toward the northwest is a resistive body that slightly becomes shallower from 300 m depth to 220 m depths. This body becomes more resistive toward the centre.

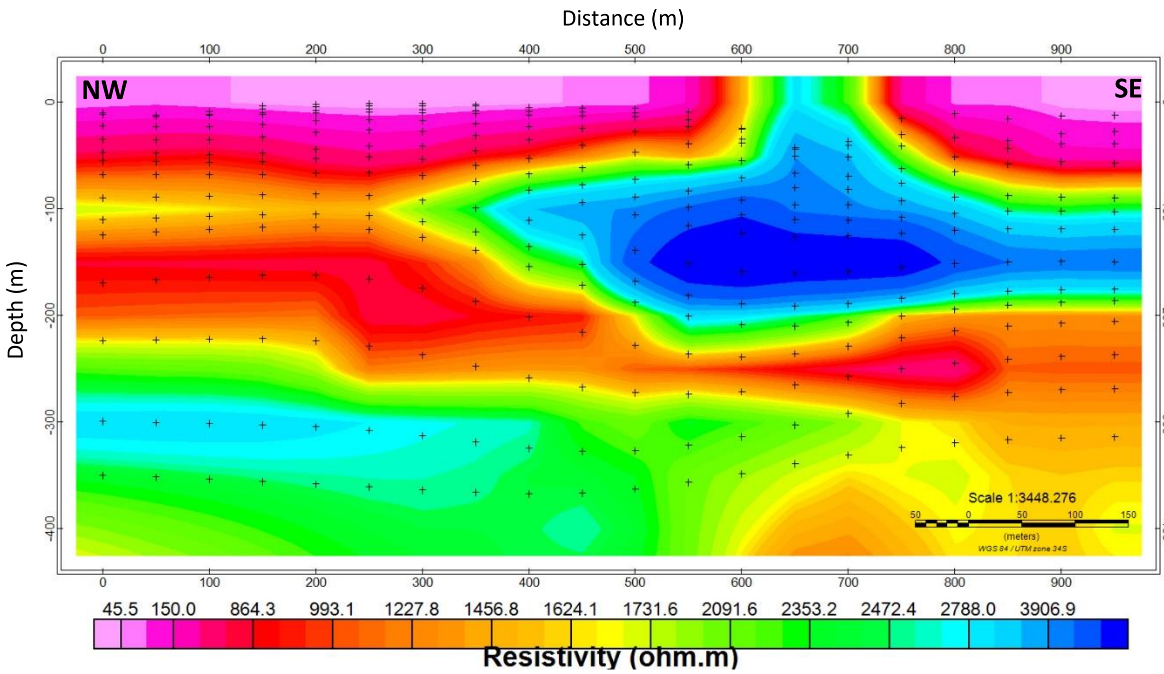

Figure 3.18. CSAMT resulting depth section map of data measured across the IP anomaly and along the second gravity line from the north. The line is 1 km long and the achieved depth of penetration is 400 m. Black ticks are data points. This survey line is approximately 10o m away from the AMT stations.

The CSAMT data acquired ~100 m away from the 1 km CSAMT profile, along the same stations as the AMT stations are presented in Figure 3.19. The resulting 2D cross section map revealed resistive features up 1 km depth. The sections shows three distinct layers: lesser resistive top layer (0 - 9 kOhm.m), moderate range resistivities (9 – 18 kOhm.m) and high resistivity amplitude (18 – 27 kOhm.m) mapped at depth. The conductive layer starts off very conductive on the surface and gradually decrease until it merges with the second layer. This is observed from 3000 m horizontal distance to the southeast. The highly resistive layer at depth shows undulations. From 3000 m to the west the subsurface layering changes and not mapping the high amplitude resistivities at depth mapped toward the southeast.

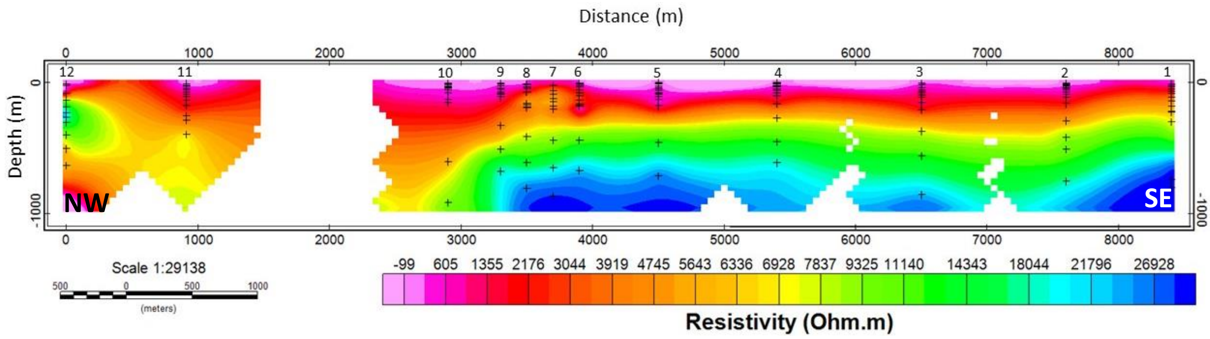

Figure 3.19. CSAMT resistivity 2D cross section of data measured on the AMT stations. The method was able to reach approximately 1 km depth.

The resulting AMT soundings were modelled for 1D surface (Figure 3.20) and inverted for 2D surface (Figure 3.21). the 1D model is of the TM mode of the apparent resistivity for stations 3, 5 and 7. Station 5 model shows at least three layer subsurface reaching 3 km of good fit. Station 5 shows a lesser resistive section of the traverse mapping at least three layers to a couple of kilometres depth of good resolution. Station 7 is more resistive of the 3 stations, indicating at least four layers and penetrating a few kilometres deep.

The resistivity variations mapped by the AMT method shows changes on the subsurface for up to 5 km depth over a 10 km profile (Figure 3.21). The 2D cross section shows three main features: less resistive (1 – 100 ohm.m), moderately resistive (100 – 40 kOhm.m) and highly resistive features (40 kOhm.m - $1x10^6$ ohm.m). The lesser resistive layer is mapped at the top 500 m depth. The conductor mapped below 2 km depth at 2 km horizontal distance is interpolated and may not be a geological feature. The moderately resistive layer is thinner than the less resistive layer. This layer present as a transition zone between less resistive and highly resistive layer, approximating few to tens of meter. The undulation and moderately resistive vertical feature under stations 4 and 5 are considered as not an artifact. Below 500 m depth a very resistive layer is mapped extending to 5 km depth with a notable decrease in resistivity at around 6000 m horizontal distance, revealing a SE dipping vertical feature.

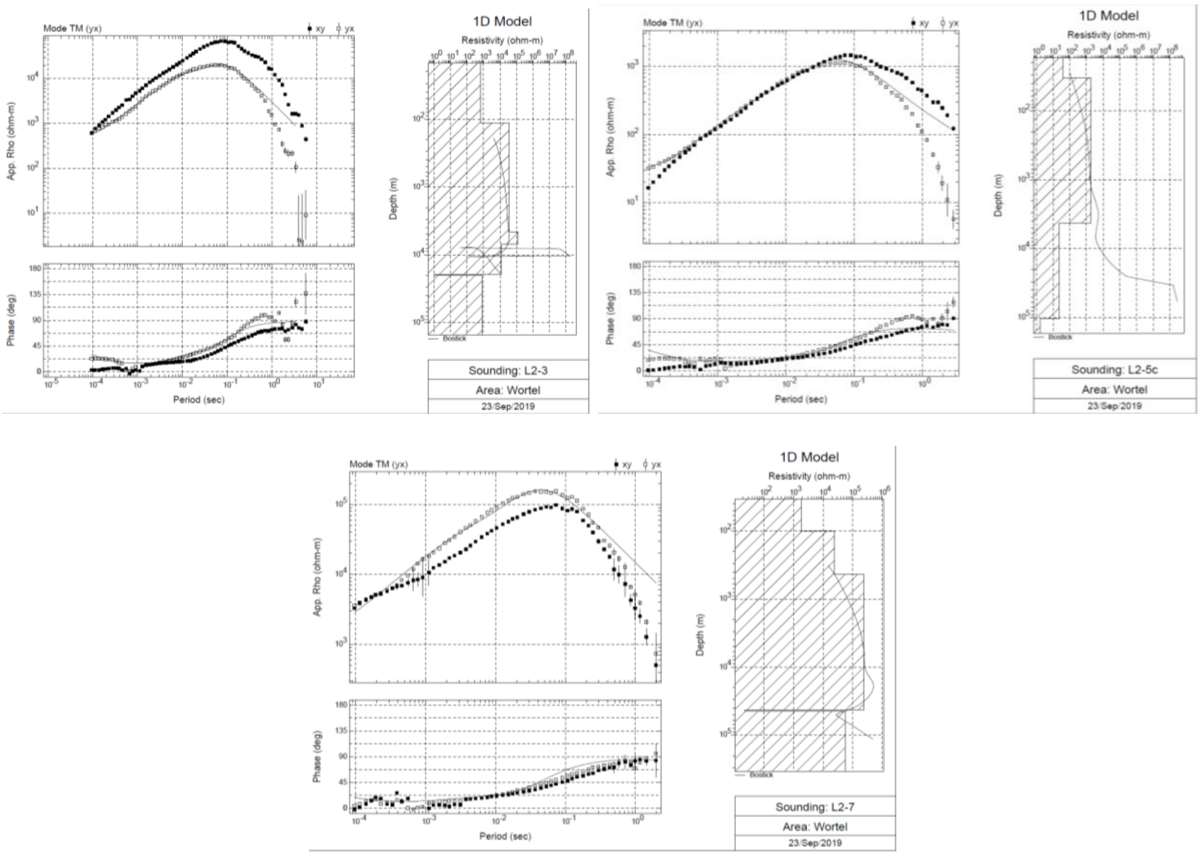

Figure 3.20. 1-D model of the TM modes for stations 3, 5 and 7.

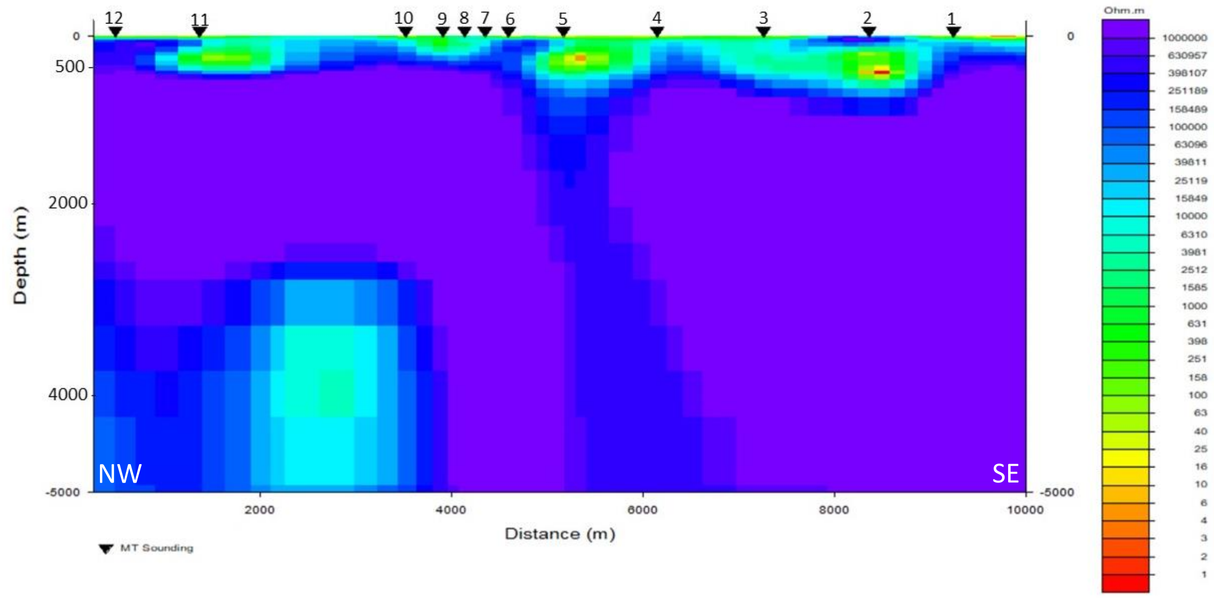

Figure 3.21. AMT resistivity 2D cross section measured toward the north end of the IP anomaly. The map shows variation of resistivity with depth.

3.4. Rock Magnetic Characterisation

In attempt to understand better the magnetism of the study area and possibly identify rocks responsible for the mapped magnetic fabrics on the farm, 43 sun-compass-oriented rock samples were drilled out across the farm. Figure 3.22 shows the drilling locations and lithologies coinciding with the site, Figure 3.23 is the Google Earth terrain map overlain with drill locations and Figure 3.24 is the TMI map overlain with drill sites. Severe weathering and limited access made it difficult to drill much more samples. The samples were analysed for: bulk susceptibility, natural remanent magnetisation (NRM), Koenigsberger ratios (Q-ratio) at local geomagnetic field and after alternating field demagnetization, determining the declination and inclination.

Measured magnetic susceptibility is the sum of the magnetism of all rock forming minerals magnetism (i.e. ferromagnetism, diamagnetism, etc), defined by $Ji = \chi H = \chi B/\mu_0$ where *Ji* is induced in a material of mass susceptibility χ by an applied field $B = \mu_0 H$ (Collinson, 1983; Telford et al., 1990). Generally, a rock magnetism consist of remanent or induced magnetism, or both (Reeves, 2005). The Q-ratio, which is described as Q = remanent magnetisation/(susceptibility x induced magnetisation) is commonly measured under local and alternating geomagnetic fields. According to Clark (1997), Q>1 indicates remanence being more dominant than induced magnetisation, and Q<1 indicates induced magnetisation to be more dominant.

The samples drilled are approximately 20 mm in diameter while the length varied. Each sample was divided into 2-4 smaller specimen for measurements. The bulk susceptibility was measured with MFK1-FA Kappabridge manufactured by AGICO at 200 A/m peak field and at 976 Hz operating frequency. The magnetic intensity and direction of magnetisation were measured with a AGICO JR6 dual speed spinner magnetometer. Alternating field (AF) demagnetisation was calculated in small incremental steps reaching the lowest of 15 mT, to determine stable calculated remanance. The stable calculated demagnetisation/AF in the area is 12.5 nT which is used to measure the Q-ratio at alternating field. The Q-ration at local geomagnetic field was calculated at 30 179 nT.

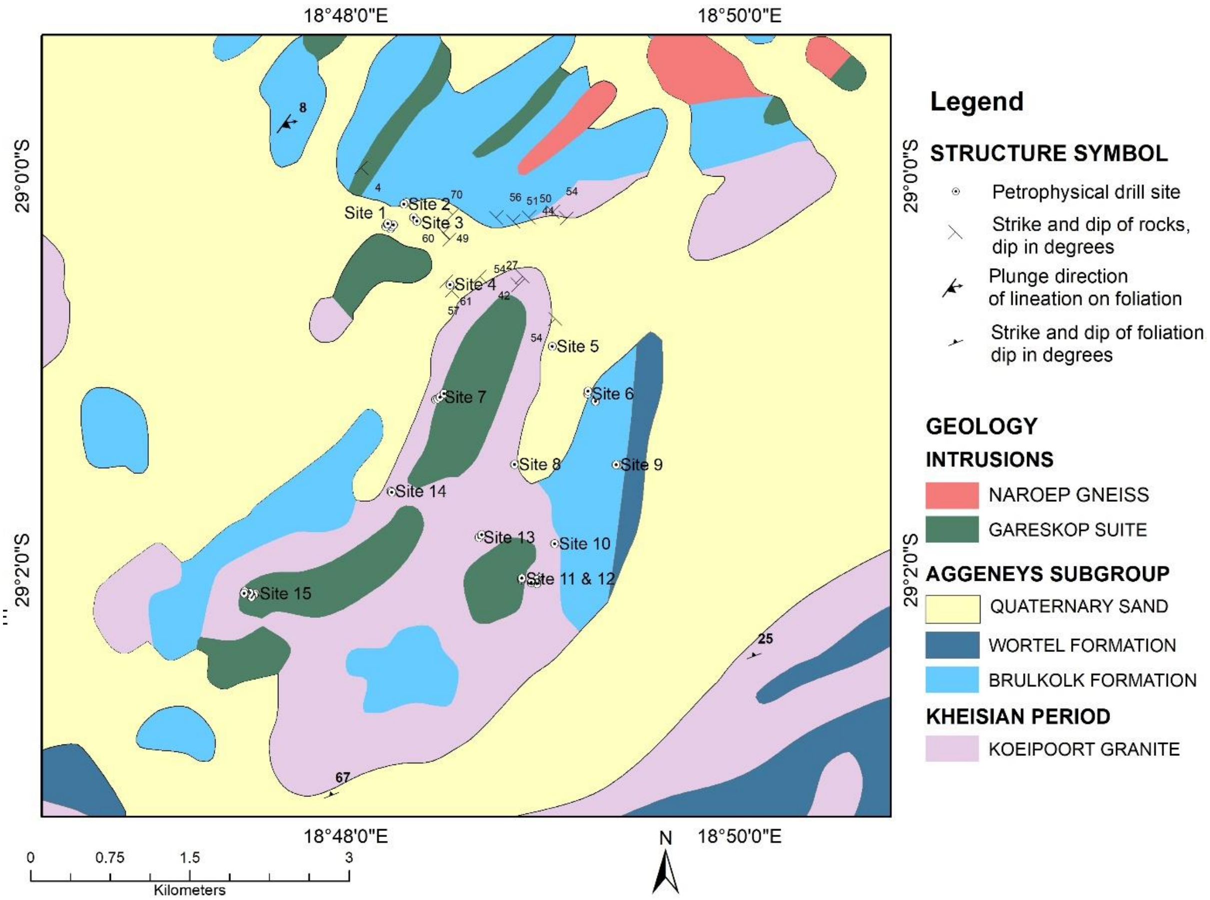

Figure 3.22. An excerpt from the 1:250 000 scale Pofadder geological map of the study area, as published by Council for Geoscience (2007), overlaid with drill sites, mapped structure symbols including dip direction and angle mapped on the ground during the course of this study.

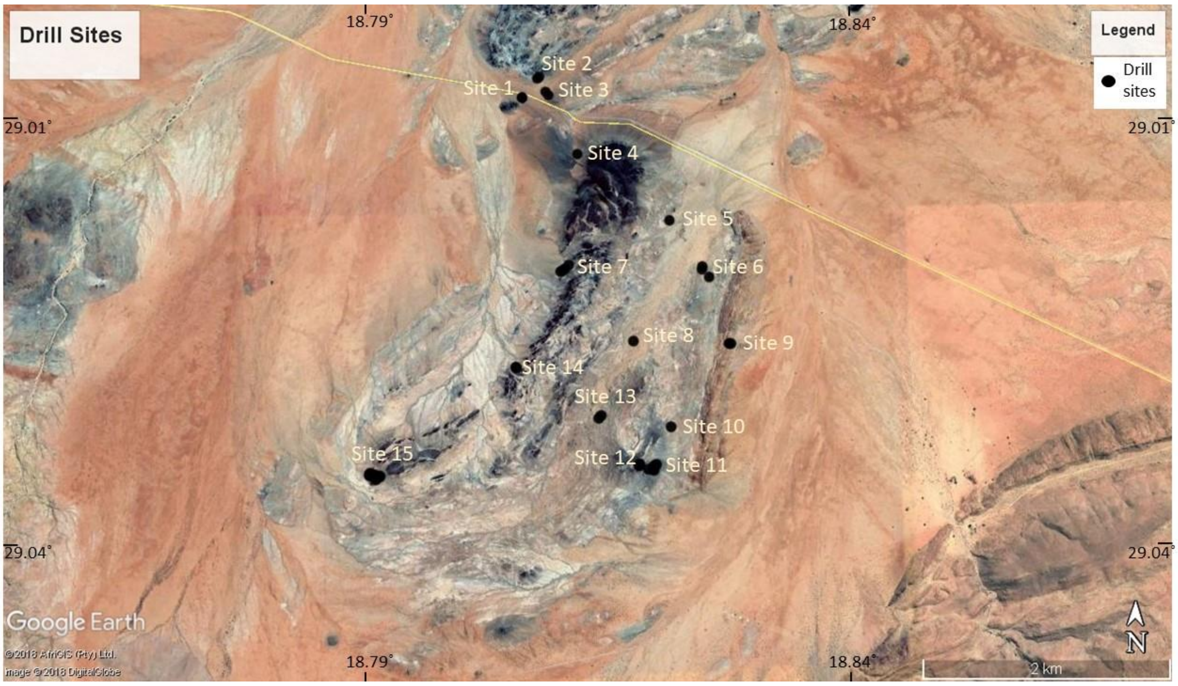

Figure 3.23. Google Earth terrain map of the Wortel Farm study area outcrop overlaid with palaeomagnetic drill sites (Google Earth, 2018b).

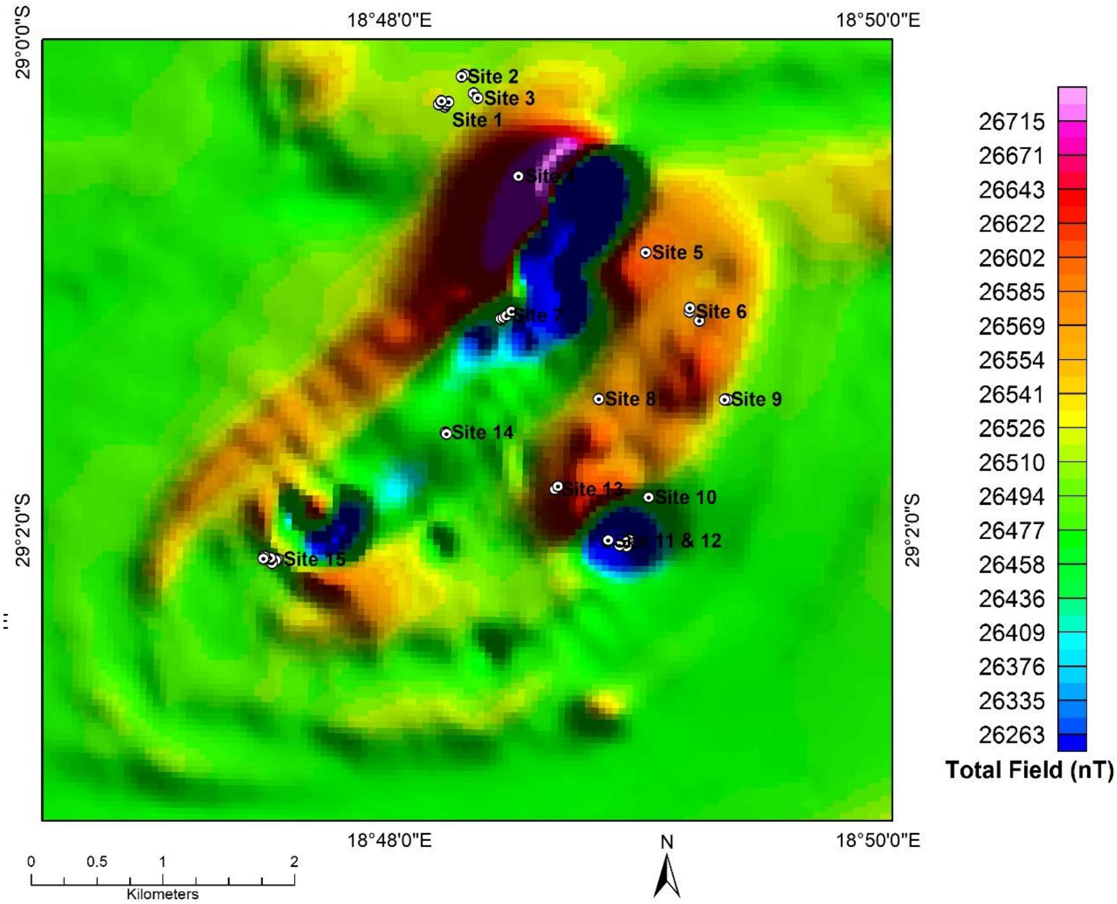

Figure 3.24. TMI map of the Wortel Farm study area overlaid with palaeomagnetic drill sites. This site shows where the sites are located with respect to the magnetic anomalies mapped.

The resulting palaeomagnetism data are presented in Table 3.5. These magnetic properties are commonly used for constraining data interpretations, inversion, modelling and many other applications. Natural remanent magnetisation is plotted against susceptibility (Figure 3.25) to graphically present lithologies with high remanent magnetism and high susceptibilities.

Table 3.5. Summary of magnetic properties results of the Wortel Farm study area. *N:* number of samples, *Q*: Konigsberger ratio. The mapped lithology column is taken from a 1:250 000 scale geology map of the area (Figure 3.22).

Site #	Sample ID	Lat	Long	Mapped Lithology	Identified Lithology	Susceptibility (*10^{-3} SI)	NRM (*10^{-3} A/m)	Q-ratio (0) (H=30179 nT)	Q-ratio (AF = 12.5 nT)	Declination (˚)	Inclination (˚)	*N*
1	1722001 - 004	-29.004	18.804	Sand cover	Gabbro	15.2– 28.8	637 – 7260	1.57 – 13.78	0.09 – 2.08	75.2 – 213.4	-74.8 – 59.90	4
	1722005 - 006				Pegmatite	-0.00652 - 0.00773	0.517 - 0.792	-3.30 - 4.27	-3.18 - 8.75	116	-32.70	2
2	1722007 - 008	-29.002	18.805	Brulkolk Formation	Gneiss	0.144 – 16.5	0.374 - 331	0.11 – 0.84	0.05 - 0.08	-	-	2
3	1722009	-29.004	18.806	Sand cover	Granite	17.6	5120	12.09	2.67	-	-	1
	1722010				Schist	0.73	17.5	1.00	1.01	-	-	1
4	1722016	-29.009	18.809	Sand cover	Pegmatite	0.533	12.3	0.96	0.55	76.40	-64.50	1
5	1722032	-29.014	18.818	Sand cover	Amphibolite	3.04	234	3.20	0.76	105.6	-37.00	1
6	1722034			Brulkolk	Gabbro	27.0	685	1.05	0.11	244.50	47.80	1
	1722035	-29.019	18.821	Formation	Pyroxenite	26.0	449	0.72	0.06	153.90	30.20	1
	1722036				Granite	11.9	157	0.55	0.13	64.00	45.10	1
7	1722037			Granite/	Gabbro	0.57	44.1	3.22	0.65	346.60	62.20	1
	1722038	-29.018	18.808	Amphibolite	Marble	0.0758	25.7	14.14	0.40	314.20	49.30	1
	1722039			Dyke	Granite	17.0	54.7	0.13	0.05	201.80	-63.10	1
	1722040				Amphibolite	63.4	1420	0.93	0.22	288.60	47.10	1
8	1722041	-29.024	18.814	Granite	Pegmatite	1.61	372	9.60	2.03	4.20	55.20	1
9	1722042	-29.024	18.823	Brulkolk	Meta-quartzite	1.61	16.1	0.42	0.40	170.50	-61.00	1
	1722043			Formation	Granite	13.6	252	0.77	0.50	153.50	-76.80	1
10	1722044	-29.031	18.818	Granite	Gabbro	67.6	6190	3.81	2.91	25.70	-78.10	1
11	1722017 - 018	-29.034	18.816	Amphibolite	Gabbro	0.448 – 1.16	3.81 - 243	0.35 – 8.72	0.27 – 0.30	129.30– 158.20	37.50 – 59.90	2
	1722020 - 021			dykes	Granite	2.22 – 31.9	77.7 - 698	0.91 – 1.46	0.57 – 0.71	33.90 – 84.90	4.10 – 10.50	2
	1722019				Schist	0.397	2.39	0.25	0.27	189.10	49.40	1
12	1722011			Granite	Gabbro	0.466	0.551	0.05	0.02	289.40	-30.00	1
	1722013	-29.034	18.815		Granite	12.1	55.9	0.19	0.02	35.30	-45.80	1
	1722012				Schist	36.9	6800	7.68	1.09	117.2	-11.80	1
13	1722014	-29.030	18.811	Granite	Granite	10.3	1740	7.05	0.22	219.40	-33.20	1
	1722015				Pegmatite	-0.000149	0.40	-111.7	-32.11	267.30	43.30	1
14	1722022 - 023	-29.026	18.804	Granite	Gabbro	0.886 – 1.66	16.6 – 4210	0.78 – 105.82	0.94 – 34.72	167.30– 349.40	57.80 – 69.70	2
15	1722024, 026, 030			Amphibolite	Pyroxenite	0.537 – 0.612	0.842 – 1.55	0.07 – 0.11	0.04 – 0.12	258.00– 334.50	-58.60 – 42.90	3
	1722027	-29.035	18.792	dykes	Gabbro	0.281	0.554	0.08	0.06	19.90	60.90	1
	1722025, 028, 031				Granite	0.946 – 13.3	9.86 – 3310	0.43 – 23.47	0.12 – 9.10	8 – 355.80	-60.20 – 64.00	3
	1722029				Gneiss	16.9	112	0.28	0.13	351.90	45.60	1

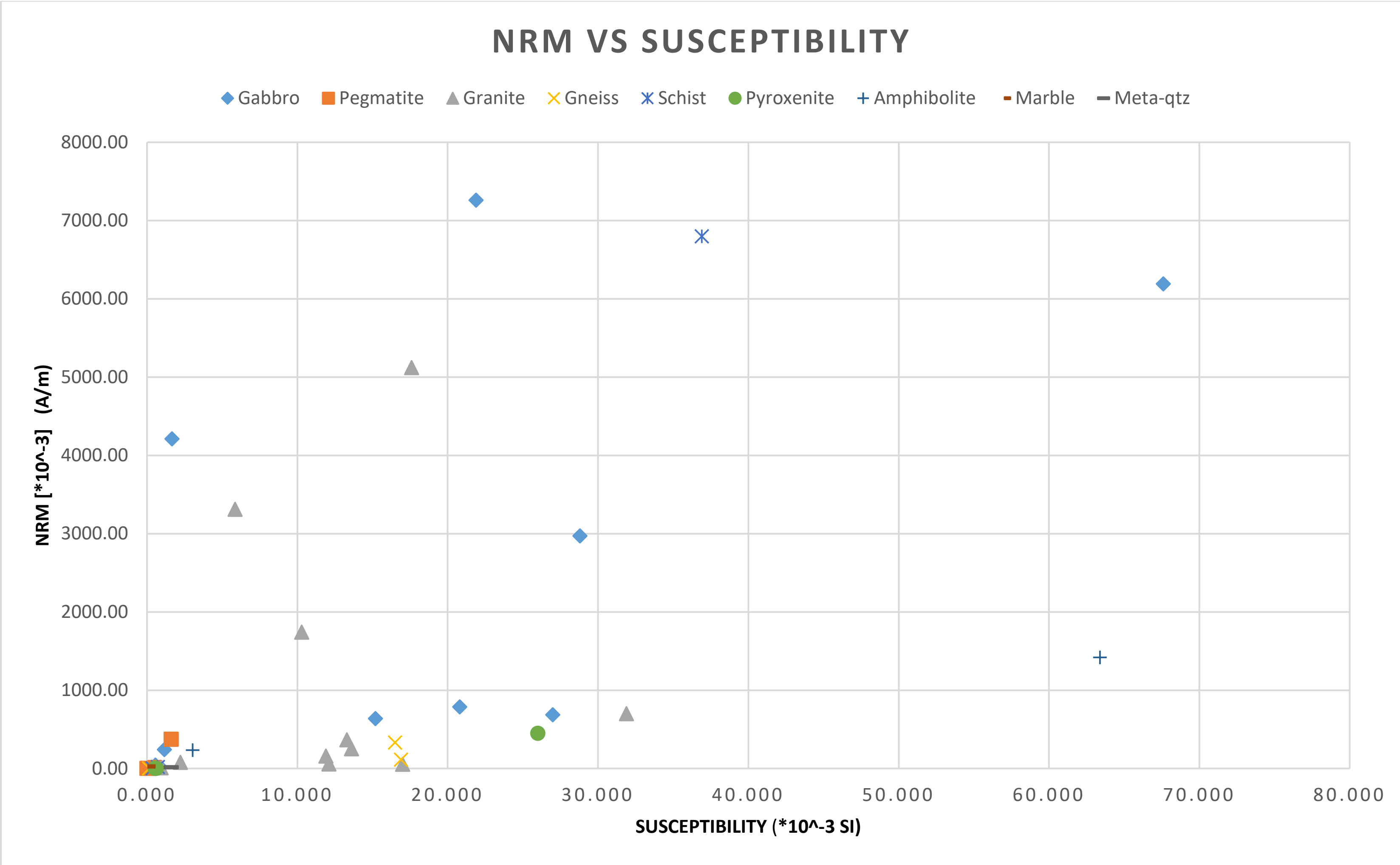

Figure 3.25. A graphical presentation of the rock samples NRM and susceptibility. What is apparent from the chart is that half the samples measured have low NRM and susceptibility, while the other half shows varying distribution. The gabbro, granites and few schist samples indicate high magnetism present on these rocks.

The results (Table 3.5) shows that most samples carry induced magnetisation, according to the Clark (1997) criteria. Gabbro, granite and pegmatite specimens of the Brulkolk Formation and Gareskop Suite are among the samples that carry remanent magnetism.

When the sample sites are plotted on the geology map (Figure 3.22), Sites 1, 7, 12 and 14 coincide with the mapped Gareskop Suite rocks. Based on the susceptibility, NRM and Q-ratio measurements, gabbro, amphibolite, granite and schist rocks appear to be the main carriers of magnetism in the Gareskop Suite. Gabbro in sites 1 and 7 is more magnetised than that of site 12 and 14 while granite is highly magnetised in site 14. Sites 5, 8, 10, 11, 13 and 15 coincides with the mapped Koeipoort Granite rocks and the four lithologies that, according to the data, carries the majority of the magnetisation are the granite, gabbro, pegmatite and amphibolite rocks. Sites 3, 6 and 9 coincides with the mapped Brulkolk Formation and the rocks that carry more magnetism are gabbro, granite and pyroxenite rocks.

The metamorphism that the rocks in the region experienced most-likely re-worked the primary mineral composition thus affecting the magnetic fabrics in the rock. Thus the measured magnetic properties represent the magnetisation post deformation after deposition. The varying inclination and declination within one mapped rock unit indicate that part of this rock unit possible experienced metamorphism and/or parts of minerals were remagnetised. The inclination values opposite to the current inclination reading is a strong indicator of present remanent magnetisation in the measured rocks.

Dip directions as well as dip angle were measured during the course of this study in a small section of the farm (Figure 3.22). The dip angle results, NW-strike with SE-dip followed by NE-strike with SW-dip, reveals folding of the rocks that span from few meters in the farm to a kilometre in the Aggeneys region; and the dip direction reveals that although the rocks are folded they maintain a similar NE-trend observed in and around the rocks mapped in the area.

3.5. Observed structures photographs

A few images of some structures seen along the farm are presented below.

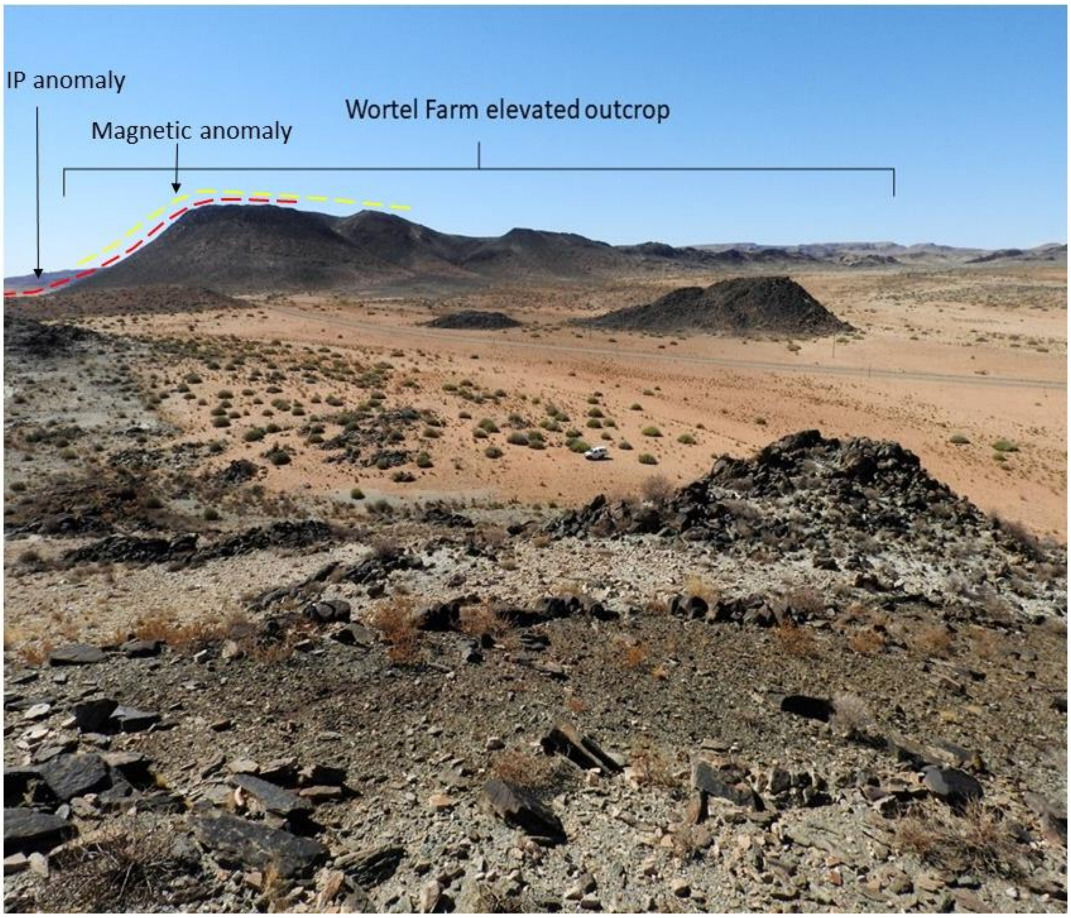

Figure 3.26. Overall overview of the Wortel Farm outcrops with some surrounding outcrops, also showing the mapped coinciding anomalies location of the IP and magnetic anomaly. Bakkie used as scale. Photo credits: Mr Nick Baglow (CGS, 2016).

Figure 3.27. Small folding structures seen on the farm. Many of these folds indicate the level and scale of deformation that occurred on the farm. The folds varied in scale.

Figure 3.28. This image shows vein-like structures seen throughout the main outcrop and some of the veins are quartz-veins. Image taken with no scale, few hundreds of meter from the outcrop, facing east direction.

Figure 3.29. Google Earth image of the farm showing location of some the images presented.

Figure 3.30. A boudinage structure imaged a few meters outside the study area. This structure also indicates the level of deformation that occurred in this area. The photographer was facing NW, few tens of meters from the outcrop.

3.6. Geochemical Data

Regional geochemical mapping program was carried out over the 2918 Pofadder 1:250 000 scale area in 2015 by CGS. A total of 21000 samples were collected and analysed for more than 60 elements. The resulting maps were created from the statistically analysed datasets (Elsenbroek et al., 2018). Of the 60 elements analysed 9 elements were anomalous on the Wortel Farm: Bismuth (Bi), Cobalt (Co), Chromium (Cr), Copper (Cu), Iron oxide (Fe), Lithium (Li), Magnesium (Mg), Nickel (Ni) and Tungsten (W). The resulting maps are presented below (Figure 3.31 and Figure 3.32).

The Bismuth is known to concentrate in pegmatites, hydrothermal veins polymetallic deposits (Robb, 1986). In the region and the farm the Bi anomaly coincides with the Aggeneys Subgroup rocks and Koeipoort granite and measuring 0.9 – 4 ppm on the farm (Figure 3.31) (Elsenbroek et al., 2018). The Cobalt elements are enriched in ultra-basic igneous rocks and hydrothermal veins, in this region they occur over the Karoo Dolerite and ultramafic dykes and sheets of the Gareskop Suite that intrudes the Koeipoort granite amongst many others and measuring between 15 – 98 ppm on the farm (Agenbacht and Oosterhuis, 2013; Elsenbroek et al., 2018). Chromium is present in chromite, magnetite and clays and here associated with the Brulkolk Formation and most distinct anomalies coinciding with the Gareskop Suite (Colliston et al., 1989; Wilson and Anhaeusser, 1998). On the farm the Cr element reads between 80 – 1000 ppm. Copper tends to concentrate in intermediate igneous rocks and black shales in sediments, clays and Fe-Mn oxides soil. On the farm copper is a mapped occurrence and the geochemistry analyses links it with dykes and sheets of the Gareskop Suite and measuring 87 – 1390 ppm. Iron is enriched in mafic igneous rocks. Although metallic or native iron is rarely found on surface as it tends to oxidise but the oxides represent the primary ores. In the region, the strong Fe anomalies corresponds with the Karoo Dolerite Suite, Namaqualand Suite and Gareskop Suite (Figure 3.32) (Elsenbroek et al., 2018; Levinson, 1974). On the farm iron measured between 5 – 7 ppm. Lithium concentrates in felsic igneous rocks and shales in sediments and is a pathfinder for pegmatite deposits. The Li enrichment on the farm and neighbouring area is associated with pegmatites and measures between 30 – 136 ppm. Magnesium are predominantly anomalous in basalts and ultrabasic igneous rocks and sedimentary carbonate rocks. The Gareskop Suite intruding the Brulkolk Formation are expected to be the source of elevated Mg in the area and measure 11800 – 76000 ppm on the farm (Agenbacht and Oosterhuis, 2013; Colliston et al., 1989; Cornell et al., 2006). The Nickel ore concentrates in mafic-ultramafic igneous rocks and shales in sediments. The Brulkolk Formation and Gareskop Suite coincided with the elevated Ni concentrations however the Gareskop Suite is expected to the true source of Ni, similarly to the Li concentrations. The Ni measures at 30 – 460 ppm on the farm. Tungsten mineral occurrence are mapped on the farm and generally associated with pegmatites and a similar correlation is drawn on the farm (Robb, 1986). The W measures at 7 ppm on the farm (Figure 3.32) (Elsenbroek et al., 2018).

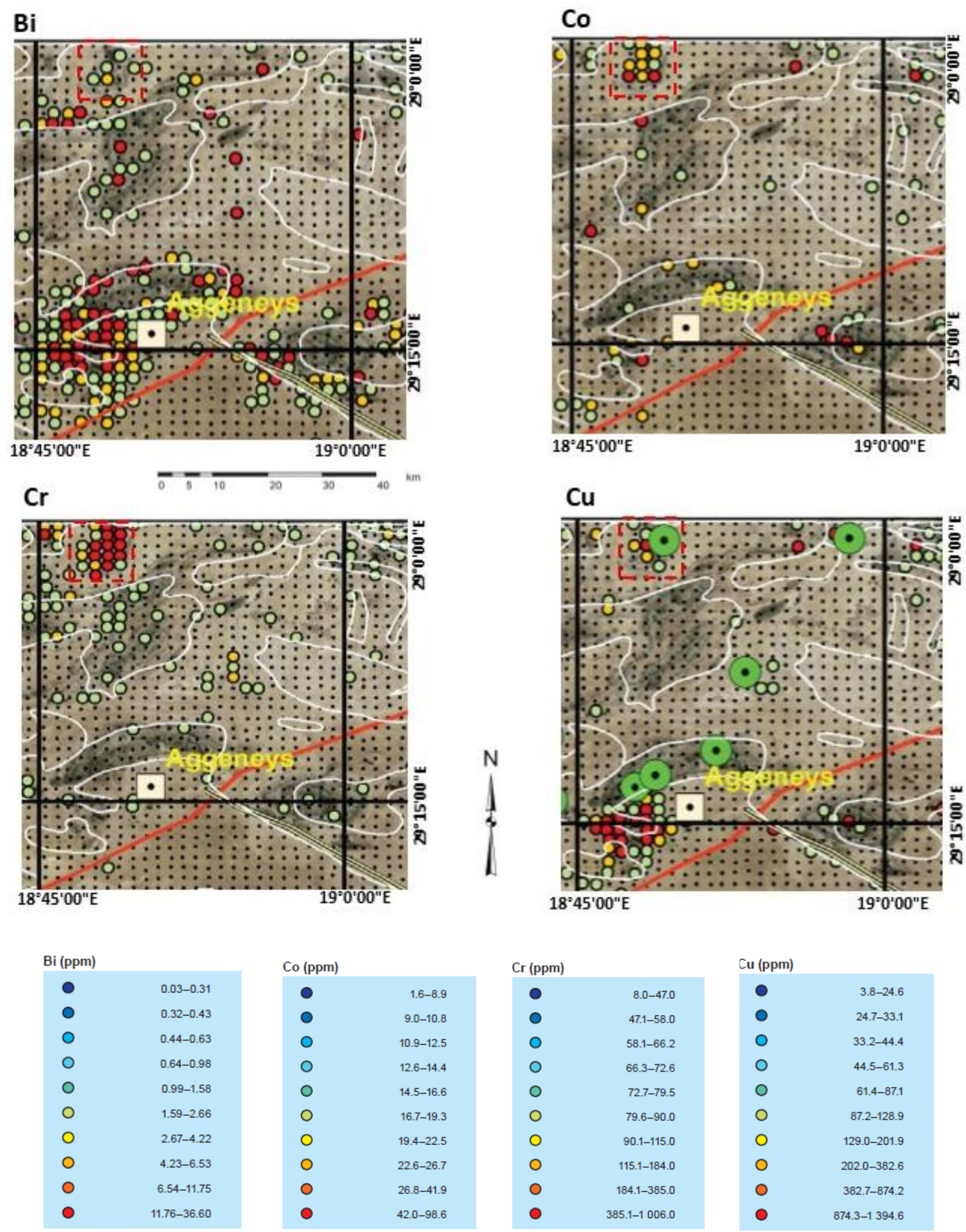

Figure 3.31. Regional geochemical distribution map of Bi, Co, Cr and Cu for the 2918BB Pofadder map sheet and surroundings. The Wortel Farm study area is outlined by a red-hatched rectangle overlay. The mapped mineral occurrences are marked by larger green circles.

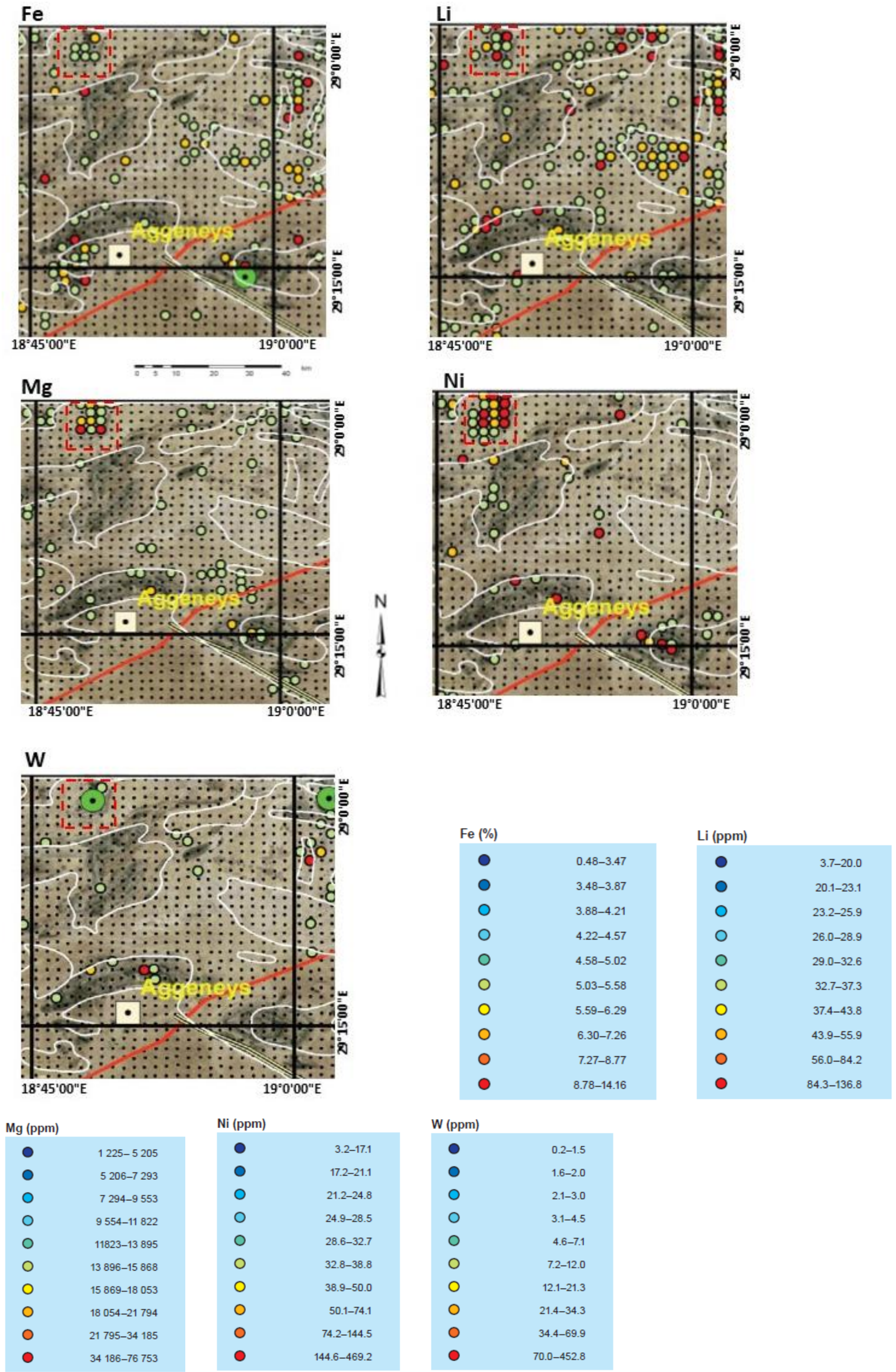

Figure 3.32. Regional geochemical distribution map of Fe, Li, Mg, Ni and W for the 2918BB Pofadder map sheet and surroundings. The Wortel Farm study area is outlined by a red hatch-rectangle overlay. The mapped mineral occurrences are marked by larger green circles.

All the data presented in this chapter are interpreted and compared with mapped geological lithologies and other datasets in Chapter 4, to understand the geology of the area better and determine the potential of the mineral prospect present.

Chapter 4: Results Interpretation

Interpretation of various responses and physical properties (observed from the data) and inferences drawn when compared with the mapped geology are discussed in this chapter. The datasets are presented in the order: magnetics, IP and DC resistivity, gravity, ERT, CSAMT and AMT.

4.1 Magnetic Results

The magnetic data presented and interpreted in this chapter had an IGRF value of 26645 nT removed as it is the Earth's main magnetic field (however not the regional magnetic field of the area) and revealing the magnetic response due to the rocks in the area, artificially sun-shaded from the NE and colours manipulated to enhance anomalous bodies (Figure 4.1). The yellow – red (warm) colour is high positive magnetism and blue the high intensity negative magnetism, the rest is background. The Wortel Farm study area is located within a regional NE striking sheared geological setting (Figure 2.4 and Figure 4.1). The magnetic map of the study area shows part of the magnetized regionally sheared geological units labelled B and C. The magnetic body B is subdivided further into B1 and B2 that appear to be disrupted by the oval shaped magnetic feature (A) in the center of the map thus forming two separate lineaments (Figure 4.1). Body B1 is approximately 2.5 km x 700 m and B2 at least 4.5 km x 400 m in dimension. These lineament could be correlated to the Koeipoort granites or alternatively dykes following the strike direction of the regional rocks. The lineaments magnetism amplitude increase from B1 at -53 nT to approximately -25 nT (with IGRF removed) at B2. This increase in magnetism could be due to high concentrations of magnetic minerals in those areas or the magnetic source being closer to the surface. On the geology map the lineaments coincide with alluvium sand cover, the causative magnetic body is buried under the sand. The anomaly labelled C coincides with sheared outcropping Koeipoort granites, Wortel (shale, schist and quartzite) Formation rocks (Figure 4.2). The observed elevated magnetic response could be due to the magnetic parts of the granites and/or Wortel Formation rocks present in the area.

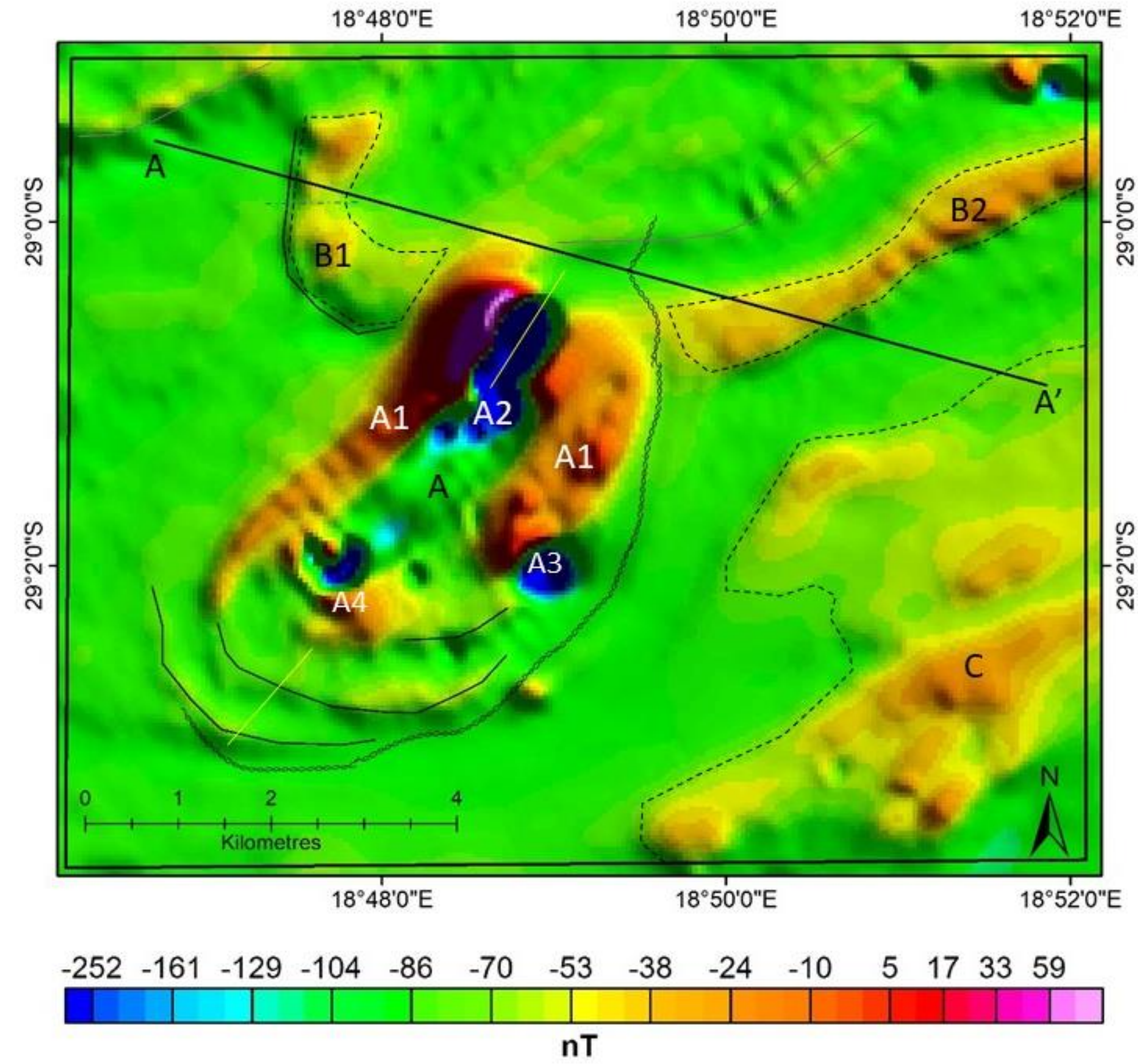

Figure 4.1. IGRF-residual magnetic map of the Wortel Farm study area with an IGRF value of 26645 nT removed. The resulting map shows that the area carries isolated remanent magnetisation, because of the strong magnetic low amplitude associated with some of the bipolar magnetic anomalies. The magnetic body are labelled according to their relative magnetic field strength amplitude.

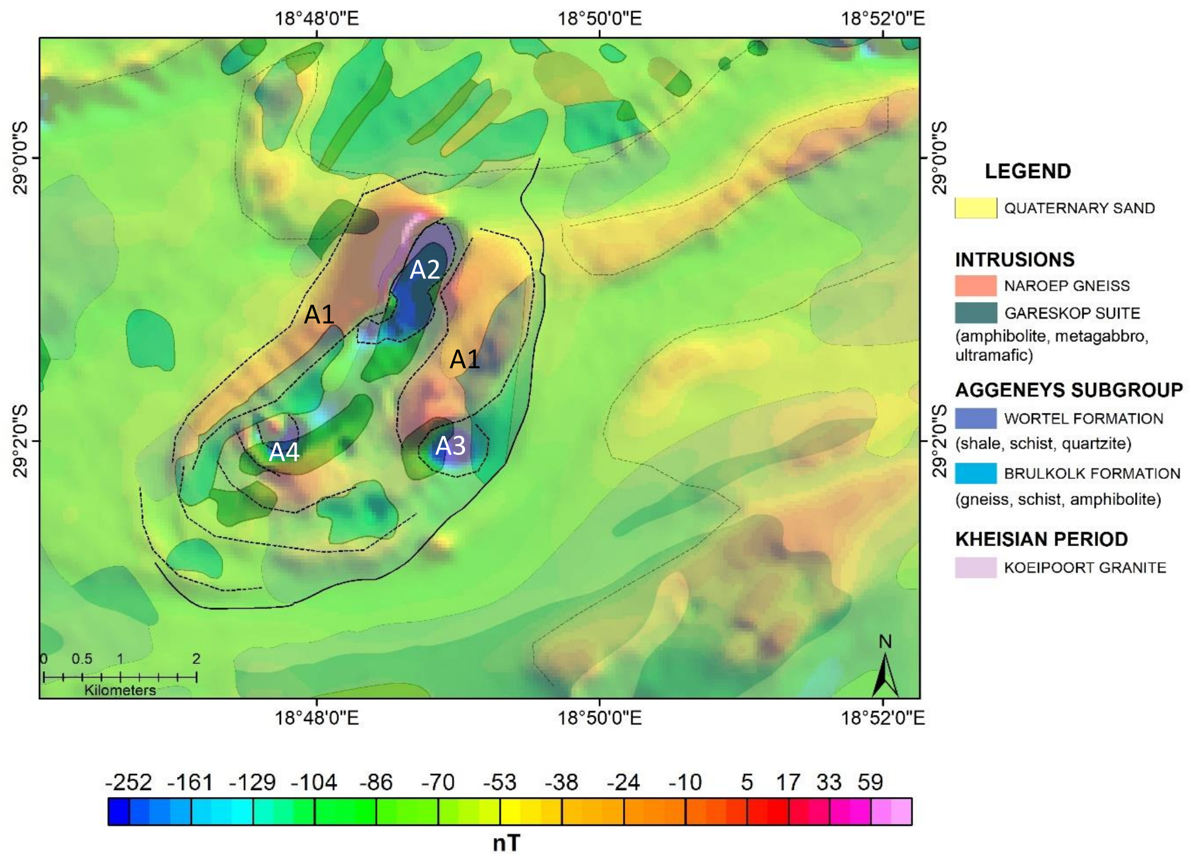

Figure 4.2. A half-toned IGRF-residual magnetic map of the Wortel Farm overlain on the geological map of the Wortel Farm, which is an excerpt from the 1:250 000 scale Pofadder geology map.

The elliptically shaped magnetic anomaly labelled A has the highest magnetic amplitude in the study area and is the motivation and focus of this research. The magnetic body is subdivided further based on the magnetic field amplitudes.

Any magnetic anomaly has a "north-seeking" and "south-seeking" pole and in the southern hemisphere the south seeking pole is a magnetic low or negative when the IGRF is removed. The boundary of the causative magnetic body lies between the maximum of the magnetic high and minimum of the associated magnetic low. If a proper regional field has been removed the north seeking pole is a "positive" magnetic high and the south seeking pole is a more subdued "negative" magnetic low, provided that the magnetism of the magnetic body is induced (Reeves, 2005). If the magnetic low is pronounced it is a sure indication that the influence of the remanent component of the rock magnetism is strong as is seen in Figure 4.1 for the area labelled A2 and A3.

The A1 anomaly coincides with the mapped Koeipoort granite and Brulkolk Formation rocks, largely following the Brulkolk Formation outlines (Figure 4.2). The magnetic amplitudes for anomaly A1 diminish from NE to SW and could indicate uneven distribution of the magnetic minerals within the source rocks and/or the magnetic source deepens to the SW of the body. Of the drilled core samples, sites 4, 5, 6, 8 and 12 coincides with the A1 anomaly. Site 4 revealed the presence of magnetic pegmatite that could be amongst the contributors to the plus 60 nT magnetic amplitude. The rest of the sites encountered magnetic amphibolite, gabbro, pyroxenite, pegmatite, schist and granite which could account for the mapped lower amplitudes of -10 – 5 nT in relation to the IGRF removed value. The high susceptibilities of the schist indicate that the Brulkolk Formation rocks attribute significant magnetism to the measured anomalies. What is also evident from the core sample analyses and identification is that the mapped granite unit is composed of more than one lithology and the presence of schist is evidence of alteration due to low grade green schist metamorphism.

The A2 negative anomaly is highly anomalous and is inferred to be the south seeking pole of A1 with an area of at least 1.7 km x 400 m dimensions and a high negative anomaly of -255 nT. This anomaly coincides with mapped amphibolite dykes of the Gareskop Suite which could be main contributors to the magnetism. The coinciding site 7 mapped magnetic gabbro and meta-gabbro, granite and amphibolite rocks. The magnetic gabbro is taken as evidence that it is of an intrusive nature postdating the Namaqua event (Bailie et al., 2007; Pettersson, 2008). The Gareskop Suite intruded the north section of the granite and has strong remanence (indicated by south seeking A2 anomaly and north seeking elevated positive amplitude north of A1 anomaly).

The anomaly labelled A3 and A4 mainly coincide with mapped amphibolite dykes of the Gareskop Suite and Koeipoort granite. The A3 anomaly indicates a strong remanently magnetized pipe-like body with its north pole indicated by the elevated positive rim on the southern tip of the eastern A1 lobe. Anomaly A3 coincides with sites 11 and 12 that were mapped as gabbros and magnetic granites and schists rocks. The presence of schist is yet another indicator of alteration induced by the intrusions if not previous deformation events. Anomaly A4 consist of a 300 x 150 m -250 nT body surrounded by relatively wider -20 nT magnetic body. Site 15 coincides with A4 and the mapped geology corresponds to pyroxenite, gabbro and a magnetic granite and gneiss rocks (Figure 4.2).

Geologically mapped structures that were recognized on the magnetic dataset and new ones inferred: i) the mapped shear zone confirmed by a sharp decrease in magnetism between A1s and B2, indicating a discontinuity, and ii) interpreted folding to the south of anomaly A extending the mapped shear zone outline. iii) More folded lineament impressions are mapped in the south region with some that appear to be connecting the A1 anomalies. The north of anomaly A appears to consist of a folded unit as indicated by the two A1 anomalies mirroring each other and separated by a possible intrusive body. This fold is also confirmed by dip measurements (Figure 3.22). The Gareskop Suite could have intruded after folding occurred following the fold axis (weakness in the rock). Anomaly B1 appears slightly folded. The B1 anomaly has areas of decreased amplitude and interpreted as rock contact or weathered joints in the rock.

From the paleomagnetic analyses, the magnetic declination result revealed that all the sampled rocks were emplaced when the magnetic field was opposite to the current declination position (Table 3.5). The measured magnetic inclination yielded positive and negative values, the positive inclination direction indicate remanent magnetisation in the area, which is also seen on a large section of A2-A4 anomalies.

4.2 Induced Polarization and DC Resistivity Results

The chargeability map shows three distinct amplitude ranges: high amplitudes of 8 – 11 mV/V labelled C, intermediate amplitudes of 6 – 8 mV/V unlabelled and low amplitudes of 4 – 6 mV/V labelled D (Figure 4.3). Anomaly C is 4 km long x 1 km wide and N-S striking. On surface, the anomaly C coincides with the barren outcrop, mapped as Gareskop Suite and Koeipoort granite (Figure 4.5), the outcrop at the top of the hill from its southern side to the hill flanks and foothill in the north consisting of hard rocks (granite, Brulkolk Formation, intrusion) to weathered material, quartz vein, rubbles and sand cover. Topographically, anomaly C1 sits on outcrop of the top of the hill, hill flanks and foot hill with elevation changes of 100 m. However the chargeability anomaly amplitude remain the same through these elevation changes. This could indicate that the chargeable material either follows the topography or the concentrations of the chargeable material varies but due to the topography/depth to source the amplitude appear the same. On a geology map the IP and DC resistivity anomalies coincides with amphibolite dykes of the Gareskop Suite, granites and Brulkolk Formation rocks and sand cover (Figure 4.5), and anomaly C is largely confined within the dykes, parts of the granites, Brulkolk Formation rocks with varying degrees of metamorphism and deformation (Figure 4.4). The contact of these lithologies cannot be definitely identified given the nature of the IP method in mapping volumetric rock properties (Airo, 2015). The lack of lithological boundaries where IP anomalies are mapped indicate a possibility that chargeable material post-date the geological formation and is more structurally confined than stratigraphically. The high chargeability could be due to clay and sediments formed due to weathering, metamorphism and depositional processes, and/or metallic material in the rocks. Literature publication (Dentith and Mudge, 2014b; Telford et al., 1990) shows that rocks like schist, gneiss, quartzite, gravels and sandstones can have a chargeability of 3 – 30 mV/V and copper and pyrite between 12 – 13 mV/V. Based on these readings, the anomaly C could be a combination of all these materials. Anomaly C is subdivided further into C1 and C2, highlighting areas with higher amplitudes (10 – 11 mV/V). These anomalies could indicate areas with higher chargeable material concentrations closer to the surface. Anomaly C3 and C4 appear disconnected from the anomaly C although they have higher chargeable amplitude (8 – 10 mV/V) like that of C. This could indicate the existence of more chargeable material like that of C that could exist on the farm in varying dimensions.

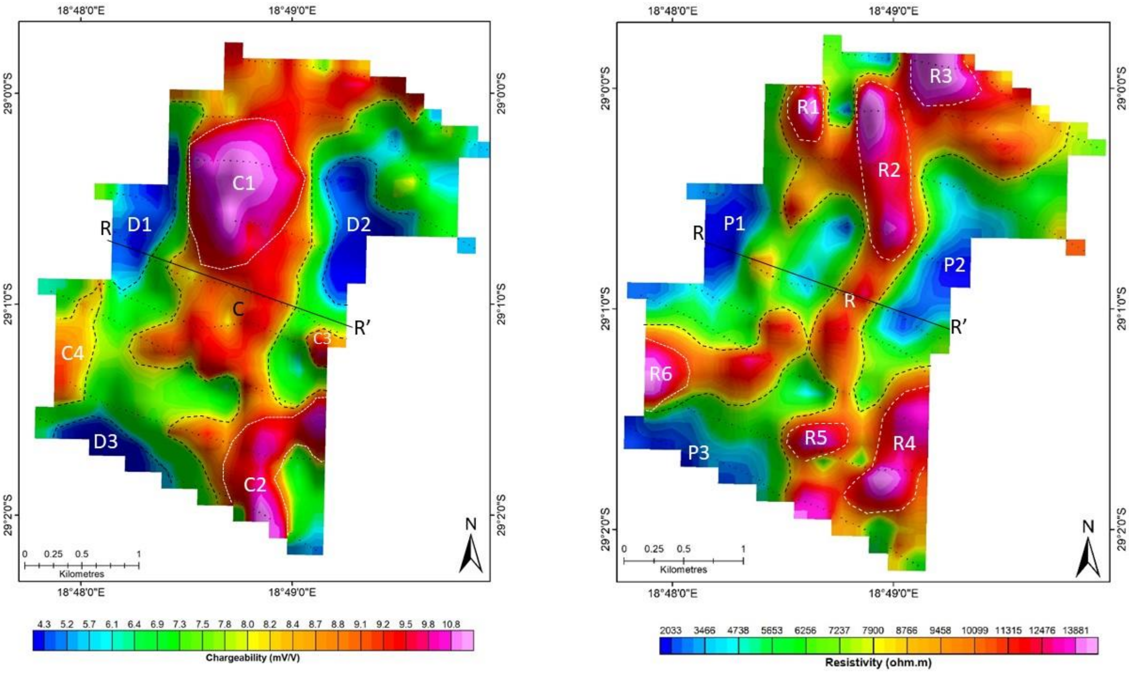

Figure 4.3. Chargeability and DC resistivity maps overlaid with qualitative interpretation drawn from the data. The labelling of the anomalies is guided by the chargeability and resistivity amplitude of the anomalies and mapped rocks.

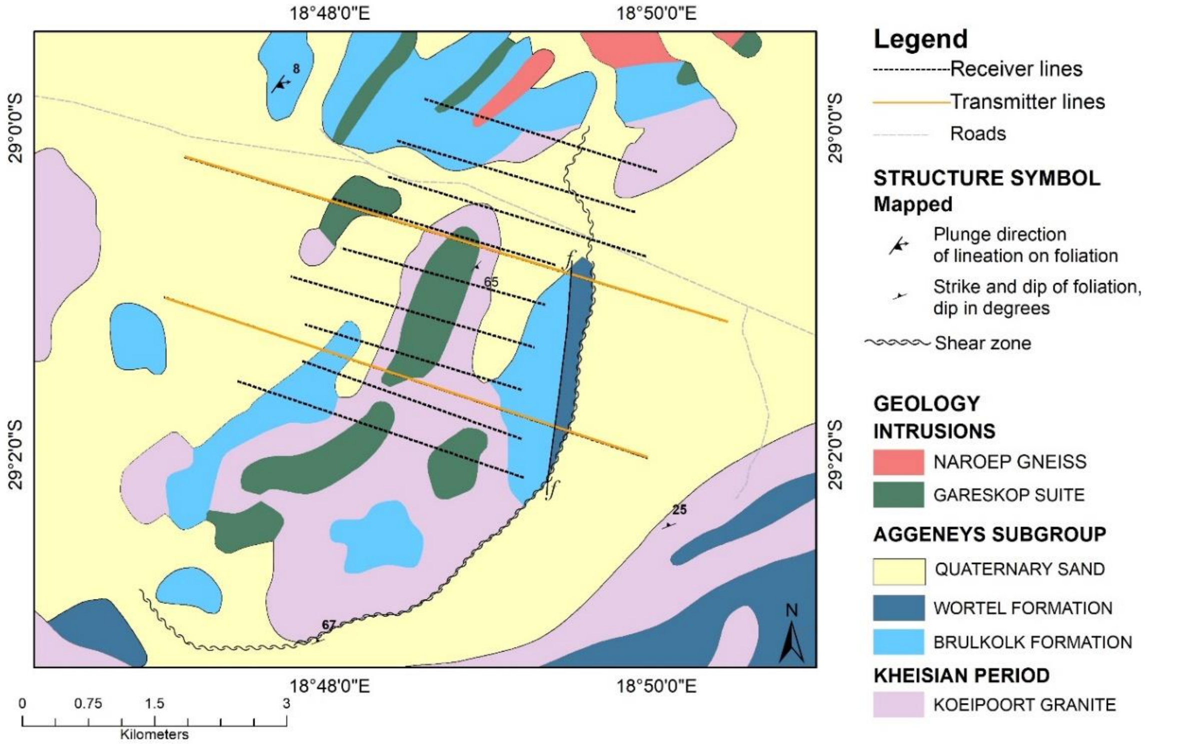

Figure 4.4. An excerpt from the 1:250 000 scale Pofadder geology map of the Wortel Farm study area, as published by Council for Geoscience (2007), overlaid with IP and Resistivity transmitter and receiver survey lines.

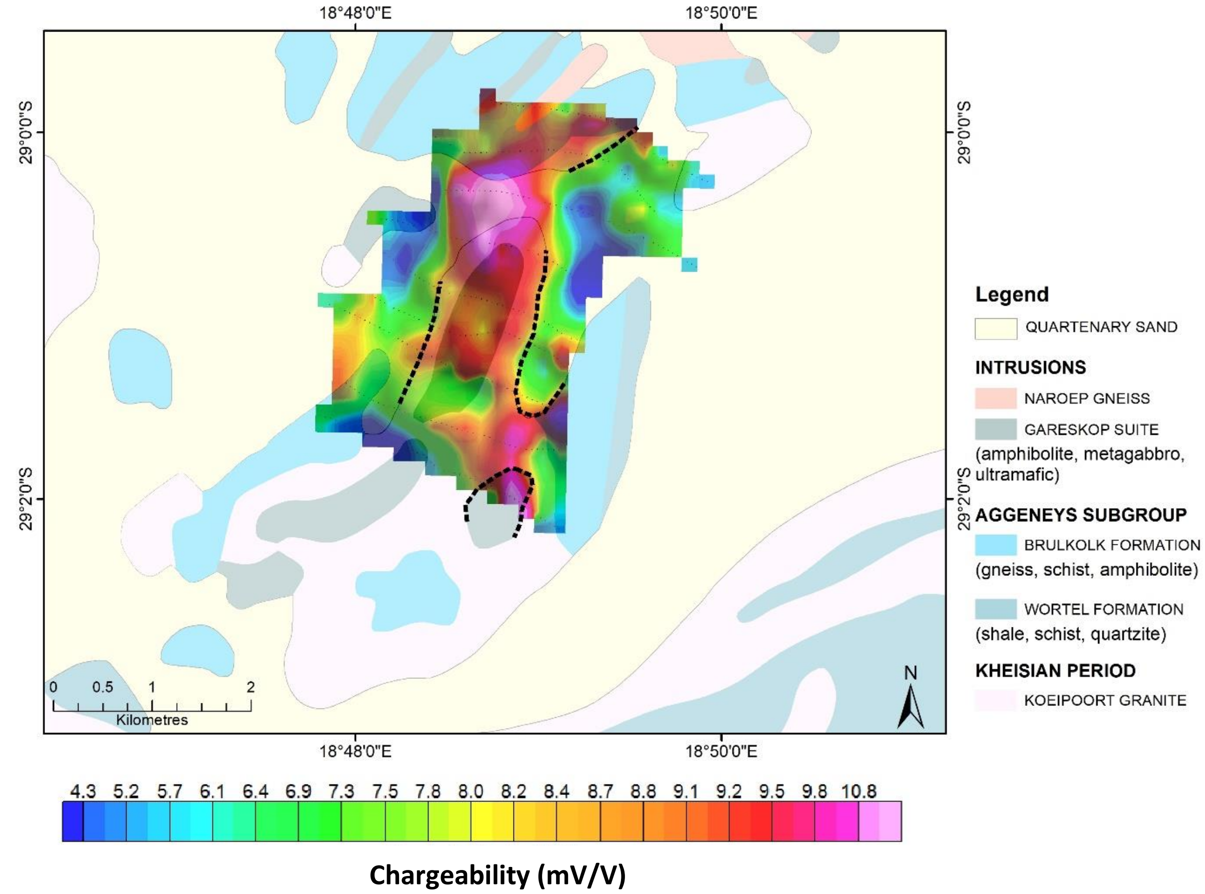

Figure 4.5. Chargeability map of the farm overlain on an excerpt from the 1:250 000 scale Pofadder geological map. The line demarcation indicate the mapped lithology contacts mainly following the Koeipoort granite and amphibolite dykes and parts of the Brulkolk Formation rocks.

The resistivity map shows on average high resistivities of the subsurface at shallow (~25 m) depth, with good resolution (half that of station spacing) (Figure 4.3). For ease of interpretation and reference to the map it has been labelled with the following criteria: high amplitude resistivity (7500 – 14 000 ohm.m) labelled R, intermediate amplitudes resistivity (4700 – 7500 ohm.m) not labelled and low amplitude resistivity or conductivity (0 – 4700 ohm.m) labelled P. The high resistivity readings are expected in such desert terrains that host metamorphic rocks due to the dry conditions, limited vegetation and hard rock (granite and gneiss) present (Simpson and Bahr, 2005). The resistivity bodies demarcated R appear well connected throughout the grid with few areas of discontinuity which could be due to contouring and filtering processes. This body labelled R is 4 km long, striking N-S and at least 200 m wide. Geologically, the high resistivity amplitudes coincides with mapped Koeipoort granite and gneiss of the Brulkolk Formation (Figure 4.4), however within the same rock unit the resistivities vary considerable indicating possible weathered areas, existence of different lithologies and/or change of lithology with depth. The P anomalies coincides with sand cover except for P3 which coincides with an outcropping granite, however this section of the outcrop could consist of weathered material or accumulated sand/clay.

The comparison of the two datasets revealed that most of the C1 anomaly (10 – 11 mV/V) coincides with high resistivity amplitudes (10 – 15 kOhm.m) and the remainder with lesser resistivity amplitude.

The rest of the chargeable areas coincides with high and intermediate resistivity (Figure 4.3). Low chargeable areas coincides with lesser resistive areas (D on the chargeable map and P on the resistivity map). Based on this data, the chargeable material appear to be confined within the resistive rocks in most parts of the investigated areas and trending the same direction as resistivity structures, NE. This could indicated that the chargeable material may be structurally controlled.

The profile extracted along profile R-R' is presented in Figure 4.6**.**

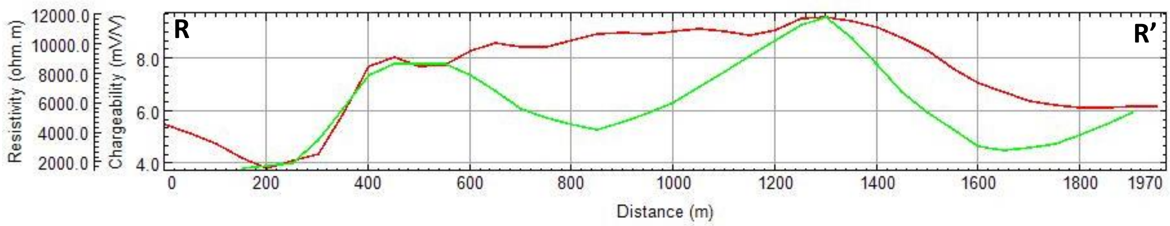

Figure 4.6. Profile R-R' of extracted from the chargeability (red) and resistivity grids (green).

The high chargeability and lower resistivity amplitudes could be areas with accumulated sands, weathered material and/or clay. The decrease in resistivity between 600 and 1200 m distance on Profile R-R' could indicate weakness in the rock or dipping of the resistive geology allowing a local valley-like features to form.

4.3 Gravity Results

The residual gravity map shows geological units and features of high and low gravity anomalies coinciding with mapped Brulkolk Formation rocks, Koeipoort granite and sand cover (Figure 4.7, Figure 4.8 and Figure 4.9). The map is sub-sectioned into elevated gravity values features: G1 and G2; low gravity amplitudes: H1 and H2 and background labelled C (Figure 4.8). Feature G1 covers ~ 800 m x 400 m in surface area with residual gravity anomaly of up to +0.25 mGal. Most areas of G1 coincides with mapped rocks of the Brulkolk Formation (gneiss, schist and amphibolite rocks) but the high gravity anomaly feature also extends to the mapped sand cover. The continuity of the elevated gravity values (above +0.109 mGal) indicate that the Brulkolk Formation rocks continue southward beneath the sand cover and/or amphibolite dykes extends toward the north-east. The high gravity values coincides with high magnetic anomalies that are interpreted as due to amphibolite dykes and Brulkolk Formation rocks. Within G1 there are areas with decreased residual gravity amplitudes which are linear, these areas are interpreted as possible faults but could also be weathered joints in the rock. Feature H1 has low (negative) gravity residuals of -0.53 to -0.1 mGal. The gravity intensity of this feature increases outwards. On the surface this section of the grid coincides with the foot of the elevated outcrop mapped as Koeipoort Granite. The dimensions of feature G2 are 200 m x 250 m with gravity residual between 0.01 and 0.25 mGal. This feature could indicate that the amphibolite dyke continue beneath the sand cover toward the NE. Mapped feature H2 coincides with mapped granites (Figure 4.9). Based on the mapped lithology and literature publications (Dentith and Mudge, 2014a), the elevated gravity residual for structures G1 and G2 are interpreted as deeper structures whose extents matches the mapped gneiss/schist of the Brulkolk Formation and amphibolite dykes of the Gareskop Suite. The low gravity amplitudes H1 and H2 are interpreted as being correlated with the Koeipoort granites.

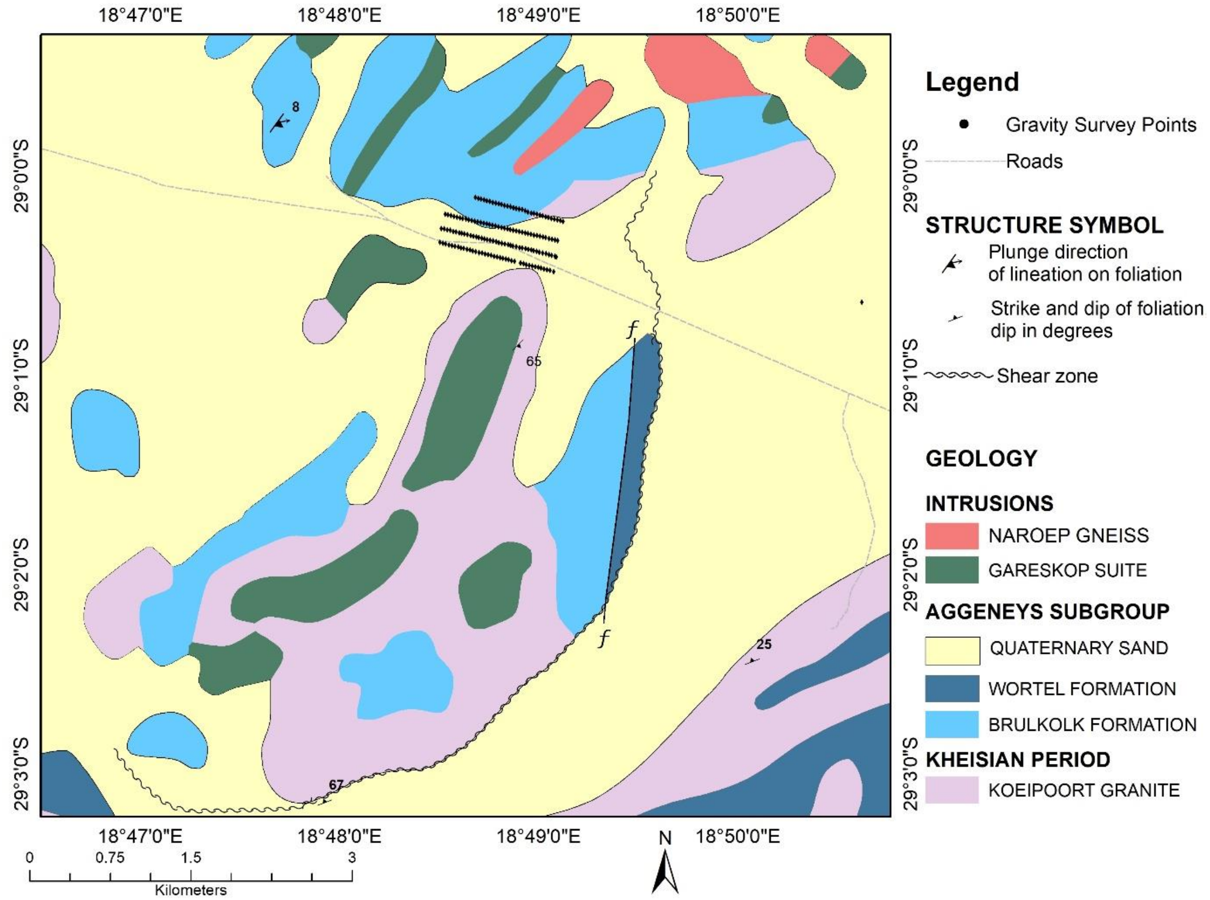

Figure 4.7. An excerpt from the 1:250 000 scale Pofadder geology map of the Wortel Farm study area, as published by Council for Geoscience (2007), overlaid with the gravity survey traverses.

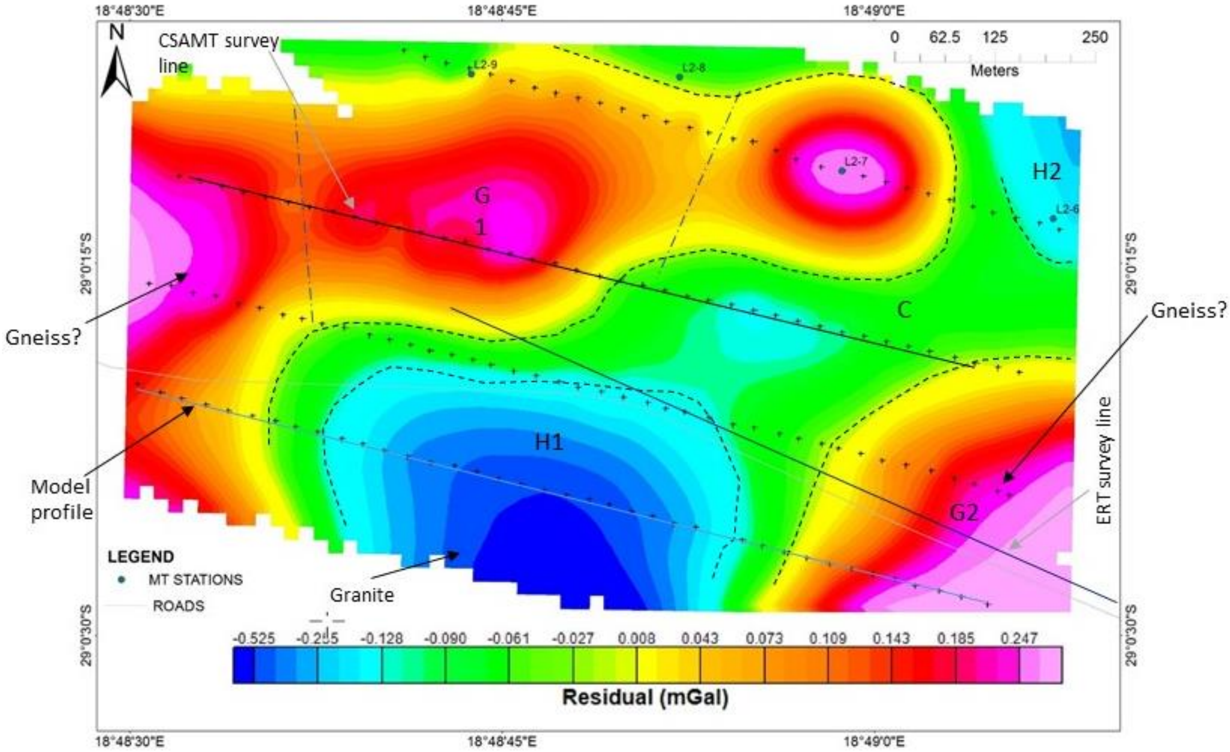

Figure 4.8. Qualitatively interpreted residual gravity map highlighting gravity variations of the present rocks. The overlay include the ERT survey line, CSAMT and modelled profile.

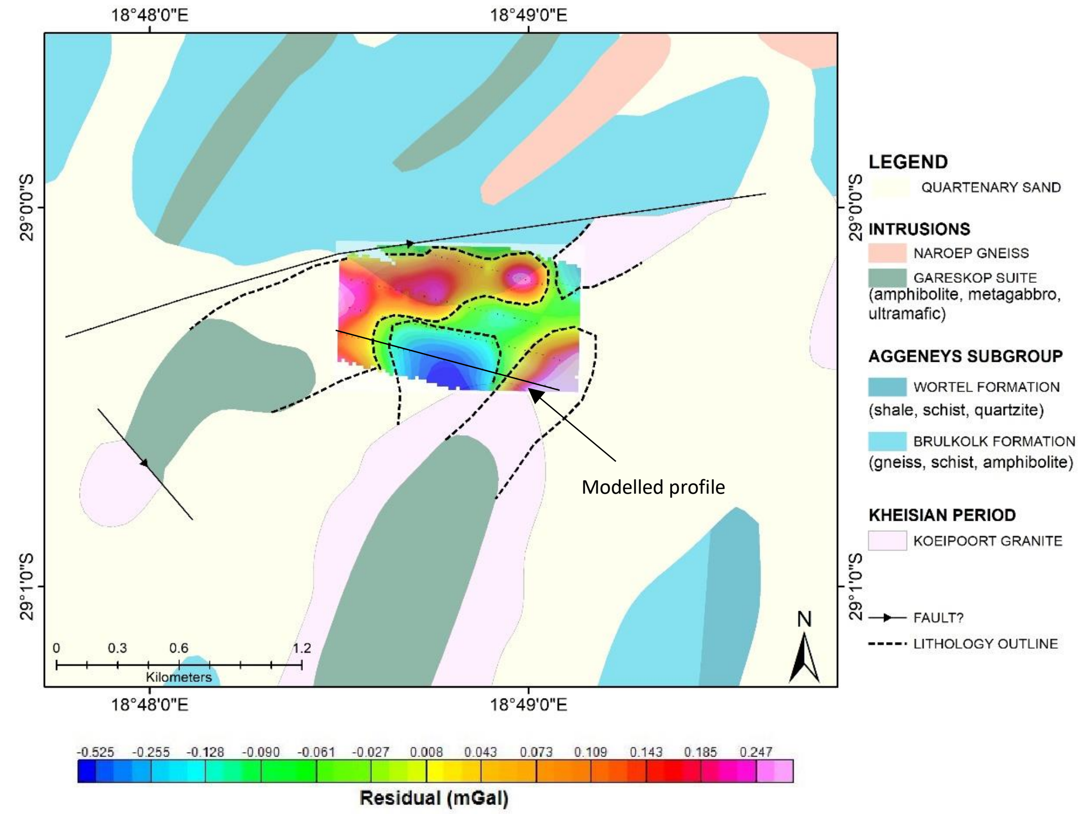

Figure 4.9. A residual gravity map of the farm overlain on a halftone excerpt from the 1:250 000 scale Pofadder geological map. The demarcating lines links the anomalies with the interpreted possible lithology source as well as modelled profile.

A gravity profile is modelled with Grav2dc 2.5D software developed by Dr G. Cooper (Cooper, 1998). The profile modelled shows elevated gravity values from the NW. The gravity values decreases along the traverse toward the SE and eventually increases again after 600 m distance along the traverse. The profile coincides with mapped sand cover indicating that the rock(s) are under sand cover. The gravity variations indicate that there are at least two lithologies. Based on the surrounding outcrops and the interpretation of the residual gravity map, two major lithologies are identified: gneiss of the Brulkolk Formatoin or amphibolite of the Gareskop Suite indicated by high gravity values and Koeipoort granite indicated by low gravity values. The model is shy of 1 km depth.

This geological model solely based on the residual gravity data and 1:250 000 scale geology map, reveals that the rock with lesser gravity readings sits between high gravity values of the Brulkolk Formation and/or Gareskop Suite rocks (Figure 4.10). In Figure 4.10 the fitted layers indicate that the oldest rock unit (Koeipoort granite) in the area is surrounded by the younger rocks. The values used are summarised in Table 4.1. The modelled lithologies are presented in densities however the fitted data is still in mGal.

Table 4.1. List of lithologies modelled and the densities used.

Lithology	**Density (g/cm^3)**
Koeipoort granite	2.40
Gareskop Suite/Brulkolk Formation	2.78

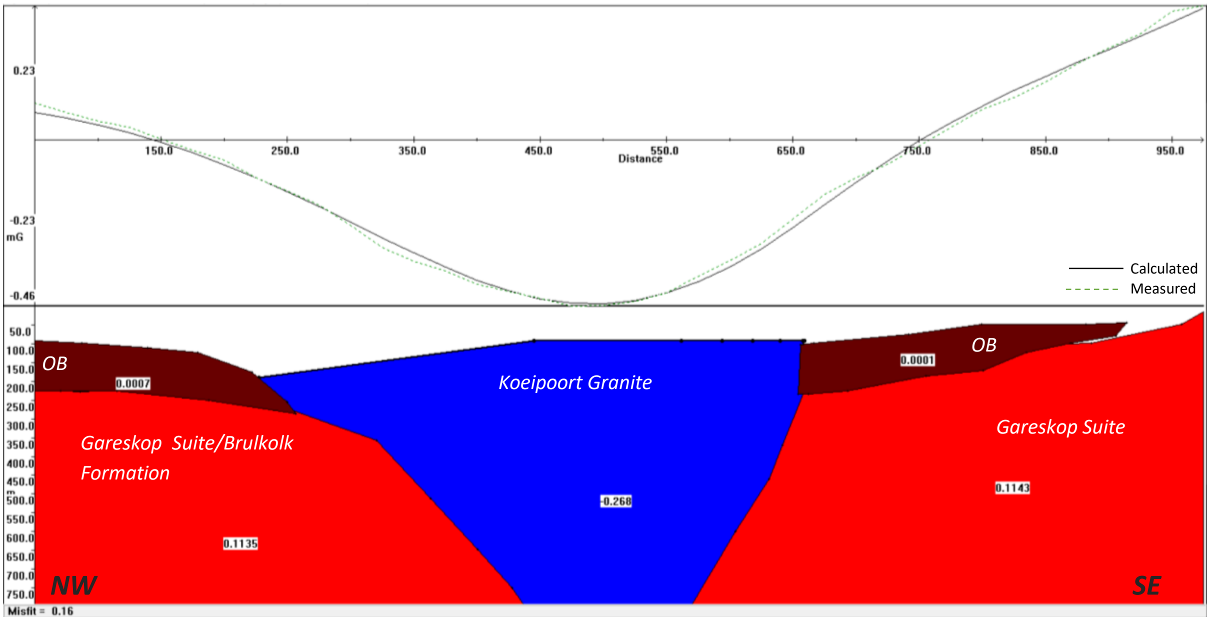

Figure 4.10. A 2.5D gravity model fit for the gravity profile, first profile from the south of the grid. The granite has lesser densitiy and sits between high density lithoogies interpreted as Gareskop Suite and/or Brulkolk Formation. OB is the overburden below 50 m depth. The achieved misfit is 0.16% and distance in meters.

4.4 Electrical Resistivity Tomography Results

The ERT inversion 2D cross section shows lateral changes in resistivity and with depth. This method mapped resistive geology up to 75 m depth, over a 1 km long traverse, mapping rocks with resistivities up to 14 kOhm.m (Figure 4.11). On the geology map the ERT traverse coincides with the Quartenary Kalahari sand cover (Figure 4.12). The top 26 m of the cross section reveals less resistive (conductive) subsurface with varying textures, indicated by the varying resistivities amplitude (10 - 250 ohm.m.). The resistivity table (Palacky, 1988) links these values with weathered metamorphic rocks, sandstones, gravels and sand. The conductive subsurface coincide with the sand cover that could be mixed with other weathered material and gravels. At 0 – 300 m distance along the traverse the subsurface is consistently conductive up to a 26 m depth, which could indicate that the Quartenary Kalahari sands are potentially hosting brackish ground water. Similar conductive pockets-like features are observed along the traverse at shallow depths. Below the 26 m depth the resistivity increases reaching more than 14 kOhm.m, such high reading are correlated with unweathered metamorphic and sedimentary rocks. While between 0 – 720 m horizontal distance the resistivity increases gradually with depth, at 720 m distance toward the north-west the resistivity sharply increases with depth. This could indicate that to the southeast the high resistivity amplitude rocks are seated deeper than the rocks in the northwest. The observed increase in resistivity at shallow depth at the 720 m distance along the traverse could indicate faulting or thrusting or the Koeipoorts granite being near to surface. Another inferred fault is at 300 m along the traverse indicated by a sharp change in resistivities. The undulation observed throughout the section could indicate uneven layering or weathering abrasions shown by minor ridges and valleys. The inferred fault at 720 m distance maps within what looks like a monoclonal fold. The resistivity profile (Figure 4.11), extracted from the DC resistivity map acquired along with the IP data, confirms the resistivity trend seen on the ERT data, of a gradually increasing resistivities to the west. The residual gravity profile (Figure 4.11) shows that the resistive rocks and corresponding geological units at depth have lower gravity response than the outcropping Brulkolk Formation gneiss. The rock units with at least a 10 kOhm.m apparent resistivity are interpreted as being granites, based on the mapped geology at surface.

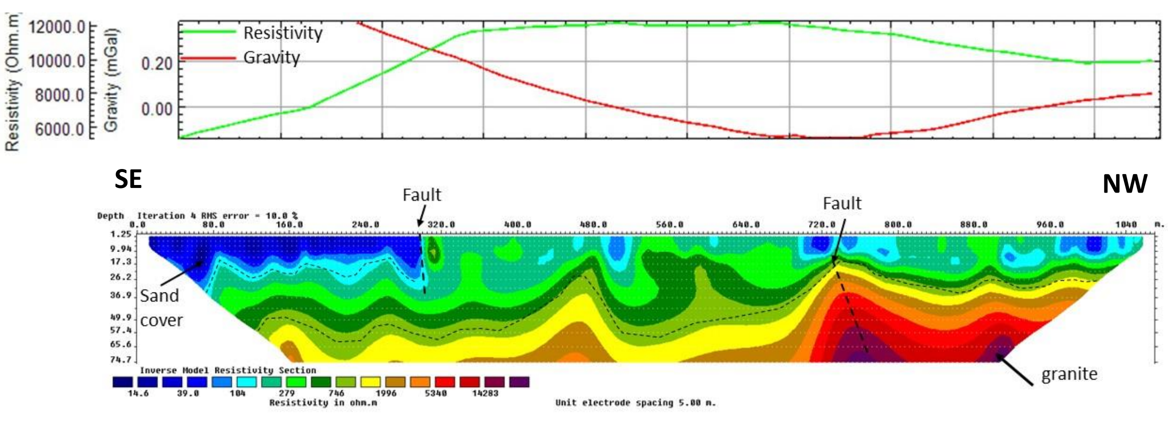

Figure 4.11. ERT 2D cross section map measured across parts of the IP anomaly, overlaid with interpretation. The gravity profile is extracted along the ERT traverse from the residual gravity map and the resistivity from the DC resistivity map acquired along with the IP data. The highly resistive material measures low densities.

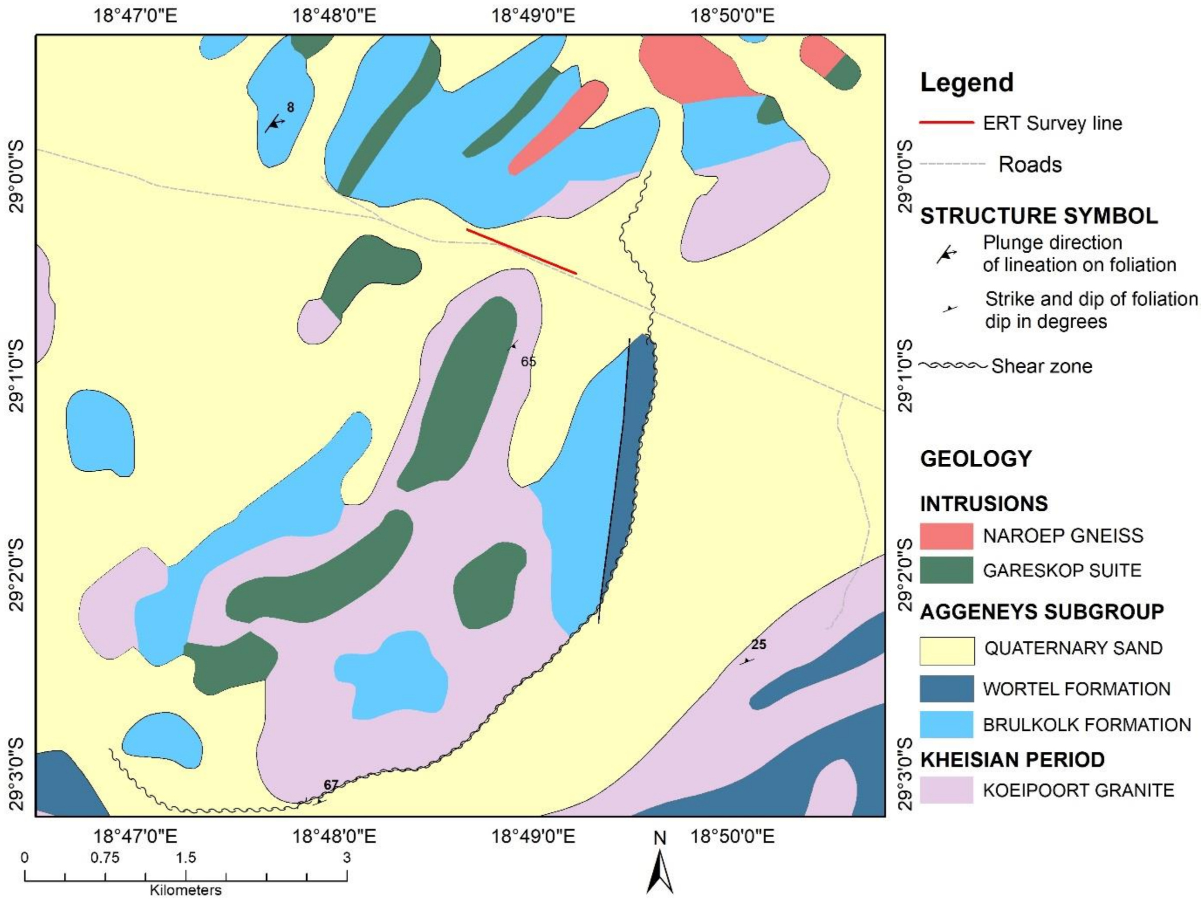

Figure 4.12. An excerpt from the 1:250 000 scale Pofadder geology map of the Wortel Farm study area, as published by Council for Geoscience (2007), overlaid with the ERT survey line.

4.5 Magnetotelluric Results

The CSAMT data were acquired along the second traverse from the north of the gravity survey grid (Figure 4.14) and across the IP anomaly C1 coinciding with mapped rocks of the Brulkolk Formation and sand cover (Figure 4.13). This CSAMT traverse is called CSAMT1. The 2D cross section revealed the subsurface geological settings and resistivity properties up to 400 m depth and 1 km along the traverse. The colour bar presented shows: lowest resistivity in pink and highest in blue, following the geophysics community standard of presenting MT data. Between 0 and 100 m depth a lesser resistive (conductive) layer occurs but is intercepted by a resistive oblate body centred around 600 m horizontal distance along the traverse where a resistive structure CR1 protrudes. The conductive layer at surface, with average resistivity of ~1000 ohm.m, could indicate that it is composed of different materials, including the mapped sand cover, weathered rock types and gravels that are expected to be somewhat conductive in this area (Palacky, 1988). The protruding (outcropping) feature CR1 with resistivity of 2600 – 4000 ohm.m, due to its oblate form increases in width with depth, reaching a 700 m width, up to 200 m depth extent and is surrounded again by slightly more conductive material, laterally and in depth as depicted in Figure 4.14. Below these units is a somewhat conductive layer CS2 of approximately 1200 ohm.m that is at least 50 m thick and overlying CR2 with 1800 – 3500 ohm.m resistivity. The pinching of CR1 at 250 m and sloping toward the pinch between 200 and 300 m depth, and 250 and 550 m distance could indicate a possible thrust faulting and/or shearing. A similar feature labelled *f2*, parallel to *f1*, occurs between 150 and 250 m distance, below 200 m depth that could also be a thrust fault. The anomaly CR2s resistivity increases toward its core, similar to CR1, which could indicate that CR2 is composed of different lithologies or the same rock unit with varying texture or the varying in resistivity is due to regularisation in the contouring algorithm. A residual gravity and DC resistivity profiles were extracted along the same CSAMT1 survey line. The highly resistive body CR1 coincides with low to negative gravity amplitudes while conductive bodies CS1, CS2 and resistive CR2 coincide with an increasing gravity amplitudes, similar to the trend observed on the ERT cross section. The resistivity profile response corroborate the resistivity features of CSAMT1. The resistive material (CR1 & CR2) is interpreted as the Brulkolk Formation rocks that were thrusted at depth and displaced. The breccia material (indicated by relatively lesser resistivity) then filled the thrust zone.

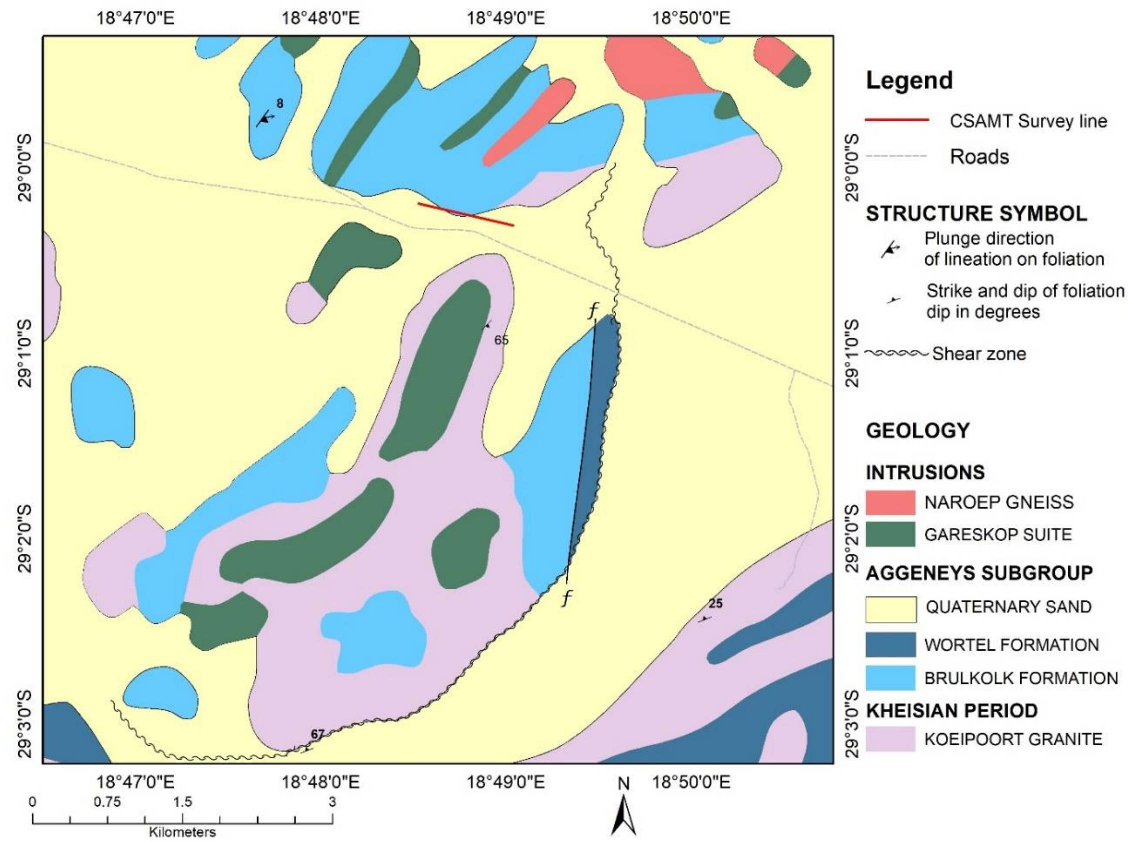

Figure 4.13. An excerpt from the 1:250 000 scale Pofadder geology map of the Wortel Farm study area, as published by Council for Geoscience (2007), overlaid with the CSAMT1 survey line.

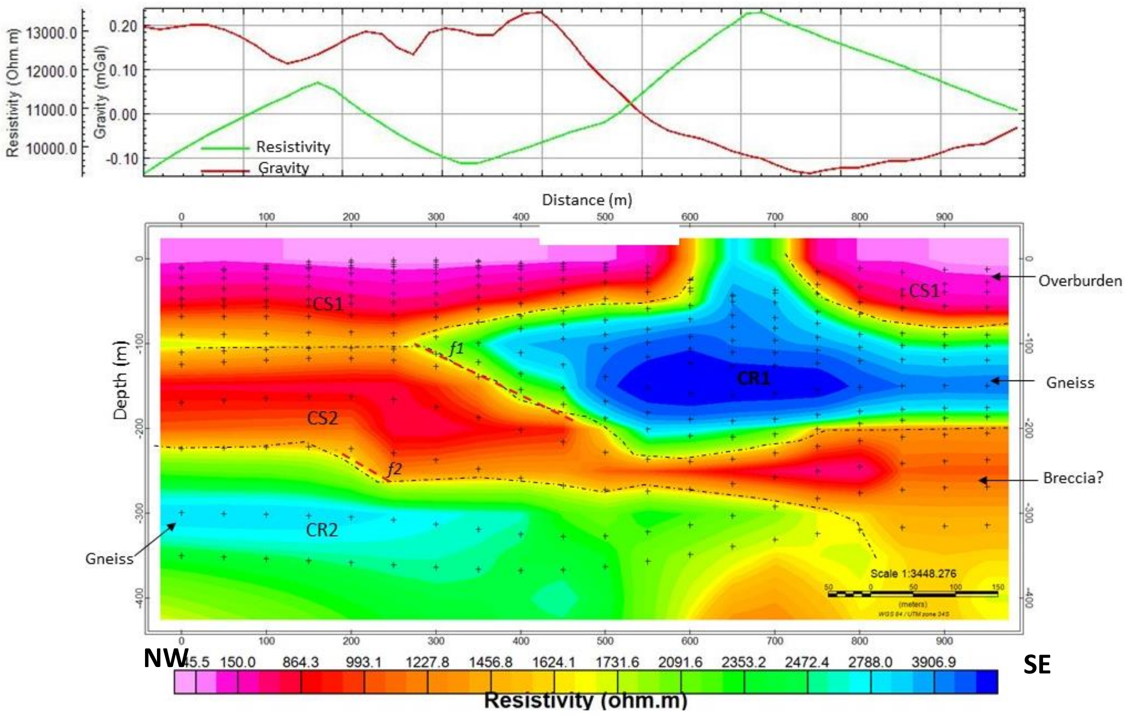

Figure 4.14. CSAMT1 resistivity 2D cross section map overlaid with qualitative interpretation. The added profiles are extracted from the residual gravity and DC resistivity maps along the CSAMT1 traverse. The DC resistivity maps at least 25 m depth of good resolution.

This CSAMT 2D cross section shown in Figure 4.16 stems from a much longer traverse undertaken parallel to CSAMT1 and is called CSAMT2. It reveals the subsurface geological layering up to 1000 m depth, over 10 km distance along the traverse consisting of 12 CSAMT/AMT stations. The profile coincides with outcropping Brulkolk Formation, Gareskop Suite and granite rocks partially overlain by a sand cover (Figure 4.15). The cross section is subdivided into units labelled L1-L4 based on depth and resistivity ranges (Figure 4.16). L1 has resistivity range of 0 – 2500 ohm.m, L2 between 2500 and 7000 ohm.m, L3 between 7000 and 19 000 ohm.m and L4 between 19 000 and 27 000 ohm.m. The resistivity increases gradually with depth indicating changes in lithology or rock composition with depth. Based on mapped geology, resistivities and thickness of the layers, L1 could consist of sandcover, weathering material of the Brulkolk Formation rocks, dykes and granite. With increasing depth, the outcropping rocks texture changes approaching a semi-consolidated material, indicated by increasing resistivities. Layer L2 is correlated with a lesser weathered rocks of the Brulkok Formation and granites. The increasing resistivities with depth are interpreted as with depth the Brulkolk Formation and granite rocks are more compact and less exposed to weathering elements. Between stations 6 and 9, where chargeable anomalies are mapped, L2 is dome shaped. The doming can be associated with the outcrop labelled CR1 in Figure 4.14.

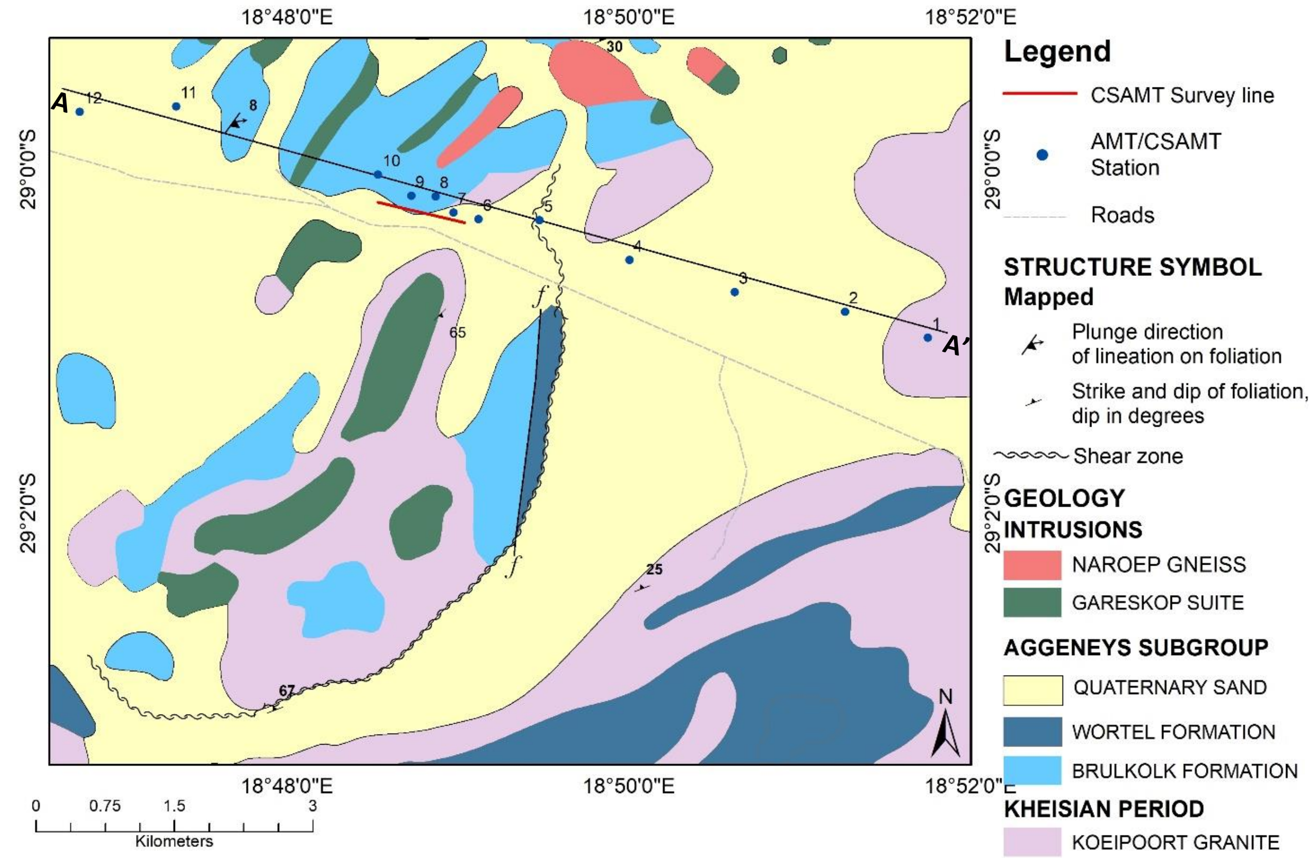

Figure 4.15. An excerpt from the 1:250 000 scale Pofadder geology map of the Wortel Farm study area, as published by Council for Geoscience (2007), overlaid with the CSAMT/AMT survey stations.

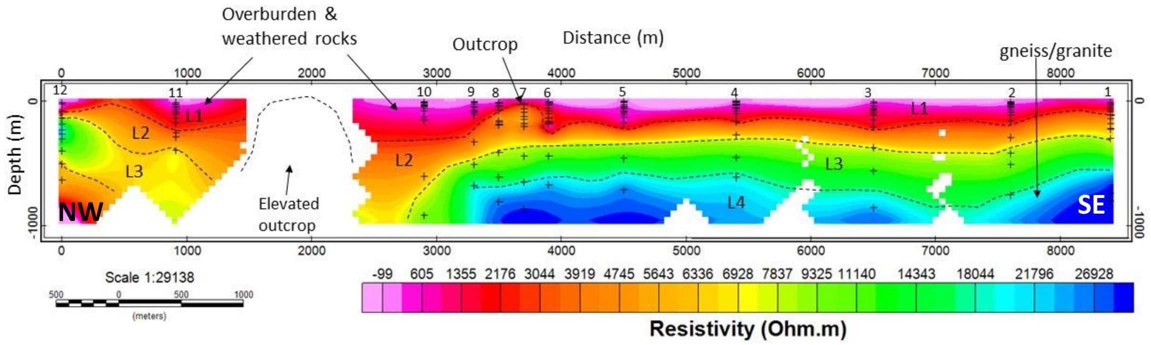

Figure 4.16. The CSAMT2 resistivity 2D cross section of the data collected along AMT stations, overlaid with qualitative interpretation.

The AMT 2D cross section shown in Figure 4.17 follows the same long traverse of CSAMT2 and labelled AMT2. It reveals the much more simplified subsurface geological structures based on resistivity changes, along a 10 km profile consisting of 12 stations. The achieved depth of penetration is 5 km and resistivity amplitudes ranges between 1 - $1x10^6$ ohm.m which is expected in this terrain due to dry metamorphosed rocks (Simpson and Bahr, 2005).

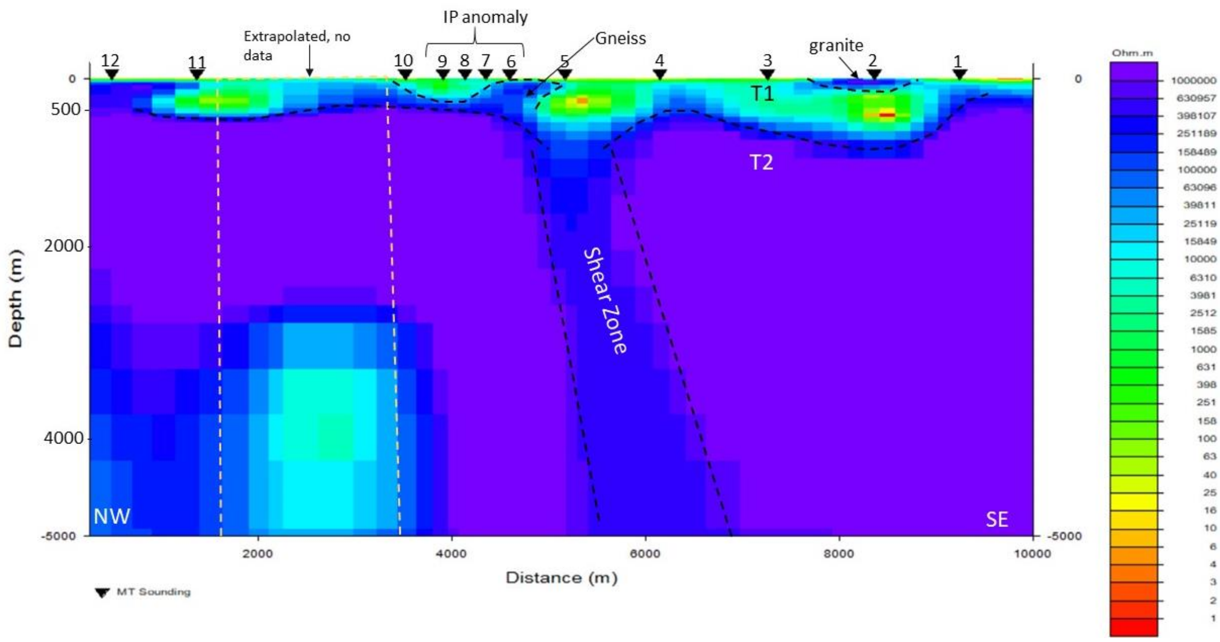

Figure 4.17. An AMT inversion section taken along the same CSAMT2 stations and the A-A' profile shown on the magnetic map, Figure 4.1 & Figure 4.15.

Geologically, the profile coincides with mapped Koeipoort granite, Brulkolk Formation and Gareskop Suite rocks and sand cover (Figure 4.15). The top 500 m depth shows more conductive very shallow crustal material below which are the highly resistive rocks of the slightly deeper crust. The AMT cross section has been subdivided into T1 for ±500 m and lesser depths and T2 for 500 m and deeper.

The T1 section shows mixture of relatively intermediate to high resistivity amplitudes (60 – 40 kOhm.m). According to Simpson and Bahr (2005) the dry igneous and metamorphic rocks records higher resistivity values. The conductive areas (1 – 6 kOhm.m) are mapped at stations, 2-5, 7-9 and 11 and they coincide with mapped Koeipoort granites, Brulkolk Formation rocks (gneiss, conglomerate, amphibolite and schist) and sand cover. The lesser resistive areas could be sand cover, sand with moisture, weathered material and thrusted zones. The more resistive structure could the less weathered parts of the Brulkolk Formation and granite as seen on CSAMT1 map including thrusting zones. The resistive dome observed between stations 5 and 7 act as a cap on the SE dipping conductor under station 5 and is similar to the dome feature mapped on CSAMT2. Undulation is also mapped throughout this profile at larger scale compared to the ERT data and interpreted as weathering abrasions that left the layering uneven. Section T2 consist of very high resistivities with few areas showing a slight decrease in resistivity. Under stations 11 and 12, below a 2 km depth is a less resistive amplitude feature that appear extending past the mapped 5 km depth. This could indicate that there is a different lithology at depth beneath the gneiss and schist of the Brulkolk Formation and Koeipoort granite, or it could be an indicator of a deformed rock(s) like faulted and thrusted areas at depth. The SE dipping linear structure apparent under station 5 coincides with mapped shear zone as marked on the geology map (Figure 4.15). This indicates that the AMT method mapped the shear zone as well as its width (ca 1 km) and depth extent. The shear zone could have also acted as pathway for material that caused an uplift in stations 5-8. This dome feature coincide with parts of the IP anomaly C1 and could be the contributing source of the IP anomaly.

4.6 Modelling

A magnetic profile A-A’ (Figure 4.1) was extracted along the CSAMT2/AMT2 traverse, modelled and presented below (Figure 4.18). The objectives of this model are to further understand the magnetic response on the farm and the rocks that could be related to it and how they relate/corroborate with CSAMT/AMT datasets for the top 1000 m depth. The model is carried out on PyGMI modelling and interpretation software (Cole, 2012) and magnetic physical properties used for the model are listed in Table 4.2 below.

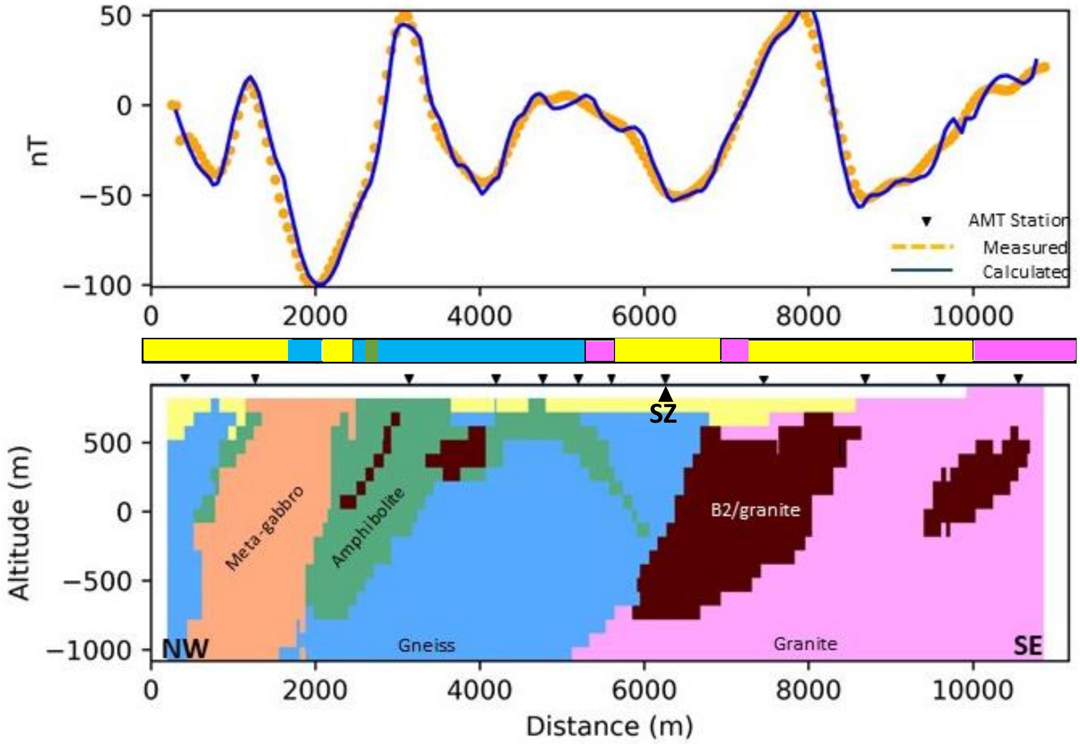

Figure 4.18. A postulated magnetic model of profile A-A’ based on the mapped lithologies and magnetic responses. SZ indicate the position of shear zone as mapped and confirmed by AMT data. The horizontal bar with colours indicate the mapped lithologies.

Table 4.2. List of magnetic physical properties used for the model presented in Figure 4.18.

Lithology	Mapped lithology	Susceptibility (x10-3 SI)	Remanent Magnetic Intensity (nT)	Remanent Magnetism (A/m)	Inclination (°)	Declination (°)
Granite	Koeipoort granite	0.0176	796.71	0.634	-66.2	-22.8
Granite (Intrusion)	Sand cover	0.026	682.4	0.54	61	100
Gneiss	Brulkolk Formation	0.01	48.7	0.4	66	300
Amphibolite	Brulkolk Formation	0.003	71.15	0.06	-37	105.6
Meta-gabbro	Gareskop Suite	0.02	820.6	0.65	62	-142
	Sand cover	-	-	-	-63	-17

The profile is modelled up to 1 km depth using magnetic parameters from the palaeomagnetic results and National Petrophysical Database of the CGS (CGS, 2019b) and mapped geology.

From the NW, largely guided by the outcropping geology and magnetic response, at horizontal distance 0 - 6.1 km is the Brulkolk Formation package (gneiss, amphibolite and schist) intruded by the Gareskop Suite (amphibolite dykes, meta-gabbro and ultramafic rocks) between AMT stations 10 and 11. Between distance 6.1 – 10.4 km is the Koeipoort granite outcropping at stations 1, 4, 5 and 7. The continuation of the granite between station 1 and 7 was assumed, guided by the surrounding outcrops. The high amplitude anomaly around 8 km horizontal distance forms part of the B2 lineament demarcated in Figure 4.1 and the anomaly around the 10 km distance forms part of body C. the distinction between the 2 granites is based on the magnetic response that indicate increased magnetic material within the package.

Based on the mapped geology the most abundant/basement like rock are Koeipoort granite and Brulkolk Formation rocks, and they fitted background response well. The high magnetic amplitudes (both negative and positive) and geology indicate a presence of another source with higher susceptibility. From the NW, the negative anomaly is associated with the Gareskop Suite package, here labelled as meta-gabbro known for its remanence in the area, followed by a positive anomaly associated with amphibolites. Toward the SE on the granite are two positive anomalies associated with B2 and edge of C anomalies (Figure 4.1). The interpretation inferred lineament (B2) or high concentration of magnetic material on C. Minor traces of B2/B1 are presented along the traverse indicating that it could be source of anomalies elsewhere or a rock with similar properties. The disappearing of L3 layer on CSAMT2 profile could be associated with the intrusion that displaced the Brulkolk Formation, indicated by the decrease in resistivity.

The comparison of the model with CSAMT2/AMT2 section indicates that the uplift at stations 5-8 (where high concentration of chargeability are mapped) coincides with decrease in magnetism. The uplift/chargeable material could have replaced the magnetic minerals. The mapped shear zone on the AMT map is only visible from at least 1 km depth, beyond the modelled section. The folded amphibolite between 4 km and 6 km horizontal distance follows the dome-like structured mapped on CSAMT2 and AMT maps.

The model presented here is a simplified interpretation of the magnetic subsurface and is one of many possible best fits.

All the results presented thus far, including geochemical data, will be discussed further in Chapter 5 as they are integrated and geologically corroborate and more inferences drawn.

Chapter 5: Discussion

Results presented and interpretations made in the previous chapters are discussed further in this chapter, including elaborations on the geological meaning of the interpretations, further inferences and conclusions that could be drawn from the integration of the data, in view of possibly identifying mineralised areas and the potential of the mineralisation. The datasets are discussed in the order: magnetic, gravity, ERT, CSAMT, AMT, IP and DC resistivity, geochemical and dataset integration, for better presentation of the discussion.

The magnetic data showed that high magnetic amplitude anomalies indicating elevated magnetic susceptibility values is confined to body A while the surrounding geological units register lower susceptibility (Figure 4.1 & Figure 5.1). A comparison of magnetics with the mapped geology correlates the positive anomalies with the Brulkolk Formation rocks (gneiss, schist and amphibolite) mapped outline or a buried unknown magnetic rock with a similar outline, negative anomalies are associated with the amphibolite dyke intrusions of the Gareskop Suite and indicate a strong remanent magnetic component being associated with this rock type. The interpretation of the Aggeneys mineral deposit shows a high magnetic amplitude associated with amphibolite, gossans and iron formation of the Gams Formation also known as Aggeneys Formation, which hosts the Aggeneys mineralisation (de Beer, 2015).

Various authors (Bailie et al., 2007; Cornell et al., 2006) mapped and published the deformation events that occurred throughout the Namaqua Sector. Evidence of some of the deformations is seen on a small and large scale, with some having been mapped geologically and some mapped through the geophysical surveys conducted during this study (Figure 5.1). Mapped structures that were confirmed by magnetic data were shear zones while additional folds and faults were inferred. Based on the mapped geological structures those observed from these data, the following sequence of events is deduced:

- Thrusting and shearing that established the NE-trending on the surrounding geology,
- More shearing followed, occurring around body A and causing folding. These events caused the separation of anomaly B2 from B1,
- Fracturing and faulting that may have existed before shearing and folding developed further along the fold axial and became the pathway for amphibolite dykes to intrude to the surface,
- Finally, the dykes intruded (Figure 5.1).
- At 1200 – 950 Ma a tectonic event occurred (Bailie et al., 2007; Cornell et al., 2006) that possibly affected the initial deposition of the rocks in the area leaving the rocks in this position (Figure 5.1).

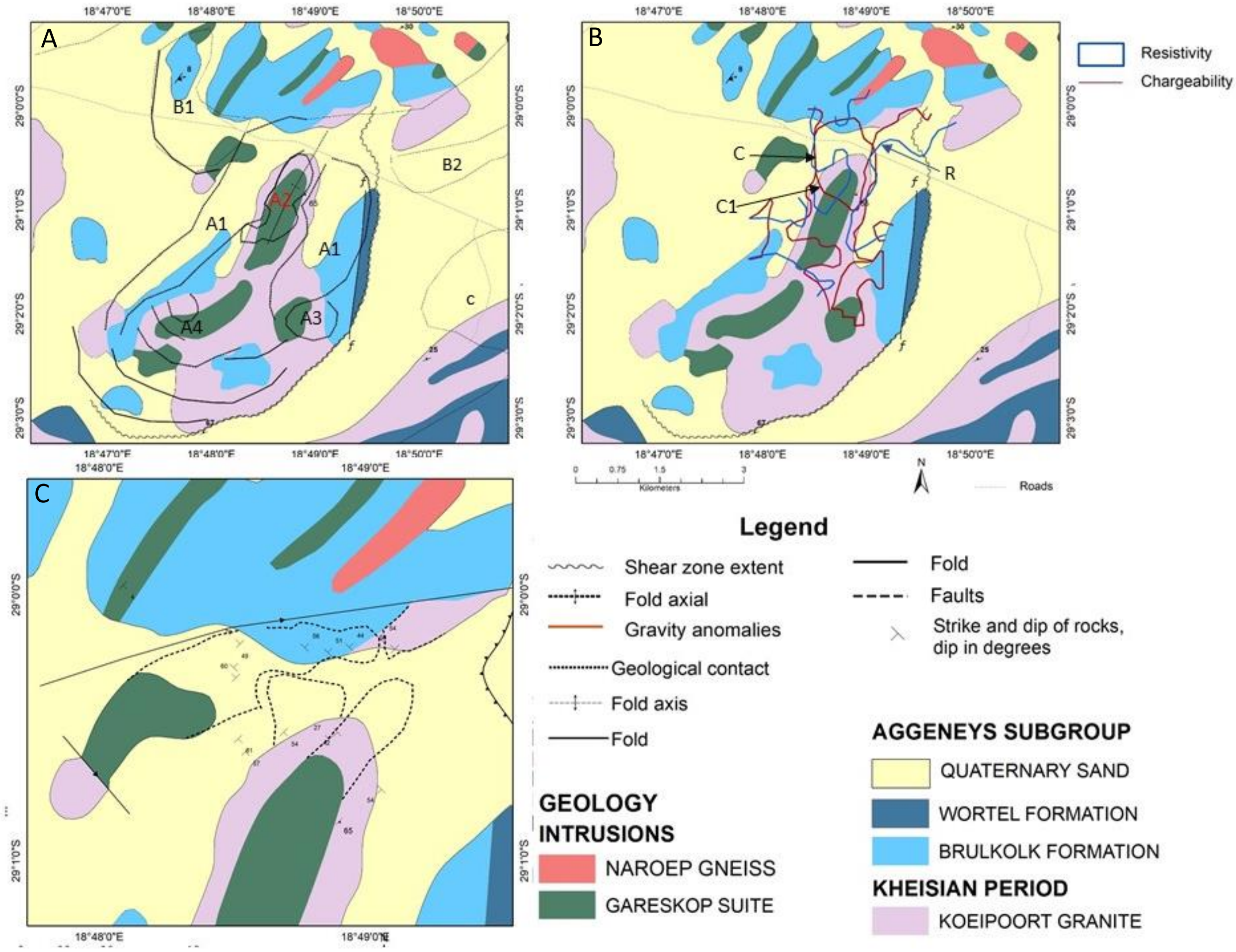

Figure 5.1. An excerpt from the 1:250 000 scale Pofadder geology map, as published by the Council for Geoscience (2007), overlain with qualitative interpretations. Map A is overlain with magnetic trends, B overlain with chargeability and resistivity trends and C overlain with mapped structural and gravity trends (red marking gravity high and blue gravity low).

The drilled palaeomagnetic core samples data revealed that the sampled rocks possesses both negative and positive inclination directions indicating that the deposition/magnetism occurred at different times and positive inclination direction shows that some rocks carries remanent magnetisation. As such positive magnetic declination of the rocks indicates that the sampled rocks were magnetised when the magnetic north was to the east of the geographic north.

The gravity data, although covering a smaller section of the study area (Figure 5.1), indicated that there are at least two main structures: 1) E-W-trending high gravity readings and 2) low gravity amplitude geological units. The extent of the high gravity amplitude structure correlates with the Brulkolk Formation rocks, especially the gneisses and the low gravity amplitude rock is interpreted as being due to Koeipoort granites, which in some areas overlies the gneiss. Post Namaqua events the Brulkolk Formation (1.9 – 1.2 Ga) was left underlying the Koeipoort granite (~2.0 Ga) in some areas on the farm.

The ERT cross section revealed that the depth to bedrock (regolith thickness) ranges between 20 and 50 m along the mapped traverse and can vary considerably elsewhere on the farm. Areas that may retain water were also mapped along the traverse and coincide with sand cover. Undulation of varying scales was interpreted as uneven layering due to weathering abrasions. Two interpreted faults with one located on the steep dipping monoclinal fold (Figure 5.1C), were identified. The low gravity amplitude rocks correlated with high resistivity rocks.

The 1 km CSAMT1 2D resistivity cross section profile showed that thrusting occurred at depth that resulted in a breaking of a resistive feature, and a section of it ending up close to surface while the other at depth.

The 10 km CSAMT2 2D resistivity profile mapped the top 1 km regional geological settings of the subsurface, revealing an increase in resistivity with depth which is associated with change in crustal rock texture with depth. The change in layering and resistivity between stations 10 – 12 is associated with the intrusions occurrence (Gareskop Suite) including the dome-like structure between stations 6 – 9 (Figure 4.16), that registered a relatively lower resistivity and affected the layering.

The AMT2 cross section mapped the structural setting up to 5 km depth over the same CSAMT2 10 km long profile. The undulations observed at 500 m depth and deeper are similar to the undulation mapped on the ERT and CSAMT2. The comparison with the geological map correlates the interpreted shear zone with a mapped shear zone that is ~1 km wide and extend beyond the mapped 5 km depth. The mapped dome-like structure at stations 6 – 9 is also apparent here (Figure 5.2) and correlating with high chargeability zones.

The geochemical results showed notable populations of Cr, Co, Cu, Fe, Li, Mg and Ni elements that are associated with pegmatite in the Koeipoort granite and Gareskop Suite dykes on the Wortel Farm study area. High chargeability areas, mapping volumetric response of metallic and clay materials, are interpreted as deposits and source of the geochemically mapped mineral occurrences. The confirmed presence of these element led to conclude that the high chargeabilities could be due to the elements and some clay soil.

Comparison of chargeability and DC resistivity maps made it clear that chargeable materials are hosted by the highly resistive rocks however not stratigraphically confined. Further comparison of chargeability with gravity and magnetic datasets revealed the following (Figure 5.1 and Figure 5.2):

- The gravity grid designed to map parts of anomaly C1 revealed two distinct lithologies, however, the chargeable materials occur across both litholigies further confirming the structurally confinement of the materials.
- Anomaly C1 (10 – 11 mV/V) and C2 (8 – 10 mV/V) correlates with most parts of the A2-A4 anomalies associated with amphibolite dykes of the Gareskop Suite, granite and sand cover. Another indicator of structural confinement.

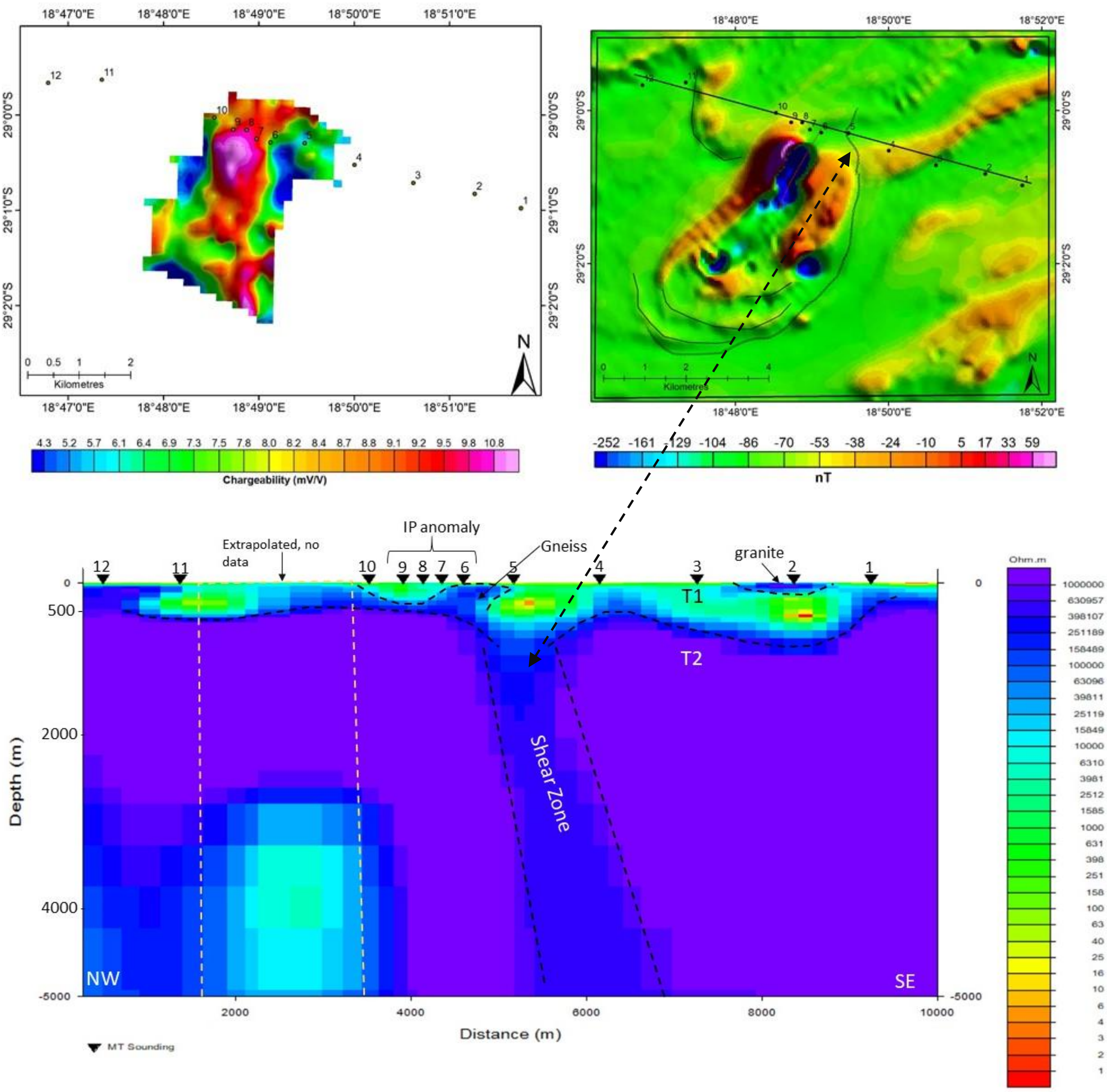

Figure 5.2. A comparitive montage of IP, magnetic and AMT datasets showing a resistivity feature correlated with the mapped shear zone and high chargeabilities location with regards to the AMT profile.

The chargeability responses interpreted as the indicators of the source location of the mapped occurrences and clay material further demonstrates that the inferred occurrence may be found on the dykes and granite but not confined to those regions. Thus, the following conclusions are drawn regarding the source of the elements/mineral occurrences:

i) The mineral occurrences are hosted in the Gareskop Suite and Koeipoort granite, due to weathering and other geological processes over time the residual of the deposit spread across the surrounding rocks, or

ii) The mineralisation occurred with and/or after the intrusion through mineralising fluids like hydrothermal fluids that occurs throughout the Earth's crust, generated by geological processes, and transported to the surface through intrusions pathways, shear zone and faults and settled across lithologies following the weak areas on the farm. A possible copper-porphyry-type hydrothermal mineral deposit. The porphyry is known to occur along faults related to intrusions and is associated with dykes and pipes, in this case the amphibolite dykes. Alteration by products such as tin, tungsten and molybdenum is usually associated with this deposit. The hydrothermal fluids deposited alters the host rocks and metallic minerals replacing the other minerals in the rock. Quartz veins are among the main indicators of alteration (and are observed across the farm and on chargeable zones) and marble is usually found between the altered and unaltered zones (Ayuso et al., 2010; Berger et al., 2008; Briggs, 2014; Lowell and Guilbert, 1970; Singer et al., 2008).

A copper-porphyry is mapped in the Vioolsdrift Suite of the Richtersveld Subprovince in Namibia, north of the study area and close to the South African boarder, where a hydrothermal study showed that the alterations were associated with base metal mineralisation. Similarly, the O'kiep copper deposit, 140 km SW of the farm, is said to be similar to the Haib deposit (Barr and Reid, 1992). The O'kiep deposits presented with highly irregular geometries and distribution to which the occurrence of mineralisation in the rock and source is yet to be determined (Gibson and Kisters, 1996). Or,

iii) A combination of the presented scenarios and alternatives.

The anomalous coinciding magnetic and chargeability bodies (Pardo et al., 2012), magnetic, DC resistivity and chargeability bodies (Pezzot, 2005) also supported by MT resistivity structures (Lee, 2015) have been the indicators of porphyry deposits associated with intrusions, where in most cases the deposit is known. Airo (2015) concluded that a combination of magnetic, chargeability, density and conductive responses is a straightforward way of identifying copper-porphyry deposits, however because of changing geology the resistivity is not the strongest exploration tool.

Based on the literature and the work presented here, two areas with possible mineralisation were identified: M1 and M2 (Figure 5.3). Area M1 has anomalous responses of magnetic, DC resistivity, chargeability and feeder pipe (shear zone) mapped on the AMT. Area M2 has relatively lesser magnetic, DC resistivity and chargeability amplitudes.

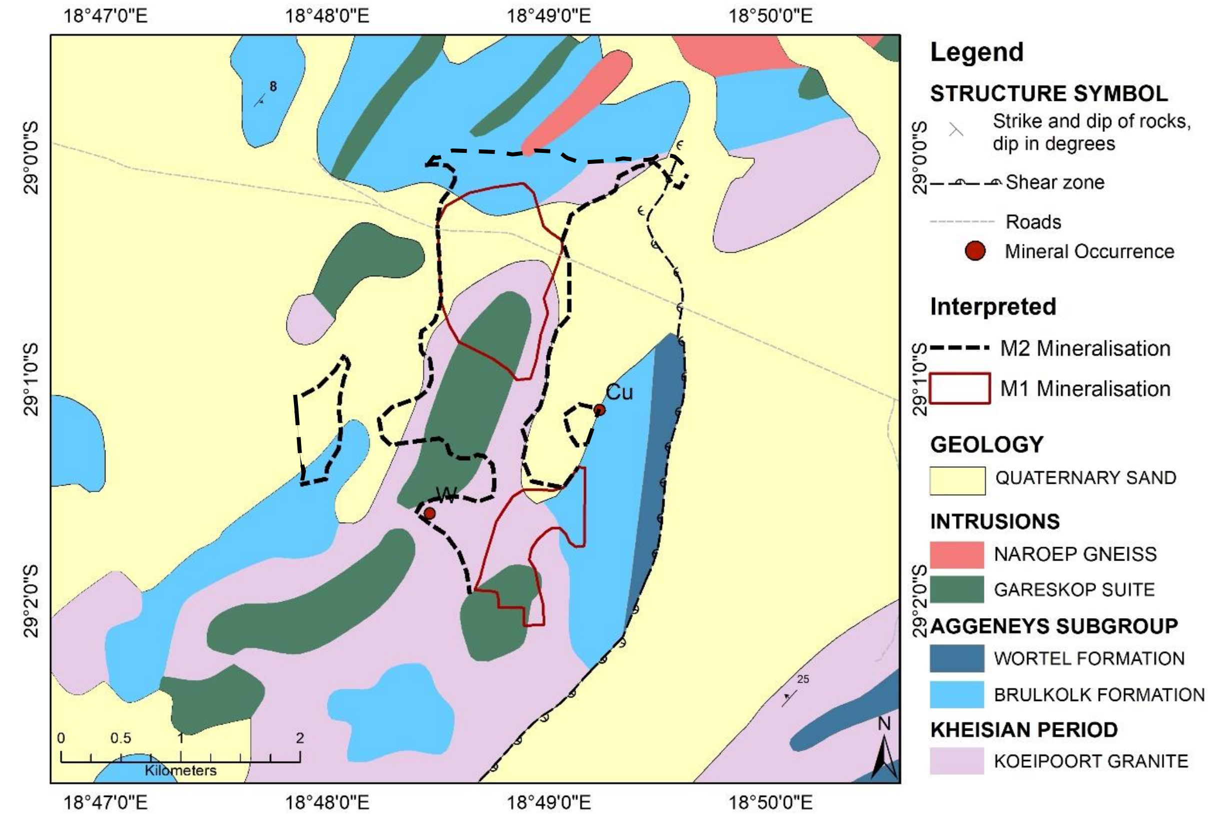

Figure 5.3. An excerpt from the 1:250 000 scale Pofadder geology map overlain with inferred areas of mineralisation. The areas are grouped into M1 and M2, where M1 are areas with high amplitudes of magnetism, DC resistivity and chargeability and M2 are areas with relatively lesser DC resistivity, magnetic and chargeability amplitudes.

Comparison between mapped geology and magnetic map shows the Brulkolk Formation and amphibolite dykes of the Gareskop suite to be magnetic, but differently polarised due to remanence confirmed by petrophysical measurements. The Koeipoort granite has low gravity amplitude compared to Brulkolk Formation (schist, gneiss and amphibolite rocks) and/or amphibolite dykes. The chargeable material, structurally confined, are correlated with the Gareskop Suite rocks that may have been subjected to mineralising fluids whose alteration zone was beyond the suite boundaries.

The gravity map interpretation indicate that the Brulkolk Formation and Gareskop Suite are magnetic with high gravity values and the Koeipoort granite with lesser gravity values. The geophysical data altered the presented geology indicating rock contacts mapped from gravity and magnetic maps, folding and faulting visible on the magnetic and ERT maps (Figure 5.4). The rock outline indicating contact drawn from the magnetic interpretation could be of the outcropping rock or a buried source.

The following could be the series of events that occurred on the farm: th mapped N-S shear zone occurring adjacent to the magnetic body A exerted stress on A that lead to folding of A and separating of the B anomalies and fracturing. Folding of the granite and Brulkolk Formation post-dates the Gareskop Suite intrusions. More folding, thrusting and faulting is seen on ERT, CSAMT, AMT and dip directions. Thrusting mapped at 200 m depth indicate discontinuities in lithology with depth. A detailed rock mapping is required to confirm and/or disapprove these findings and provide greater detail of lithology and structural set-up.

To conclude, the presented data indicate that the farm sits on a sheared region of the NE-trending rocks and the main outcrop experienced shearing, thrusting, folding and faulting of various scales post all rock deposition and intrusions that pre-dates the mentioned deformation. The extent of the mapped shear zone reaches beyond mapped 5 km depth and at 1 km below surface. Change in crustal structure with depth is visible on magnetotelluric datasets including intrusions deposited on the Brulkolk Formation and attribute to the dome-like structure.

The structures such as faults, folds, rock contacts, dips and shear zones and their extents mapped from these data are combined and overlain over the current 1:250 000 scale geology map (Figure 5.4).

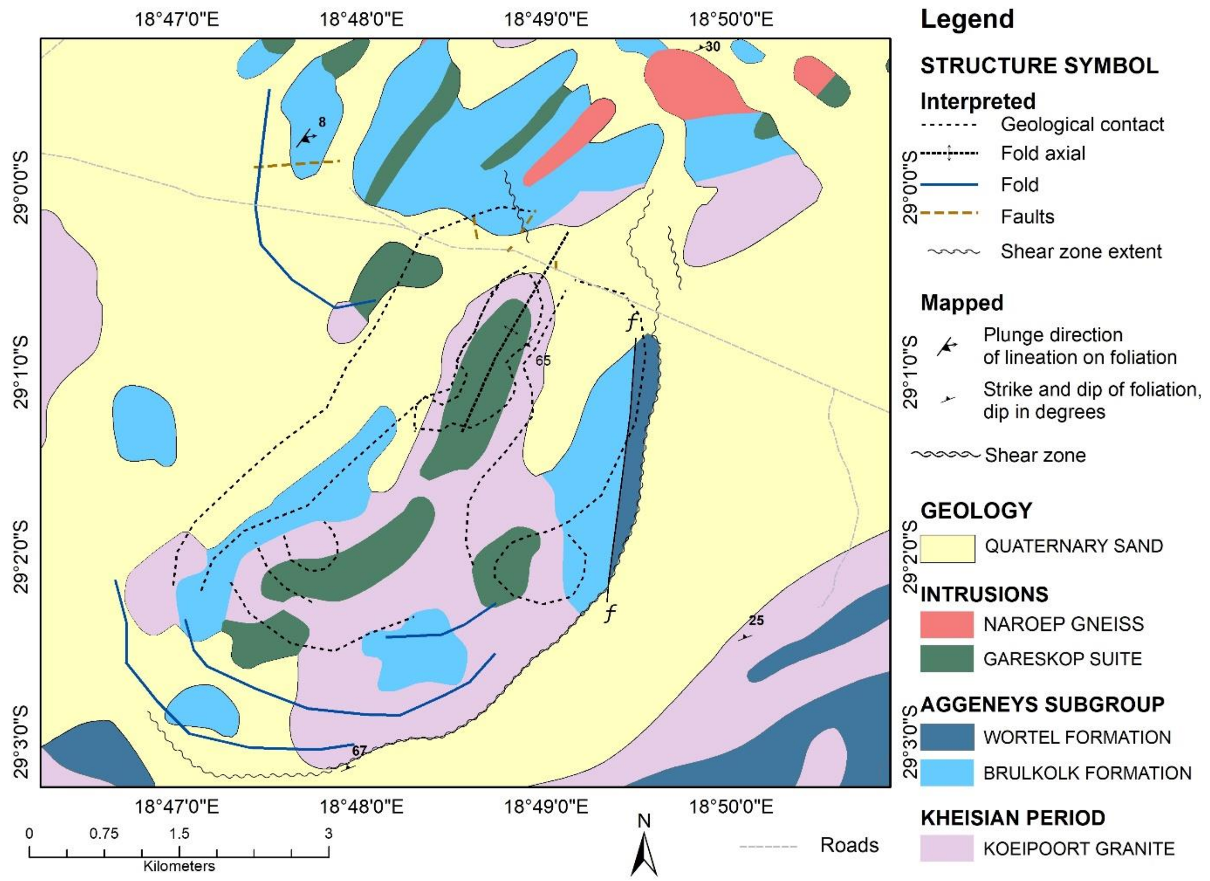

Figure 5.4. An excerpt from the 1:250 000 scale Pofadder geology map of the study area, as published by Council for Geoscience (2007), overlain with interpreted structures and some mapped geological structures.

The Namaqua tectonostratigraphic subdivisions are separated by major tectonic boundaries that are distinguished on the basis of lithostratigraphy, tectonic history, isotopic signature and metamorphic grade. The Bushmanland Terrane is largely composed of amphibolite, gneisses and granites dated at between 1210 and 1020 Ma with migmatitic gneisses dated at ca 1.85 Ga present locally. The Wortel Farm study area is dominated by amphibolites, gneisses, schists and amphibolites and Koeipoort Granite. The latter has a deformation fabric of the early Kheisian Era (~ 2.0 Ga) (Bailie et al., 2007;

Cornell et al., 2006). The Wortel Farm is known to have low-to-high-grade metamorphic rocks, with at least four deformation ($D_2 - D_5$) event structures and one M_2 metamorphic event imprinted on the rocks (Bailie et al., 2007; Cornell et al., 2006; Eglington, 2006). Based on these criteria, the terrane boundary as presented by Cornell et al. (2006) may need to be shifted further north of the area (by ~10 km toward the Hoogoor Suite outcropping rocks) and the rocks re-categorised as belonging to the Bushmanland Terrane.

Chapter 6: Conclusions and Recommendations

The aim of this research was to map a mineral prospect using geophysical methods to determine the potential of the prospect. The study area has mapped copper and tungsten mineral occurrences and high magnetic amplitude anomalies that matches the magnetism of the Aggeneys mineral deposits 20 km south of the area.

Based on the mapped mineral occurrences, magnetic anomaly, proximity to the Aggeneys mineral deposits and Bushmanland Group rocks mapped on the farm that belongs to the Richtersveld Subprovince, the now erroneous hypothesis of this project was that the Wortel Farm study area's copper and tungsten mineralisation is similar (in deposition and origin) to that of the Aggeneys mineral deposits and may have been transported during the deformation events and ended up 20 km away.

The analyses of the results revealed the following:

1. The geochemical results showed that there are high concentrations of Cr, Co, Cu, Fe, Li, Mg and Ni elements on the farm.
2. The mapped high chargeabilities (8 – 11 mV/V) are associated with host/deposit bodies, of undetermined source, of these mapped elements and mineral occurrences.
3. These deposits, according to the chargeability results, could exist as a larger connected body or discontinuous bodies forming pockets across the farm and neighbouring region with no clear lithology link.
4. The chargeability, magnetic, MT and DC resistivity datasets indicates occurrence of alterations on the farm that could be due to the intrusions and deposition of hydrothermal fluids.
5. Mapped fractures, faults and shear zones may have been the travelling pathway for the hydrothermal fluids that could have resulted in copper mineralisation and its by-product tungsten.
6. Magnetism on the farm is attributable to amphibolites and grabbros of the Brulkolk Formation and amphibolite dykes of the Gareskop Suite while, for the Aggeneys mineral deposit magnetism is due to amphibolite, gossans and iron formation of the Gams Formation.
7. The current geology map (1:250 000 scale) is too simplified for this study area, as evidence pf alteration and the existence of more than one lithology was found in a mapped geological unit.
8. Mapped structures were confirmed and new structures mapped including folds mapped through strike and dip measurements and geophysical data; faults, thrusting and shearing though geophysical data that may have occurred during the $D_2 - D_5$ deformation consisting of thrust, tectonic duplication, ENE-trending asymmetric folds, monoclonal fold, NE-strike slip faults and shear zones.
9. The structures, deformations and stratigraphy present in the study area indicate that the terrane boundary between the Bushmanland Terrane and the Richtersveld Subprovince may have to be shifted further north of the area instead of seen as passing through the Wortel Farm.

In conclusion, except for the Bushmanland Group rocks in the area, common deformation and geological structures similar to the Aggeneys deposits, it is clear that the Wortel Farm mineral occurrences and magnetism are not associated with/linked to the Aggeneys mineral deposits, but are of a pervasive nature as seen in Springbok and Aggeneys vicinity that this region was subjected to mineralizing fluids of post Namaqua age and yet unknown source. Per the assessment of the data presented, it is inferred that the mineral occurrence could be a porphyry-type occurring with the amphibolite dykes through the crustal fractures mapped and detectable with the IP method. As such, it is my interpretation that the farm hosts potential mineral deposits.

The geochemical data identified prominent ore elements on the farm and the geophysical methods used in this study area contributed information to the structures, deformation degree and subsurface geological settings and indicated the possible zones of mineralisation. However, the geophysical methods were not able to determine with certainty the depth extent of the mineralisation present, especially the depth, only that a deposit body possibly exist. To confirm these findings and arrive at a tangible conclusion, it is recommended that IP 2D cross sections, detailed mapping and a drilling integration studies be carried out in this area. The IP cross section surveys should be conducted over anomaly C1 to determine the present alteration and mineralisation extent at depth and around the dykes; detailed mapping is imperative in this area mainly because of the degree of deformation and alteration, as it will enable an enhanced interpretation and explanation of the responses mapped. Drilling is recommended to put an end to all speculations and to confirm or disprove all these inferences and models.

References

Agenbacht, A.L.D., 2007. The Geology of the Pofadder Area. Handbook. Council for Geoscience, Pretoria, 10-83.

Agenbacht, A.L.D., Oosterhuis, W.R., 2013. The Metallogeny of the Pofadder Area. Handbook. Council for Geoscience, Pretoria, 1-115.

Airo, M., 2015. Geophysical Signatures of Mineral Deposit types – synopsis. Geol. Surv. Finl. 9–70.

Ayuso, R.A., Barton, M.D., Blakely, R.J., Bodnar, R.J., Dilles, J.H., Graybeal, F.T., Mars, J.C., McPhee, D.K., Seal, R.R., Taylor, R.D., Vikre, P.G., 2010. Porphyry copper deposit model: 2010-5070, in: John, D. (Ed.), Scientific Investigation Report. Reston, 169. https://doi.org/https://doi.org/10.3133/sir20105070B

Bahr, K., 1988. Interpretation of the magnetotelluric impedance tensor: regional induction and local telluric distortion. J. Geophys. 119–127.

Bailie, R., Armstrong, R., Reid, D., 2007. The Bushmanland Group supracrustal succession, Aggeneys, Bushmanland, South Africa: Provenance, age of deposition and metamorphism. South African J. Geol. 110, 59–86. https://doi.org/10.2113/gssajg.110.1.59

Barr, J.M., Reid, D.L., 1992. Hydrothermal alteration at the Haib porphyry copper deposit , Namibia : Stable isotope and fluid inclusion patterns. Communs geol. Surv. Namibia 8, 23–35.

Berger, B.R., Ayuso, R.A., Wynn, J.C., Seal, R.R., 2008. Prelimenary model of porphyry copper deposits: 2008-1321, in: Open File Report. U. S. Geological Survey, 55. https://doi.org/10.3133/ofr20081321

Briggs, D.F., 2014. What is porphyry copper deposit? Min. You Tucson Citizes 1-7. http://www.geomineinfo.com/ESW/Files/Mining_a.

Briggs, I.C., 1974. Machine contouring using minimum curvature. Geophysics 39, 39–48.

Buthelezi, M., 2015. Interpretation of airborne magnetic and gamma-ray spectrometric data in Aggeneys, Northern Cape, South Africa: Report no. 2015-0073, Council for Geoscience. Pretoria.

CGS, 2019a. Gavity base station, viewed 24 October 2016, http://www.geoscience.org.za/index.php/2019-03-13-12-40-41/publications/284-geophysical-data

CGS, 2019b. Physical Properties Database, viewed 24 March 2019, http://www.geoscience.org.za/index.php/2019-03-13-12-40-41/publications/284-geophysical-data.

Chave, A. D., Jones, A.G., 2012. The Magnetotelluric Method Theory and Practice. Cambridge University Press.

Clark, D.A., 1997. Magnetic petrophysics and magnetic petrology: aids to geological interpretation of magnetic surveys. J. Aust. Geol. Geophys. 17, 83–103.

Cole, P., 2012. Development of a 3D potential field forward modelling system in Python., in: AGU Fall Meeting. ePoster, San-Francisco.

Collinson, D.W., 1983. Methods in rock magnetism and palaeomagnetism: Techniques and instrumentation, 1st ed. Springer Netherlands, Netherlands. https://doi.org/10.1007/978-94-015-3979-1

Colliston, W.P., Praekelt, H.E., Schoch, A.E., 1989. A broad perspective (Haramoep) of geological relations established by sequence mapping in the Proterozoic Aggeneys terrane, Bushmanland, South Africa. South African J. Geol. 92, 42–48.

Colliston, W.P., Schoch, A.E., 2013. Wrench-shearing during the Namaqua Orogenesis — Mesoproterozoic late stage deformation effects during Rodinia assembly. Precambrian Res. 233, 44–58. https://doi.org/10.1016/j.precamres.2013.03.007

Colliston, W.P., Schoch, A.E., 2000. Mid-Proterozoic tectonic evolution along the Orange River on the border between South Africa and Namibia. Communs geol. Surv. Namibia 12, 57–66.

Colliston, W.P., Schoch, A.E., Cole, J., 2014. The Grenvillian Namaqua-Natal fold belt adjacent to the Kaapvaal Craton : 1 . Distribution of Mesoproterozoic collisional terranes deduced from results of regional surveys and selected profiles in the western and southern parts of the fold belt. J. African Earth Sci. 100, 7–19.

Cooper, G.R.J., 1998. GRAV2DC - gravity modelling and inversion, Version 2.06. Johannesburg, University of Witwatersrand. Visited January 2019.

Cornell, D.H., Thomas, R.J., Moen, H.F.G., Reid, D.L., Moore, J.M., Gibson, R.L., 2006. The Namaqua-Natal Province, in: Johnson, M. R.; Anhaeusser, C. R.; Thomas, R.J. (Ed.), The Geology of South Africa. Geological Society of South Africa & Council for Geoscience, 325–379.

de Beer, J. & Muller, A., 2015. Geophysics in the Okiep Copper District, in: De Beer, J.H. (Ed.), The History of Geophysics in Southern Africa. SUN MeDIA Stellenbosch, Stellenbosch, 441–451.

de Beer, J., 2015. The History of Geophysics at Gold Fields, in: de Beer, J.H. (Ed.), The History of Geophysics in Southern Africa. SUN MeDIA Stellenbosch, Stellenbosch, 380–387.

de Villiers, J., Sohnge, A.P.G., 1959. The Geology of the Richtersveld, in: Memoir (Geological Survey (South Africa)). Government Printer, Pretoria.

Dentith, M., Mudge, S., 2014a. Geophysics for the mineral exploration geoscientist, 1st ed. Cambridge University Press, Cambridge, United Kingdom, 235-349.

Dentith, M., Mudge, S., 2014b. Geophysics for the mineral exploration geoscientist, 1st ed. Cambridge University Press, Cambridge, United Kingdom, 85-189.

Dingoko, O.W., Ledwaba, L., Cole, P., 2010. Redevelopment of old DOS programs into mordern windows programs: Report no. 2010-0096, Council for Geoscience. Pretoria, 1-20.

Eglington, B.M., 2006. Evolution of the Namaqua-Natal Belt, southern Africa - A geochronological and isotope geochemical review. J. African Earth Sci. 46, 93–111. https://doi.org/10.1016/j.jafrearsci.2006.01.014

Elsenbroek, J.H., Netshitungulwana, R., Strauss, S., Hlatshwayo, S.M., Ralushai, A.E., Mukosi, N.C., Bensid, M.L., Nxumalo, V., Ntikang, T., Walt, D. Van Der, 2018. Geochemical ATLAS, Regional Geochemical Mapping of the 2918 Pofadder Area at a scale of 1 : 250 000. Council for Geoscience, Pretoria, 23-159.

Erdi-Krausz, G., Matolin, M., Minty, B., Nicolet, J.P., Reford, W.S., Schetselaar, E., 2003. Guidlines for radioelement mapping using gamma ray spectrometry data. IAEA, Vienna, Austria.

Evans, D.M., Windrim, D.P., Armstrong, R.A., 2007. Age of Metavolcanic rocks at the northern margin of the Namaqua-Natal Metamorphic Province in the Karas Mountains, Namibia, defined by SHRIMP U-Pb dating of zircons. South African J. Geol. 110, 47–54. https://doi.org/10.2113/gssajg.110.1.47

Foulkes, S.E., 2014. New Geochemical Constraints on the Genesis of the Gamsberg Zinc Deposit , Namaqualand Metamorphic Province, South Africa. MSc thesis, Rhodes University.

Fransson, M., 2008. U-Pb Zircon Dating of Metasedimentary Rocks in the Areachap, Kakamas and Bushmanland Terranes in Namaqua Province, South Africa. MSc thesis, University of Gothenburg.

Geometrics Inc., 2011. Stratagem EH-4 Operation Manual 26716-11 Rev. A. https://geometrics.com/wp-content/uploads/2018/10/EH4_manual_F.pdf.

Geosystem SRL, 2011. WinGLink User's Guide, Release 2.20.12. Milan, Italy.

Gibson, R.L., Kisters, A.F.M., 1996. The geology and mineralization of the Okiep Copper District : An overview. South African J. Geol. 99, 105–106.

Google Earth Pro 7.3.0, 2018a. Aggeneys Outcrops Lat. -29.013° Long. 18.797°, elevation 800 m. Viewed 30 January 2019. https://www.google.com/earth/.

Google Earth Pro 7.3.0, 2018b. Wortel Farm Lat. -29.007° Long. 18.813°, elevation 800 m. Viewed 31 January 2019. https://www.google.com/earth/.

Hinze, W.J., Aiken, C., Brozena, J., Coakley, B., Dater, D., FLanagan, G., Forsberg, R., Hildenbrand, T., Keller, G.R., Kellog, J., Kucks, R., Li, X., Mainville, A., Morin, R., Pilkington, M., Plouff, D., Ravat, D., Roman, D., Urrutia-Fucugauchi, J., Veronneau, M., Webring, M., Winester, D., 2005. New Standards for Reducing Gravity Data: The North American gravity database. Geophysics J25–J32.

IRIS Instruments, 2003a. Elrec 6: Instrument Specification, viewed 20 January 2019, http://www.iris-instruments.com/elrec-6.html

IRIS Instruments, 2003b. VIP4000: Instrument Specification, viewed 20 january 2019, http://www.iris-instruments.com/vip-4000.html

IRIS Instruments, 2003c. Syscal Pro: Instrument Specification, viewed 20 January 2019 http://www.iris-instruments.com/syscal-pro.html

Kane, M.F., 1962. A comprehensive system of terrain corrections using a digital computer. Geophysics 27, 455–462.

Kearey, P., Brooks, M., Hill, I., 2002. An Introduction to Geophysical Exploration, 3rd ed. Wiley-Blackwell.

Ledwaba, L.; Dingoko, O.; Cole, P. and Havenga, M., 2009. Compilation of Survey Specifications for all the old regional airborne geophysical surveys conducted over South Africa: Report no. 2009-0130, Council for Geoscience, Pretoria, 34-35.

Lee, B., 2015. Three-dimensional electromagnetic imaging of porphyry copper deposit with MT and ZTEM data. MSc Thesis, University of Alberta. https://doi.org/https://doi.org/10.7939/R31R6N57H

Levinson, A.A., 1974. Introduction to exploration geochemistry, 1st ed. Applied Publishing Ltd, Illinois, USA, 924.

Loke, M.H., Acworth, I., Dahlin, T., 2003. A comparison of smooth and blocky inversion methods in 2D electrical imaging surveys. Explor. Geophys. 34, 182–187.

Lowell, J.D., Guilbert, J.M., 1970. Lateral and vertical alteration-mineralization zoning in porphyry ore deposits. Econ. Geol. 65, 373–408.

Macey, P.H., Thomas, R.J., Minnaar, H.M., Gresse, P.G., Lambert, C.W., Groenewald, C.A., Miller, J.A., Indongo, J., Angombe, M., Shifotoka, G., Frei, D., Diener, J.F.A., Kisters, A.F.M., Dhansay, T., Smith, H., Doggart, S., Roux, P. Le, Hartnady, M.I., Tinguely, C., 2017. Origin and evolution of the ~ 1 . 9 Ga Richtersveld Magmatic Arc , SW Africa. Precambrian Res. 292, 417–451. https://doi.org/10.1016/j.precamres.2017.01.013

Miller, R.M., 2012. Review of Mesoproterozoic Magmatism, Sedimentation and Terrane Amalgamation in Southwestern Africa. Geol. Soc. South Africa 115, 417–448.

Mobbs, P.M., 2004. The Mineral Industry of Namibia: USGS Minerals Yearbook - 2004. U. S. Geol. Surv. 1–7.

Morelli, C., Gantar, C., McConnell, R.K., Szabo, B., Uotila, U., 1974. The International Gravity Standardization Net 1971, 4th ed. SPec. Publ. Assoc. Geod, Paris, 194.

Moritz, H., 1980. Geodetic Reference System 1980. J. Geod. 395–405.

Naicker, I., 1993. Geographic Information System (GIS) Integration of Geological, Geochemical and Geophysical Data from the Aggeneys Base Metal Province, South Africa. MSc Thesis, University of Cape Town. http://hdl.handle.net/11427/22549.

National Oceanic and Atmospheric Administration, 2018. National Geophysical Data Center, viewed 20 November 2018, https://www.ngdc.noaa.gov/geomag-web/.

Palacky, G.J., 1988. Resistivity Characteristics of Geological Targets, in: Nabighian, M.N. (Ed.), Electromagnetic Methods in Applied Geophysics. Society of Exploration Geophysicists, pp. 52–129.

Parasnis, D.S., 1979. Principles of Applied Geophysics, 3rd ed. Chapman and Hall Ltd., London, 4-139.

Pardo, O.H., Alexander, G.C.E., Pintor, I.M.B., 2012. Geophysical exploration of disseminated and stockwork deposits associated with plutonic intrusive rock : a case study on the eastern flank of Colombia ' s western cordillera. Earth Sci. Res. J. 16, 11–23.

Pettersson, Å., 2008. Mesoproterozoic crustal evolution in Southern Africa. Doctoral Thesis A117, University of Gothenburg, 1-28. https://doi.org/http://hdl.handle.net/2077/17269

Pezzot, E.T., 2005. Induced Polarization and Magnetic Surveys. S. J. V. Consult. LTD Report. http//www.mindoro.com/i/pdf/LoboGeophysicalReport.pdf 1–89.

Praekelt, H.E., Schoch, A.E., 1997. Stratigraphical Synthesis of the Metasediments of the Aggeneys Terrane in the Namaqua Mobile Belt. South African J. Geol. 100, 85–100.

Reeves, C. V., 2005. Aeromagnetic Interpretation and Rock Magnetism. First Break 7, 275–286.

Robb, L.J., 1986. Uraniferous leucogranites from the Namaqualand Metamorphic Complex. Part I - geology, geochemistry and petrogenesis, in: Anhaeusser, C.R., Maske, S. (Eds.), Mineral Deposits of Southern Africa. Pretoria, 1609–1627.

Rogers, S., 2015. V5 System 2000 MTU/MTU-A User Guide, Version 3. Phoenix Geophysics, Toronto, Canada, 1-116.

Sasaki, Y., 1992. Resolution of resistivity tomography inferred from numerical simulation. Geophys. Prospect. 40, 453–464.

Scintrex Limited, 2012. CG-5 Scintrex System Operational Manual, part #867700 Revision 8. [WWW Document]. https://scintrexltd.com/wp-content/uploads/2017/02/CG-5-Manual-Ver_8.pdf.

Simpson, F., Bahr, K., 2005. Practical Magnetotelluric, 1st ed. Cambridge University Press, Cambridge, 1-45.

Singer, D.A., Berger, V.I., Moring, B.C., 2008. Porphyry copper deposits of the world: database and grade tonnage models, 2008. U. S. Geol. Surv. 45.

Smith, W.H.F., Wessel, P., 1990. Gridding with continuous curvature splines in tension. Geophysics 55, 293–305. https://doi.org/10.1190/1.1442837

Stettler, E.H., Kleywegt, 2015. Geophysics at the Geological Survey and Council for Geoscience, in: De Beer, J.H. (Ed.), The History of Geophysics in Southern Africa. SUN MeDIA Stellenbosch, Stellenbosch, 257-301.

Swain, C.J., 1976. A FOTRAN IV program for interpolating irregularly spaced data using the difference equations for minimum curvature. Comput. Geosci. 1, 231–240.

Telford, W.M., Geldart, L.P., Sheriff, R.E., Keys, D., 1990. Applied Geophysics, 2nd ed. Cambridge University Press, Cambridge, 6-609.

Tenzer, R., Mikuška, J., Marušiak, I., Pašteka, R., Karcol, R., Vajda, P., Sirguey, P., 2010. Computation of the atmospheric gravity correction in New Zealand. New Zeal. J. Geol. Geophys. 8306, 333–340. https://doi.org/10.1080/00288306.2010.510171

Thomas, R.J., von Veh, M.W., McCourt, S., 1993. The Tectonic Evolution of Southern Africa: an overview. J. African Earth Sci. 16, 5–24.

Trimble Geospatial, 2018. Integrated GNNS System, viewed 21 January 2019, https://drive.google.com/file/d/0BxW3dqQ5gdnTVXJrNHhBUDZKd1E/view.

Trimble Navigation Limited, 2008. Trimble R8 GNSS Receiver User Guide, viewed 21 January 2019, https://www.al-top.com/wp-content/uploads/2018/05/TrimbleR7-R8_223A_UserGuide.pdf.

Vajda, P., Panisova, J., 2005. Practical comparison of formulae for computing normal gravity at the observation point with emphasis on the territory of Slovakia. Contrib. to Geophys. Geod. 35/2, 173–188.

Van Der Merwe, S.W., Botha, B.J. V, 1989. The Groothoek Thrust Belt in western Namaqualand; an example of a mid-crustal structure. South African J. Geol. 92, 155–166.

Walker, P., Terblanche, O., 2010. Characterization of the Gamsberg deposit from electromagnetic modelling, in: Geophysical Algorithms. Society of Exploration Geophysicists, Denver, pp. 4453–4457. https://doi.org/https://doi.org/10.1190/1.3513180

Webb, S.J., 2009. The use of potential field and seismological data to analyze the structure of the lithosphere beneath southern Africa. Ph.D Thesis, University of Witwatersrand. http://hdl.handle.net/10539/8003.

Weckmann, U., Magunia, A., Ritter, O., 2005. Effective noise separation for magnetotelluric single site data processing using a frequency domain selection scheme. Geophys. J. Int. 161, 635–652. https://doi.org/10.1111/j.1365-246X.2005.02621.x

Wilson, M.G.C., Anhaeusser, C.R., 1998. Mineral resources of South Africa, 6th ed. Council for Geoscience, Pretoria, Handbook, 16, pp. 740.

Yossi, M., 2015. 3D geophysical modelling used for structural interpretation in southern Mali and northeastern Guinea , West Africa. MSc Thesis, University of Witwatersrand. http://hdl.handle.net/10539/23530.

Zonge, L.J., Hughes, K.L., 1988. Controlled source audio-frequency magnetotelluric, in: Nabughian, M.N. (Ed.), Electromagnetic Methods in Applied Geophysics. Society of Exploration Geophysicists, pp. 641–711.